Ion Transport Across Ion Exchange Membranes - Fluctuations and Chronopotentiometric Studies

by

Stephen H. Stern

A dissertation submitted to the Graduate Faculty in Chemistry in partial fulfillment of the requirements for the degree of Doctor of Philosophy, The City University of New York.

1972

A dissertation submitted to the Graduate Faculty in Chemistry in partial fulfillment of the requirements for the degree of Doctor of Philosophy, The City University of New York.

Examining Committee:

Horst Hoyer

Meyer Fishman

Mentor:

Michael Green

Executive Officer:

Leonard H. Schwartz

Oct 6, 1972

Date

Abstract

ION TRANSPORT ACROSS ION EXCHANGE MEMBRANES -

FLUCTUATION AND CHRONOPOTENTIOMETRIC STUDIES

by

Stephen H. Stern

Adviser: Professor Michael E. Green

Fluctuation techniques and chronopotentiometry were used to study ion transport, under an electric field, to and across certain ion exchange membranes. Principally Na^+ and H^+ (phosphate co-ion) transport was studied, and polystyrene sulfonate membranes used. The fluctuations were studied in the form of noise power spectra, in the frequency range 10 Hz to 100 kHz. The spectra were taken at steady state, at several temperatures, concentrations and currents. Chronopotentiometric studies were made of the formation of the depletion layer as a function of the variables mentioned above. A technique was developed to determine both the voltage across the membrane, and this voltage minus the IR drop, as the depletion layer formed.

Two distinct sources of noise and two critical current densities were found. At the first critical current density, the noise is generated by diffusion of ions at the membrane - solution interface in the diluate solution. At steady-state fluxes near and above the second critical current density, a second noise source exists. It is of much greater magnitude than the other noise source and is created by bulk flow in the diluate solution. This flow provides the mechanism for maintenance and stability of high flux steady state conditions at fluxes well above the second critical current density. Several parameters characterizing the transport have been estimated.

Dedication

To M.E.G. and E.V.A.

for their empathy, encouragement and wisdom

Acknowledgements

Special thanks are extended to
My wife Dorothy
My children Sharon and Lori
Toni Barber for typing
Masao Yafuso for his inspiration

Table of Contents

Tables

Figures

INTRODUCTION

Transport processes occurring across artificial membranes separating salt solutions are of great interest to chemists, chemical engineers and biologists. Chemists and chemical engineers would like to understand the mechanism of transport so that they would be able to fabricate membranes of any desired property or properties. Biologists are forced to turn to simple artificial membranes in order to understand the behavior of complex cell membranes, in terms of established physical and chemical principles.

Ion-exchange membranes have had and will continue to have wide applicability in scientific and technological investigations. They are used to desalinate brackish and sea waters and they are utilized in various industrial processes. They have been used to decant natural skim latex,[1] to desalt amino acids[2] and to separate and characterize proteins.[3] Although the uses to which ion-exchange membranes are put seem to be limited only by the inventiveness of man, the energetics of ion-transport are still only poorly defined even in simple commercial membranes. In studying ion transport across these membranes we wish to answer fundamentally the question of the transport kinetics and of the mechanism of transport.

As is well known, when studied at sufficiently high current densities, ion exchange membranes produce a depletion layer in front of the membrane. That is, from the membrane surface, and extending perhaps a few hundred A^0 into the solution, is a region largely depleted of ions. There is a concentration gradient from this region out to the bulk solution some tens of microns away. Associated with this depletion layer is a high field. High fields and their consequences for water are believed to be of great importance in biological systems.

The membranes actually studied were Ionac cation exchange membranes, with most of the work done on MC-3142 and MC-3235. We have carried out two types of measurements: noise spectral density measurements and voltage-time measurements at constant current. The results are useful in bringing closer an understanding of how the depleted region is formed and of how ion-exchange membranes are able to continuously pass high currents well above the critical current density. This gives us a better understanding of the transport process and transport kinetics of an electrodialysis system. Since nerve membranes are ion-selective and operate at high fields, our system might be a useful partial model of nerve transport.

Electrodialysis in Ion-Exchange Membranes

Passage of current across ion-exchange membranes leads to a reduction of electrolyte concentration on the side which donates the counterions and an increase on the receiving side.

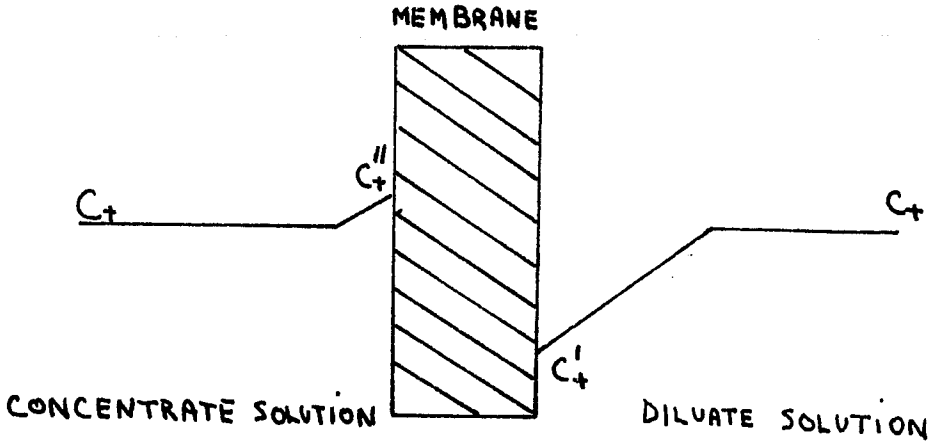

Consequently, diffusive polarization layers exist on both sides of the membrane.[4] The hydrodynamic conditions determine the thickness of both layers.

If the current density is increased to a point where convective transport is no longer adequate to maintain the flux, a more complicated series of events occurs. At this limiting current density, an alternative process must take a significant part in carrying the current. This limiting current is an important factor complicating the practical application of electrodialysis.

Earlier investigations of systems such as ours have shown "abnormal" behavior at fluxes above the limiting current density.[5-9] There has been some speculation as to what the alternative process responsible for the maintenance of flux above the critical current density really is. It has been generally accepted that this "alternative" process is water dissociation.[5,10,11] However, there is a good deal of evidence in the literature that appears to show that such dissociation could only account for a small percentage of the added flux above the critical current density.[6-9] The nature of the critical current density has itself been called into account and some investigators have speculated that there are, in fact, two critical current densities that exist in a narrow flux range.[6,8] Cooke,[7,8] in 1961, investigated the interfacial concentration at the membrane - solution interface by driving ions across the membrane under the influence of an external current source and then repeatedly interrupting that current source for 350 μs intervals. Voltage readings were then recorded 20 μs to 40 μs after interuption. These measurements were taken while the concentrated solution side of the membrane was stirred. Cooke was thus able to measure a "concentration overpotential" due to the depletion of ions near the membrane surface. In his investigation, Cooke used fluxes above and below the critical current density, but he interrupted current only until such time as depletion occurred at the membrane surface. Our work employs a different technique to measure the

overpotential and extends these measurements to times well past depletion (i.e., until steady state is reached).

Membrane Transport Theories

There are two groups of macroscopic theories on membrane transport. There are theories that include only linear terms and are first order in all gradients and there are non-linear theories[12] which would allow for the effects of non-linear convection (turbulence). Later, it will be shown that non-linear theories are sometimes needed to explain high flux transport because this is often accompanied by turbulence.

The linear theories are based on irreversible thermodynamics. The present macroscopic form of irreversible thermodynamics was suggested primarily by the statistical mechanical investigations of Onsager. However, the necessary concepts such as linear laws, entropy production and symmetry of coefficients have been confirmed by experimental data.[11]

Most electrolytic conductivity is concerned only with differences in electrical and chemical potential. If we assume that only these gradients are important and ignore all cross terms, we can derive the Nernst-Plank Equation from irreversible thermodynamics. There can be a convection term in the Nernst-Plank Equation, but it is linear and assumes only laminar flow.

When a membrane separates two solutions, there are a number of forces which may operate to cause a flow (flux) of molecular or ionic species through it. These forces operate either individually or in combination with each other. For example, an electrical potential gradient can result in thermal diffusion or a temperature gradient in chemical potential

qradient. For example, if the temperature and bulk concentration are kept constant and the pressure and electric potential are allowed to vary, we qet electrokinetic effects. These include electroosmotic pressure, streaminq potential and streaminq current.[13] Other combinations are also possible. The fundamental theorem of irreversible thermodynamics is that the forces and fluxes are chosen so as to conform to the equation

$$T\theta = \sum_i J_i X_i \qquad (1)$$

where

θ = diS/dt (rate of entropy production due to irreversible processes within the system.

T = temperature

J_i = flux

X_i = conjuqate force of flux i

If there is more than one irreversible process occurrinq, each flow is related not only to its conjuqate force but it is also linearly related to all other forces found in equation (1). If the qeneral linear coefficient is denoted by L_{ik}, the qeneral form for J_i is

$$J_i = \sum_k L_{ik} X_k \qquad (2)$$

If J_i and X_i are chosen from equation (1) and are independent, then the phenomenological coefficients L_{ik} of the linear laws satisfy the symmetry relation

$$L_{ik} = L_{ki} \qquad (3)$$

Equation (3) states the Onsager reciprocal relations.[13]

The use of irreversible thermodynamics enable one to deal not only with effects of electrical and chemical potential differences but also with cross effects. These cross effects include a variety of electrokinetic effects thermosmosis and reverse osmosis.

A third group of theories is based upon the theory of rate processes.[14] The membrane is considered as a series of potential energy barriers across which materials must pass if they are to permeate the membrane. A microscopic theory would be required to make such an approach successful. Since a microscopic picture of membrane transport is not available yet, the approach of group III is rarely used.

The Donnan Potential

Ion-exchange membranes have ionogenic groups fixed to the resin matrix (-negative groups like $-SO_3^-$, COO^- in the case of cation-exchange membranes). As a result of this they take up electrolyte quite differently than do non-ion-exchange membranes. Ion-exchange membranes exclude the co-ions (ions of same sign as the fixed groups) by electrostatic repulsion. When a cation-exchange membrane is placed in dilute solution of a strong electrolyte, there will be a considerable concentration difference in both anion and cation between the membrane and bulk solution. The anion (co-ion) concentration is larger in the solution and the cation (counter-ion) concentration is larger in the ion-exchange membrane. If the ions carried no charge, diffusion would level out these concentration differences between the membrane and the bulk solution; but ions are charged and these differences are not completely leveled out. Diffusion of counter-ions into the solution and of co-ions into the membrane takes place but only to a small extent since these processes violate the requirements of electroneutrality. Cations migrate into the solution, anions into the membrane with a resulting accumulation of positive charge in the solution and negative charge in the ion-exchange membrane. The first few ions that diffuse build up an electric potential between the two phases. This is called the Donnan Potential. It pulls anions back into solution and cations back

into the negatively charged membrane. An equilibrium is thus established where the action of the electric field balances the tendency of the ions to level out the existing concentration differences by diffusion.[15]

The Donnan Potential increases as the concentration of the external solution decreases. An increasing Donnan Potential means a greater exclusion of co-ions from the membrane. Co-ion uptake and electrolyte sorption are equivalent because of electroneutrality requirements. Therefore, electrolyte is increasingly excluded with increasing Donnan Potential. Electrolyte exclusion is more efficient with counterions of low valence and co-ions of high valence. Thus $HPO_4^{=}$ is more strongly excluded than $H_2PO_4^{-}$ from a cation exchanger.

The Donnan Potential can be derived from the Nernst-Plank Equation shown below.

$$J_i = -D_i C_i (\text{grad } \ln a_i + \frac{z_i F}{RT} \text{grad } \varphi) + \bar{C}_i V^* \qquad (4)$$

where

D_i = diffusion coefficient

a_i = activity

φ = electric field

z_i = number of charges on the ion

C_i = concentration

$\bar{C}_i V^*$ = convection of pore liquid where $\bar{C}_i$ is the concentration of counterions in the membrane phase.

V^* = velocity of movement of the center of gravity of the pore liquid.

At the membrane solution interface, the gradient of electric potential and gradient of activity become very much greater than the flux and convection term. This is equivalent to assuming equilibrium at the interface.

$$\frac{z_i F}{RT} \text{ grad } \varphi = -\text{grad ln } a_i \qquad (5)$$

$$E_{Don} = \bar{\varphi} - \varphi = -\frac{RT}{z_i F} \ln \frac{\overline{a_i}}{a_i} \qquad (6)$$

The Cation Transport Number

The transport number of a species is defined as the fraction of the electric current which is carried by the species. As a result of the Donnan Potential, the charge in the membrane will be predominately carried by the counter-ion, whereas, in the solution, the current will be carried by both charge carriers. Thus the counter-ion transport number will be higher in the membrane than it is in the solution. It will approach unity as the Donnan Potential increases. This difference in transport number means that the counter-ion will travel faster in the membrane than it travels in the solution. This causes an electrolytic depletion at the membrane surface.

The difference in transport number is made up for by increased diffusion and convection in the external solution. However, if the flux is increased, it will eventually reach a magnitude above which diffusion and convection can no longer maintain it across the still layer in the external solution. At this point, we are at the critical current density; the concentration of ions at the membrane surface has reached a minimum[7] and the electric field generated across the diffuse layer adjacent to the membrane has reached its maximum value.

Current-Voltage Curves

The relationship between the d.c. voltages across ion-exchange membranes and increasing flux is well known.[9,14,15] Current voltage curves have been plotted for many types of ion-exchange membranes bounded by many different electrolytic solutions. All of these curves have in common three distinct regions labeled below:

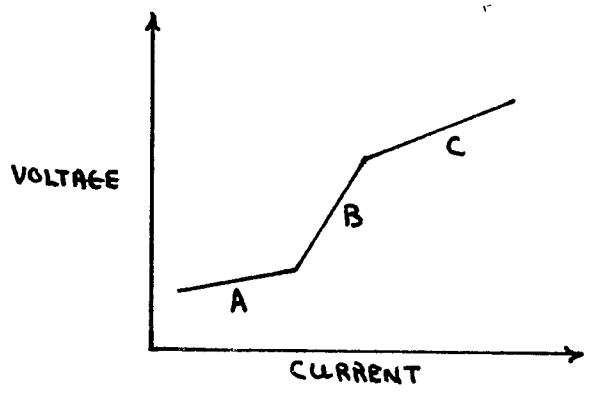

Region "A" is a region of small voltage increase with increasing current. The voltage may be accounted for by an ohmic term and by the "over-voltage" due to the concentration potential. Region "B" is characterized by a sharp increase in voltage. This large increase is believed due to the onset of the "alternative" process that will now help to maintain the flux. The fact that the voltage rise does not continue can only mean that the process is initiated in this region. Region "C" we shall henceforth call a "high polarization" region.[9] The fact that very high fluxes can be maintained for long periods of time in this region suggests that the

"alternative" process responsible for maintenance of the flux is indeed extremely efficient.

The Double Layer

Ion-exchange membranes may be considered electrodes in that a particular ion, for example H^+ ion, is in reversible equilibrium between the membrane surface and the solution phase. In the ordinary sense, the membranes are not electrodes because they do not serve as oxidation-reduction sites and also because they are somewhat permeable to water.[9] In the absence of specific adsorption, a double layer similar to that found external to ion-exchange membranes is found external to electrodes. There is a space-charge region in the metallic electrode analogous to the usual diffuse double layer of electrolyte theory and a charge-free layer.

The diffuse double layer, made up of positive and negative ions extends into the bulk of the electrolyte.[16] Models of the double layer go back as far as Helmholtz (1853) and Quincke (1861). The first detailed model is due independently, to Gouy[17] and Chapman,[18] each of whom gave an analysis which started with the same premisis as the Debye-Hückel theory (1923). Stern[19] modified the Gouy -Chapman model. The Gouy -Chapman theory treated ions as point charges and such ions could approach the electrode within any distance no matter how small it might be.

Stern postulated that ions cannot reach the electrode beyond "the plane of closest approach". This theory assumes

the double layer to be divided into two regions: the compact double layer (inner or charge free layer) between the electrode (membrane in our case) and the plane of closest approach and the diffuse double layer extending from the plane of closest approach to the bulk of the solution. The Gouy-Chapman-Stern theory is still the most widely accepted double layer theory.

Chronopotentiometry

Chronopotentiometry has been used extensively in studies of kinetics, adsorption and transport properties of a working electrode. It is an experimental procedure which involves the measurement of the potential as a function of time during polarization by constant current.[20]

Chronopotentiometric analyses of dilute solutions in contact either with a working electrode or an ion-exchange membrane are complicated by the necessity of correcting for the charging of the electrical double layer.[21] Sand's Theory describes electrolysis at constant current under the influence of electromigration and diffusion in the absence of convection. According to Sand's theory, the time required for the concentration of electrolyte to fall to zero at the place of the electrode (membrane), called the transition time, is given by

$$\tau = \frac{\pi z^2 F^2 D C^2}{4 I^2 (1-T)^2} \qquad (1)$$

where

z = valency of current carrying ion

F = Faraday's Constant

D = Diffusion Coefficient

C = concentration of the electrolyte

I = current density (total)

T = transport number of the counterion in solution

In the derivation of Sand's equation, it is assumed that the current is entirely faradaic. This is not true since some fraction of the total current must be devoted to double layer charging at every instant.[21] The total current density is, therefore, the algebraic sum of the faradaic and double-layer charging (non-Faradaic) current densities. The double layer current is given by

$$i_c = \frac{dE(t)}{dt} \cdot C_1 \qquad (8)$$

where

C_1 = the potential independent differential double-layer capacitance

E = the electric field

Thus the transition times computed from the Sand's equation will always be less than those found experimentally because the faradaic current is always smaller than the total current.[20,21] At high current densities or low concentrations, deviations from Sand's equation reportedly become more pronounced, whereas at low current densities or high concentration such deviations are imperceptible.[21]

Several models have been proposed to compensate for the effects of double-layer charging. Olmstead and Nicholson[20] evaluate four such current and compensation methods in their paper. The hope of each of these methods is to find true transition times.

It was taken for granted in the early analyses of electrolytic experiments that Faradaic and non-Faradaic processes didn't interact and that "a priori" separation was possible. Until recently however, few experiments have been undertaken to investigate coupling effects. However, MacDonald[22] clearly shows that in the "absence of an indifferent electrolyte...Faradaic and non-Faradaic processes are so coupled that they become almost indivisible parts of a single process." At present, the situation appears to be that there is no successful model for obtaining the transition times that takes the coupling of Faradaic and non-Faradaic processes into account.

Noise-Application To Ion-Exchange Membranes

Knowing that electrical noise analysis had been used successfully in the study of semi-conductors[23,24] and that a significant amount of noise theory had been developed, Green and Yafuso[10,11] recognized that noise measurements could be a valuable tool in the analysis of many other types of systems. With this insight the first extensive noise study of electrodialysis was undertaken.

Initially, Yafuso and Green hoped to study the ion-exchange process taking place within an ion-exchange membrane. However, their data quickly told them that any noise due to ion-exchange itself was dominated by a larger noise source external to the membrane, in the diluate solution. They showed that this noise was dependent on the "alternative process" needed to maintain the flux at steady state conditions above the critical current density. Their work clearly left many unanswered questions. This noise investigation is, in part, an extension of their work. It was undertaken in the hope that new information on transport could be obtained.

In the last two years, a number of papers on noise measurements have been published. These papers will be discussed later. What their publications show is that it is quickly becoming recognized that noise analysis can be extended to a large variety of different systems.

Noise Theory

Because the noise is directly related to microscopic interactions of the system under investigation, information about the system can be obtained directly from fluctuations (noise). Fluctuations may be regarded as the very means whereby a classical system in thermal equilibrium proceeds from "state" to "state". From the standpoint of noise the application of the so-called ergodic theorem (that a time average for a single system in statistical equilibrium may be replaced by an average over an equilibrium ensemble) seems very natural and we assume that this is always valid.[25]

In a generalized sense, noise is the fluctuation of a random variable. The observed parameter α, is the deviation of the thermodynamic extensive variable (a) from an equilibrium value (a_{eq}) or from some steady state value (a_{ss}).

$$\alpha = a - a_{eq}$$
$$\alpha = a - a_{ss} \qquad (9)$$

Kinetic information is contained in the correlation function, which is the time average of the product of $\alpha(t)$ and $\alpha(t + \tau_*)$. For a system in a stationary state, i.e., in which thermodynamic average (macroscopic) parameters do not vary with time,

$$C(\tau) = \langle\alpha(t)\alpha(t + \tau_*)\rangle = \langle\alpha(o)\alpha(\tau)\rangle$$

where

τ_*= the relaxation time

So far we have considered the behavior of a particular fluctuation $\alpha(t)$ in a particular system. An alternative attack would be to start by considering an ensemble of systems having various displacements (α) over a range of different values at a given time t and then to consider how this distribution will be effected as time goes on. After a sufficient passage of time an over-all statistical distribution will emerge which on the average is stationary.[26]

The correctness and applicability of the above equation is based on the system being Markoffian, i.e., that a knowledge of the value of α at time t determines the probability distribution of this variable, without reference to previous values. The time average of α is taken equal to zero, i.e., $\langle\alpha\rangle = 0$.

The variable α has a value at one instant in time and then another value at some later time. If the time interval between the two α values is short, the value at the later time will be dependent on the value at the earlier time. If we call the initial time zero and the later time t, and the corresponding α values α_o and α_t, then the average value of the product of α_o and α_t over an ensemble of systems will not equal zero.

$$\langle\alpha_o\alpha_t\rangle \neq 0 \qquad (11)$$

Over long time intervals the variable α loses all memory of what it was and

$$\langle\alpha_o\alpha_t\rangle \to 0 \qquad (12)$$

The behavior of the variable becomes progressively more uncorrelated with its previous value as the time interval lengthens. At very long time intervals the variable value at a later time t will be completely unrelated to what it was at time zero.

The total noise of a system can be analyzed into its various Fourier components by means of a filter. The output is the power spectrum: the power spectrum is a function of frequency and is equal to:

$$G(f) = \frac{V^2(f)}{R(\Delta t)} \qquad (13)$$

where

$G(f)$ = power spectrum

V^2 = voltage squared

R = resistance

The voltage squared is proportional to power since

$$PR = V^2 \qquad (14)$$

where

P = power

R = resistance

V^2 = voltage squared

The Wiener-Khintchine relationship states[17] that the correlation function and power spectrum are each others Fourier cosine transform.

$$G(f) = 4\mathrm{Re}\int c(\tau_*)e^{-iwt}dt \qquad (15)$$
$$= 4\int c(\tau_*)\cos wt\, dt$$

where

$w = 2\pi f$

t = time

When the behavior of a system can be characterized by a single relaxation time, the correlation function is

$$c(\tau_*) = \langle\alpha\alpha\rangle \exp^{-(t/\tau_*)} \qquad (16)$$

For the case a simple reaction involving an equilibrium of a dissociati

$$AB \underset{k_r}{\overset{k_f}{\rightleftharpoons}}$$

The time behavior acterized by a single relaxation time τ

$$\tau_* = \frac{}{k_f} \qquad (17)$$

$\alpha = \alpha_o e^{-}$ concentration of A^+

= concentration of B^-

The correlation functio

$$c(\tau_*) = \langle\alpha_o^2\rangle e^{-t/\tau_*} \qquad (18)$$

The power spectrum is then given by[28]

$$G(f) = \frac{4\langle\alpha_o^2\rangle\tau_*}{1 + w^2\tau_*^2} \qquad (19)$$

If we set α = voltage(V) and plot log V^2 vs log f, we obtain a characteristic power spectrum for a process with a single relaxation time. Such a spectrum is white (flat) up to the neighborhood of the frequency where w is equal to $1/\tau_*$. At higher frequencies than $1/\tau_*$ the power spectrum decays at a rate of w^{-2}.

So far we have discussed procedures to solve for the spectral densities of stochastic processes based on Fourier analysis of the fluctuating quantities. Another method of obtaining these spectral densities employs conditioned probabilities for the transport variables. This leads to solutions in terms of Green's functions. The power spectrum arising from the fluctuations can be obtained from the phenomenological equations describing the macroscopic system. The noise from transport phenomena can be calculated from the Green's function $g(x,t; x',t')$ of the transport equation.[29] The Green's function gives the value of g at x at time t due to a disturbance by a unit impulse at x' at time t'. The power spectrum is obtained by integrating the Fourier transform with respect to time of $g(x,t; x',t')$ over x and x'.

$$G(f) = 4\mathrm{Re}\int c(\tau_*) e^{-iwt} dt \qquad (15)$$

$$= 4\int c(\tau_*) \cos wt \, dt$$

where

$w = 2\pi f$

t = time

When the behavior of a system can be characterized by a single relaxation time, the correlation function is

$$c(\tau_*) = \langle \alpha\alpha \rangle \exp^{-(t/\tau_*)} \qquad (16)$$

For the case a simple reaction involving an equilibrium of a dissociating species:

$$AB \underset{k_b}{\overset{k_f}{\rightleftharpoons}} A^+ + B^-$$

The time behavior of a fluctuation is characterized by a single relaxation time τ_*, which is given by[28]

$$\tau_* = \frac{1}{k_f + k_b(c_{A^+} + c_{B^-})} \qquad (17)$$

$$\alpha = \alpha_o e^{-t/\tau_*}$$

where c_{A^+} = concentration of A^+

c_{B^-} = concentration of B^-

The correlation function is

$$c(\tau_*) = \langle \alpha_o^2 \rangle e^{-t/\tau_*} \qquad (18)$$

The power spectrum is then given by[28]

$$G(f) = \frac{4\langle \alpha_o^2 \rangle \tau_*}{1 + w^2\tau_*^2} \qquad (19)$$

If we set α = voltage(V) and plot log V^2 vs log f, we obtain a characteristic power spectrum for a process with a single relaxation time. Such a spectrum is white (flat) up to the neighborhood of the frequency where w is equal to $1/\tau_*$. At higher frequencies than $1/\tau_*$, the power spectrum decays at a rate of w^{-2}.

So far we have discussed procedures to solve for the spectral densities of stochastic processes based on Fourier analysis of the fluctuating quantities. Another method of obtaining these spectral densities employs conditioned probabilities for the transport variables. This leads to solutions in terms of Green's functions. The power spectrum arising from the fluctuations can be obtained from the phenomenological equations describing the macroscopic system. The noise from transport phenomena can be calculated from the Green's function $q(x,t; x',t')$ of the transport equation.[29] The Green's function gives the value of q at x at time t due to a disturbance by a unit impulse at x' at time t'. The power spectrum is obtained by integrating the Fourier transform with respect to time of $q(x,t; x',t')$ over x and x'.

Noise Measurements in Different Systems

It was mentioned earlier, that noise measurements have been made on a number of different systems."1/f-noise" is used to describe a noise source whose power is inversely proportional to the frequency. The cases where such noise is found will now be discussed.

The phenomenon of 1/f noise has been observed commonly in semiconductors. In a series of experiments it has been shown that 1/f noise of homogeneous metal samples and of semiconductors can be expressed as[30-33]

$$\frac{\Delta R}{R}^2 = \frac{x}{N} \frac{\Delta f}{f} \qquad (20)$$

where

N = the total number of mobile charge carriers found in the homogeneous samples

x = an experimental constant with a value of 2.1×10^{-3},

f = the frequency

Δf = bandwidth

R = the resistance

Hooge and Goal[34] showed that 1/f noise is also present when current flows through a thermocell and that the 1/f noise can be described as fluctuations in the internal resistance of the cell.

It is well known that in addition to thermal noise a d.c. voltage applied to carbon resistors causes "flicker noise". This noise is characterized by a 1/f power spectrum and although the origin of it is not well understood, it is possible to explain it by assuming resistance fluctuations of the resistor.[35]

Fluctuations with a 1/f spectrum were found in the conductance of ionic solutions and in the voltage of concentration cells.[33] In this case, the 1/f noise is associated with carrier concentration fluctuations. The noise was said to be current noise whose magnitude in the bulk solution was determined by the number of charge carriers present. Noise across small patches of squid axon membrane were also found to have a 1/f type dependence.[36]

Diffusion Noise

Lax and Merqert,[37] showed that fluctuations in the total number of carriers plux a term associated with the transport of these carriers across a boundary is associated with the noise of diffusion and drift.

Theoretical considerations show that in one dimension diffusion the low frequency spectrum has an $f^{-1/2}$ dependence and high frequency dependence of $f^{-3/2}$. For three dimension diffusion at low frequency the spectrum can be written[29]

$$G(w) = \frac{32\,\rho_o R_o}{15D} \qquad (21)$$

where

D = Diffusion coefficient

ρ_o = Averaqe Density

w = $2\pi f$

R_o = Radius of a sphere where a qiven number of particles are fluctuatinq at high frequency

$$G(w) = \frac{\rho_o (2D)^{1/2} 4\, R_o^2}{w^{3/2}} \qquad (22)$$

The first term shows no frequency dependence, the second shows an $f^{-3/2}(w^{-3/2})$ dependence. Since this $f^{-3/2}$ dependence is true of diffusion noise, reqardless of the qeometry or the number of dimensions, Lax refers to it as the "universal 3/2 power law".[37]

Summary

The successful use of noise analysis depends on finding out where the noise is being generated and then being able to identify the process causing the noise. Hopefully, the type of power spectrum obtained (frequency dependence) will enable us to do the latter and our chronopotentiometric studies both the former and the latter. Noise spectra can give us valuable insight into the process (or processes) responsible for flux maintenance across the solution which is depleted of ions external to an ion-exchange membrane as well as information about the depleted region itself.

Chronopotentiometric studies undertaken across the same membranes at the same concentrations, temperatures, and fluxes as those used in the noise studies should be very helpful in noise spectra interpretation. Such studies should help to determine where the noise is created and what causes it. The steady-state resistances and measured concentration potentials obtained from these studies should provide us with a great deal of information about the depleted region and membrane surface across which the noise is measured. However, apart from the assistance these data provide in the clarification of the noise data, chronopotentiometric studies are very valuable in that they can help to understand how the bulk solution gets depleted of ions and how charge forms on the membrane surface and in the bulk solution.

EXPERIMENTAL SECTION

In this work, we have studied transport across cation ion-exchange membranes in electrolytic solutions. A dry cell provides the energy for the transport by driving a current between electrodes on opposite sides of the membrane. When current is sent across an ion-exchange membrane separating two compartments of electrolytic solution, a Back Emf is built up. This Back Emf is, in part, a type of polarization which is a direct result of the difference in transport number of ions between the solution and membrane phase.[5,6,38] The passage of current across ion-exchange membranes (electrodialysis) also produces noise of great enough magnitude to be measured and studied.[11]

Noise measurements, at steady state conditions, were made using phosphoric acid solutions and Disodium hydrogen phosphate. The experimental procedure and apparatus will be described in this section.

A technique has been devised to simultaneously measure the Back Emf and total d.c. voltage created across ion-exchange membranes. These measurements were obtained from the time the current is first applied until steady state is reached. The Back Emf was also measured as it went from one steady state to a different steady state. Two different steady states were

obtained by placing an 11kΩ resistor between the measuring electrodes. The experimental procedure and apparatus will be discussed in this section. Both the voltage-time data and the power spectrum were measured at the same concentrations and temperatures.

The Cation-Exchange Membrane

The membranes used in this work were all obtained on 9 x 12-in sheets from the Ionac Chemical Company. The membrane used most extensively, the one for which all of the chronopotentiometric and fluctuation data is presented, is numbered MC. 3142. This is a polystyrene sulfonate cation exchange membrane. The following properties of this membrane were supplied by the Ionac Chemical Company:

a) Electrical Resistance ohm-cm^2 A.C. measurement in .1 N NaCl is 9.1.

b) % Permselectivity (.5 N NaCl/1.0 N NaCl) is 94.1.

c) Membrane thickness is 6 mils.

d) Approximate density is 196 g/m^3

e) Capacity is 0.021 -meq/cm^2.

f) Dimensional stability (ability to revert after drying) is good.

g) Chemical stability is good up to 60°C.

Circular pieces of membrane were cut out of the larger sheets with a cork borer 11 mm. in diameter.

Before the membrane piece was placed in the cell, it was soaked in .021m phosphoric acid solution for approximately 24 hours. Extensive precautions were undertaken to insure that the membrane surface remained free of surfactant materials.

Firstly, the membrane was handled only with clean tweezers. Secondly, all water used was doubly distilled and then treated to remove additional surfactant materials that were not removed in distillation.[39] Thirdly, the cell was cleaned by soaking it in a solution of strong detergent and Na_2CO_3. The detergent, X-100, was obtained from Rohm and Haas. It is an extremely water soluble, long chain hydrocarbon with hydrophilic and hydrophobic groups. The cell was repeatedly rinsed to remove all traces of X-100.

The Cell

The plexiglass cell used in this work is shown in Fig. 1. The membrane is mounted flat against the tapered hole that connects the two compartments of the cell. The membrane area exposed to transport is determined by the diameter of the hole cut in the black vinyl electrical tape ("Tiger" tape) that secures the membrane to the center partition. Once mounted, the membrane is converted to the counterion salt of interest by filling the cell with the solution to be used and passing a current of approximately 1 ma through the membrane for five to ten minutes. The solution is then changed before measurements are taken.

No additional equilibration between membrane and solution is necessary again until a different counterion or a new piece of membrane is used. The same piece of membrane can be used for a series of runs over a number of days but the solution is changed after each run. The measurements were found to be reproducible on the same piece of membrane used over a number of days as well as between different pieces of membrane.

FIGURE 1

THE PLEXIGLASS CELL

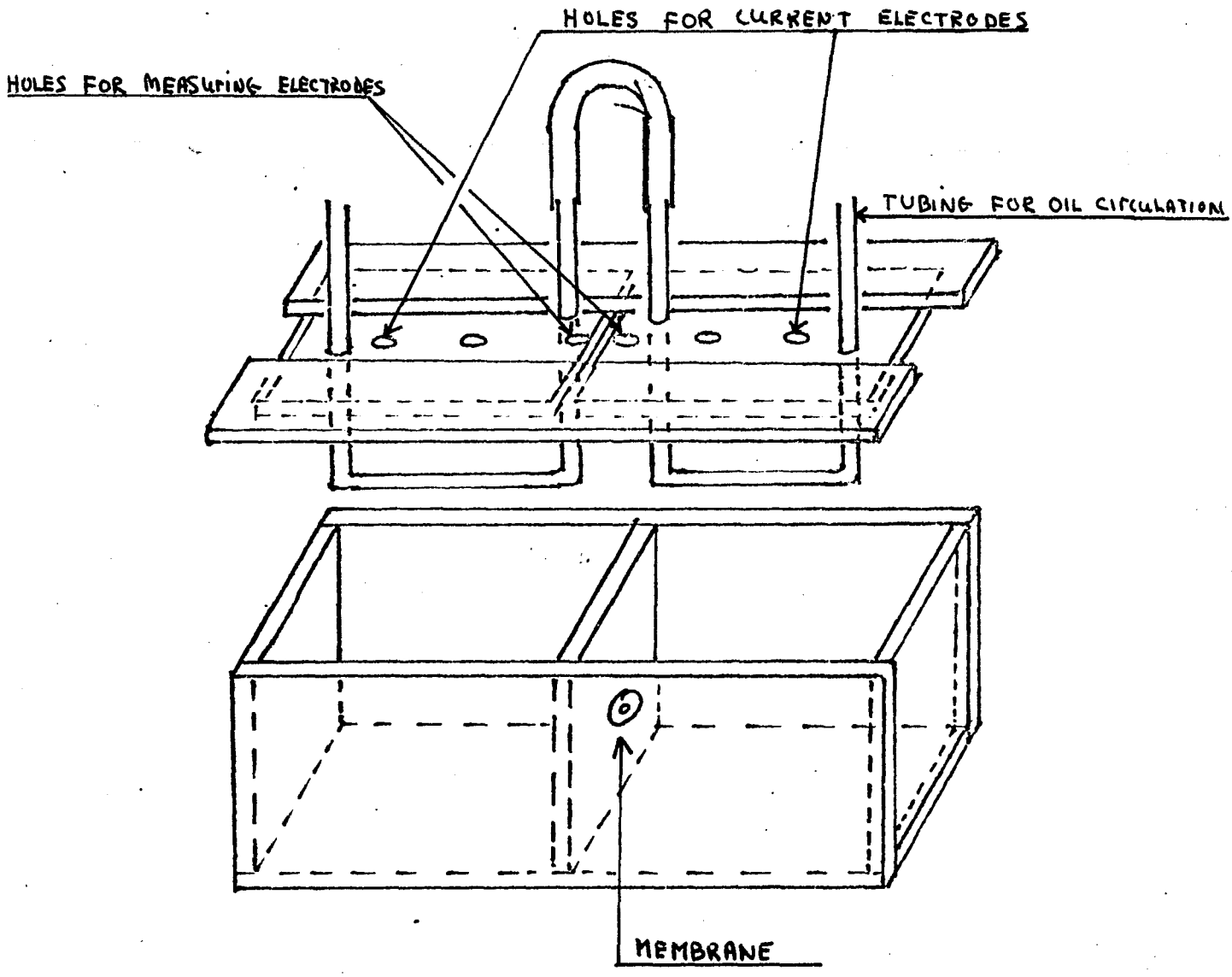

The cover for this cell has five holes above each compartment. The holes at the farthest ends of the cell are used to change solutions. Each compartment holds approximately 50 ml. of solution. The type and concentration of solution on each side of the membrane is always the same for any given run. Two of the four remaining holes above each compartment are used for circulating silicone oil through glass tubing that extends into the solution. The temperature of the circulating oil determines the temperature of the solutions to be used. A Messgerate-Werk Laude Ultra K_2 thermostat was used to set oil temperatures above 18°C. Below 18°C an icebath was used to cool the oil and a Laboratory Supplies Co. Inc. pump was used to circulate it. Silicone oil was chosen as a temperature regulator because it was found that, unlike water, alcohols and various other solvents, it did not introduce 60 Hz when circulated through glass tubing.

The two remaining holes above each cell compartment (four holes in all) are used for our Platinum electrodes (in oscillation studies copper electrodes were used). Two electrodes, one on each side of the center partition, are at a distance of ~2mm from each membrane surface. These are our inner electrodes, henceforth referred to as our measuring electrodes. Two outer Pt electrodes - current electrodes - are on opposite sides of the membrane ~2.5 cm from its surface. The current electrodes (our anode and cathode) have an exposed surface approximately eight times larger than do the measuring electrodes. The current electrodes, a 90 volt carbon-zinc battery and a 100 kilohm

potentiometer give us a low noise constant current d.c. field which causes the ions to migrate across the membrane. The 100K potentiometer in series with the battery and cells, serves both as a current control and as a swamping resistor. (See Fig. 2) The swamping resistor will keep the current constant if the solution resistance changes. All four platinum electrodes are cleaned, after a series of runs, in the oxidizing part of a Bunsen burner flame.

Before the membrane is mounted in the cell, the cell itself is checked to see that there are no leaks between the two cell compartments. This is done by placing a piece of "Tiger" tape across the center hole where the membrane would normally sit and attempting to run current across the cell using the same electrodes, 90 V battery and 100 K potentiometer that will be used in the measurements. In order to detect the current, a Weston d.c. ammeter model No. 901 was set on the 16ua scale. At all possible settings of the 100 K potentiometer (all possible currents), no current was detected flowing between the cell compartments. The cell and membrane, were repeatedly checked for leaks in the above manner.

Noise Measurements

Both noise measurements and voltage-time measurements were obtained in this work. Both types of measurements were dependent on having a flux of sufficient magnitude (equal to or greater than the critical current density) so that a depleted region of high field is formed in front of the membrane on the desalting (diluate) side.

All noise measurements were obtained at steady state conditions. The noise measuring system is shown in a circuit diagram (Fig. 2). The noise or voltage fluctuations across the membrane and external solution are seen by the "inner" or measuring platinum electrodes. The signal to be measured could be as small as 4μV. This makes it imperative that we prevent any interference from extraneous noise sources.

Shock Mounting

There are two extraneous noise sources which must be eliminated or at least controlled if we are to be able to measure the "real" noise. (This is particularly true if the "real" noise is of small magnitude.) These disturbing noise sources are 60 cycle (and/or harmonic frequences) pickup, and vibrations which shake the solution and/or the measuring electrodes. The pickup problem was controlled in three ways. Firstly, the electrodes, cell and 1st stage preamplifier were placed in a magnetically shielded box. Secondly, all ground loops in the measuring circuit were carefully eliminated. Thirdly, two high pass filters and a band pass filter were used to cut off any 60 cycle still remaining before the signal reaches the spectrum analyzer.

The vibration problem was controlled by shock mounting the magnetically shielded measuring box. This was a non-trivial problem; however, good results were obtained after some experimentation. The box was shock mounted in the following way:

1) Four standard shock mounts were placed on a flat table.
2) Six inches of firm packing material was placed on top of the shock mounts.
3) A very heavy box, (~1 foot on each side) was placed on the packing material.

4) On the very top is our magnetically shielded measuring box. It is separated from the box below by a thin layer of "air pocket" packing.

This method of shock mounting is believed to be successful because the heavy box acts like a large pendulum and converts high frequency vibrations to low frequency vibrations. These low frequency vibrations (below 40 Hz) are of no concern to us, since they can be easily cut-off and they are below our frequency measuring range. With the problems of oscillations and vibrations successfully controlled, it was found that we could record noise spectra where the total rms voltage was only 2 μV above the background noise level. Such spectra are quite interesting and informative.

Measuring Apparatus

The signal goes from the measuring electrodes through a high pass filter into a preamplifier. The filter consists of a 4μf capacitor and an 11 KΩ resistor (see Fig. 2). The capacitor sits between the positive electrode and the 11KΩ resistor. The 11KΩ resistor feeds back to the negative measuring electrode which is grounded to the magnetically shielded box. The signal across the 11KΩ resistor is read into the preamplifier minus most of its low frequency components (or d.c. signal). The preamplifier is Applied Cybernetics Model No. LA206V. It is a self-contained low-noise amplifier with a total noise level of 1.4μV. This amplifier satisfied all the major requirements needed in this investigation. It has a low noise level, a high input impedence, a wide range frequency response (up to 100 KHz) and a high gain (up to 40dB).

The preamplifier, cell and d.c. current generating system are kept in the magnetically shielded, shock mounted box. When the preamplifier output leaves the box, additional gain, if needed, is supplied by a Hewlett-Packard Model No. 466A amplifier with a maximum output of 1.5 volts rms. This second stage amplifier is labeled B on the circuit diagram. The output of this amplifier is sent to a Hewlett-Packard Model No. 3400 true root mean square voltmeter (labeled C in the circuit diagram). The total rms voltage is thus recorded during each run.

Figure 2

Noise Measurement - Circuit Diagram

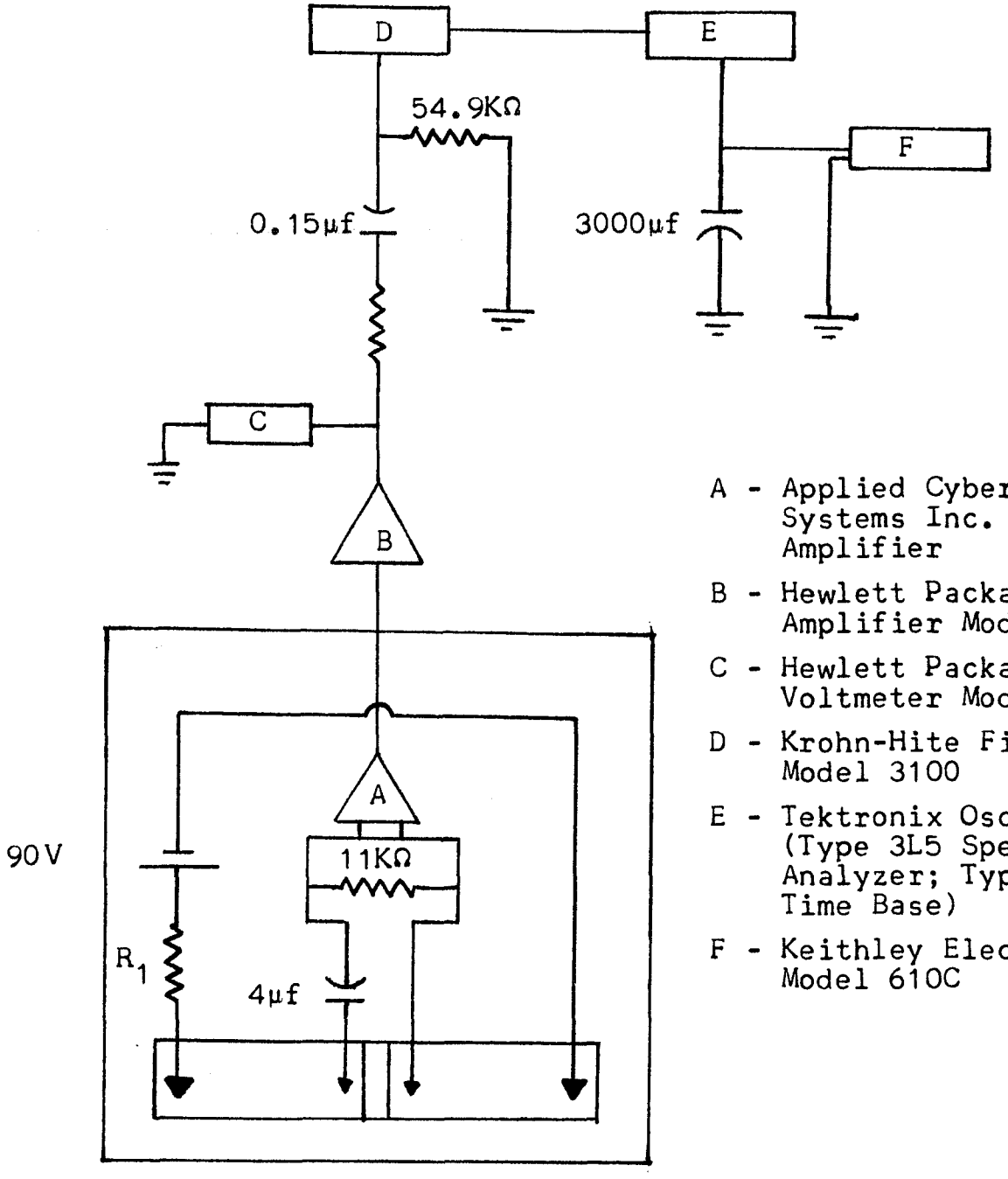

A - Applied Cybernetics Systems Inc. Pre-Amplifier

B - Hewlett Packard A.C. Amplifier Model 466A

C - Hewlett Packard RMS Voltmeter Model 3400A

D - Krohn-Hite Filter Model 3100

E - Tektronix Oscilloscope (Type 3L5 Spectrum Analyzer; Type 3B4 Time Base)

F - Keithley Electrometer Model 610C

It was found that the points on a given run were reproducible only if the rms voltage remains relatively constant. With the same piece of membrane, at the same concentrations and temperature, spectrum reproducibility is best attained if one matches total rms rather than current density.

The output of the 2nd stage amplifier is also sent through a 2000 Ω resistor into a second high pass filter. This filter is at the input of a Kronheit Model 3100A band pass filter (labeled D in our diagram) and it cuts off low frequency signals, still remaining, below 60 Hz.

The use of the bandpass filter as a variable high pass filter, enables us to selectively cut off frequencies below those being measured and to prevent overloading of the spectrum analyzer. The dynamic range of the 3L5 Tektronix spectrum analyzer (labeled E) is 30 dB. It is a vertical plug in unit oscilloscope, type 564, used with a Tektronix Type 3A72 dual trace amplifier as horizontal plug in. The frequency range, resolution and center frequency of the spectrum analyzer are all set manually. The resolution was set at 20 Hz/Div for all measurements. Setting each frequency manually offers an advantage in that it allows us to have as much time averaging as we desire.

The amplitude of the fluctuations at each point is proportional to the d.c. output of the scope. This output is read on a 610C Keithly electrometer (labeled F). A 3000 μf capacitor across the oscilloscope output provides additional averaging of

the fluctuations making it easier to average the electrometer reading by eye. A single spectrum could take between seven and fifteen minutes to obtain and could have anywhere from five to twenty points.

The response of the system was checked periodically using a General Radio 1390 B white-noise generator as a standard noise source. When white noise from this generator was fed into the noise measuring system through the measuring electrodes, the voltage output on the electrometer was constant at all frequencies. This is what we would expect for white noise, and implied that the system did not itself filter the signal. By using high pass filters, the frequency response of the electronics could be checked. This was done and the results shown in Fig. 3. This proved to be an excellent test of both the dynamic range and response of our measuring system. The above response tests were performed numerous times, with the measuring electrodes in and out of solution, with and without a membrane in the cell and with current on and off. The results were always in agreement with theoretical expectations.

Several checks were made to eliminate the electrodes as a noise source. For example, it was found that it made little difference what type or concentration of solution was used. If no membrane was placed in the cell, over the entire current range used in this work, there was no measurable noise above background. As a further check of the independence of our

measured spectra from any intrinsic property of our platinum electrodes, copper sulfate power spectrum were taken with both Pt and copper electrodes. The resulting spectra were found to be identical within experimental error, no matter what combination of copper and platinum electrodes were used. If the electrode noise was to be a factor, this would not be the case.

Voltage-Time Measurements

The voltage-time measurements were recorded with MC-3142 ion-exchange membranes. Two types of voltage-time measurements were obtained. The first type simultaneously records the total d.c. voltage (chronopotentiometry), this voltage minus all IR terms (hereafter to be called the Back Emf), and the current change across the membrane and external solution from time equals zero (time when current was turned on) to time equals steady state. The Back Emf was measured by repeatedly shutting the current off for 5ms out of 505ms of current time. The current was off ~1% of the total current time. The following section provides detailed information on how these measurements were obtained.

The circuit diagram for both types of voltage-time measurements is shown in Figure 4. The measuring system for both the first and second type voltage-time measurements is the same except that the current was not monitored in the latter case. When switch 1 (Fig. 4) is closed, there is a path between the positive measuring electrode and the negative or grounded measuring electrode. When switch 1 is open the only path between the two measuring electrodes is through the $10^{14}\Omega$ resistor of B. The second type of voltage-time curve shows how the system, after having attained steady state, goes from one steady state condition (switch 1 - Fig. 4 closed) to another steady state (switch 1 - Fig. 4 open).

The reverse process was also measured i.e., going from the steady state with the switch closed to the steady state with the switch open.

Figure 3

The Power Spectrum of White Noise That has been Passed Through a Filter

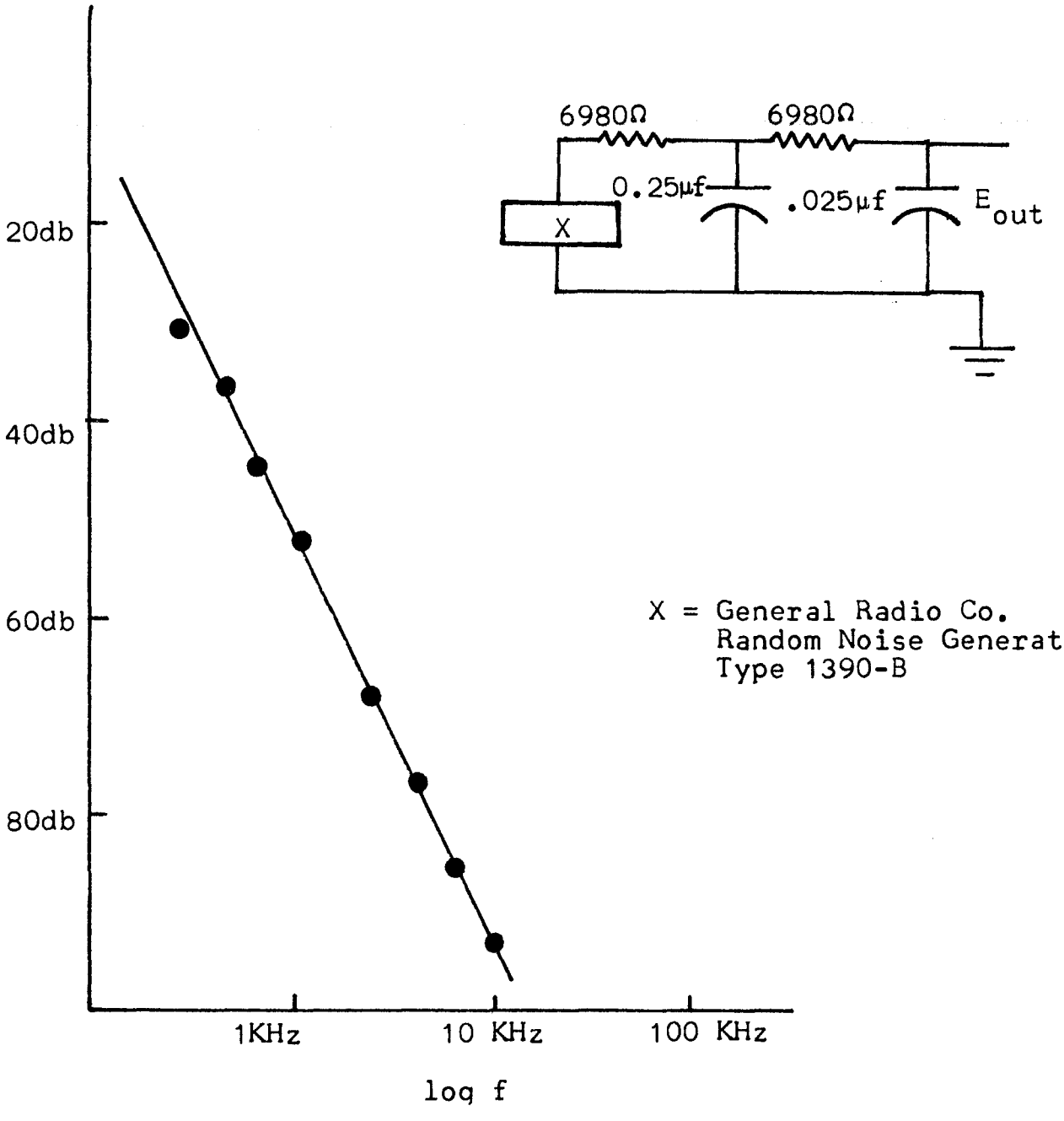

Figure 4

Voltage-Time Measurements - Circuit Diagram

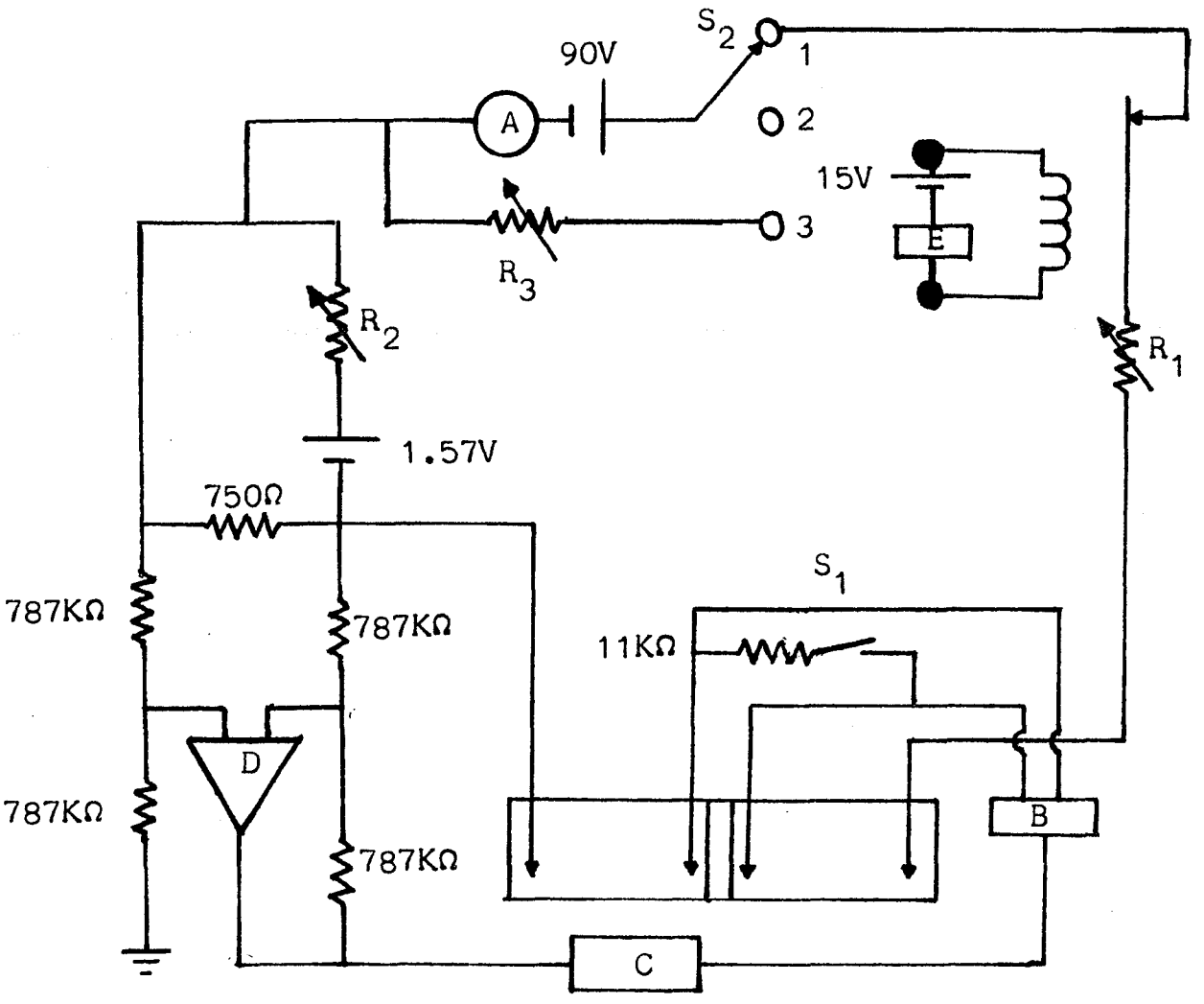

A - Weston D.C. milliammeter 901
B - Leithley Electrometer 610C
C - Tektronix Type 564 Storage Scope
D - Zeltex 1 Amplifier
E - General Radio Pulse Generator 1340

Voltage-Time Curves (From the time the current is first applied until steady state is reached)

Voltage-time measurements from time equals zero to time equals steady state were taken with both the switch open and with the switch closed. (Switch 1 - Fig. 4).

The total d.c. voltage is read into the electrometer, B. The output of B is read on one channel of a dual trace amplifier in scope C. The current change is monitored on the second channel by reading the output of a floating operational amplifier (Zeltex model Zel 1) of unity gain whose input is the voltage drop across a 750 Ω resistor in series with the cell. The 1.57V battery and the variable resistor R_2 are adjusted before each run to buck out the voltage across the 750 Ω resistor at the steady state current. The Back Emf is read by placing a relay in series with the cell. The relay, operated by a pulse generator, repeatedly shuts the current off for 5ms and keeps it on for 500 ms. The voltage recorded during this 5ms interval is the Back Emf, and it is read on channel 1 of oscilloscope C. It was found that having the current off for 5ms out of 505ms had no effect on the total d.c. voltage or current.

An additional current loop, completely independent of the cell and membrane, consists of the 90V battery and the variable resistance R_3. Before a run is to be taken, switch 2 is set in position 3 and this loop is completed. Then R_3 is adjusted so that the current in this loop will be equal to the steady state current of the run to be taken. Then switch 2 is

flipped to time = 0 position[1] and the run begins. The purpose of this additional loop is to put a load on the battery similar to the load it will feel when the actual run starts. R_1 serves the same purpose as it did in the fluctuation studies; it serves as a swamping resistor.

All runs were taken under identical conditions with the 11 K resistor in the circuit, and with the 11 K resistor out. The total voltage and Back Emf were also measured under identical run conditions but without the membrane in the cell. They were both found to be constant after the first time division of the oscilloscope graticule. The electrode values were found to be dependent on concentration and temperature. Thus runs were taken at all concentrations and temperatures, with the membrane omitted as well.

Response Check

The response of the system was checked by replacing the cell, solution and membrane with a reasonable facsimile, as shown in Fig. 5. With current running, both the total voltage and Back Emf were simultaneously read across the 2.8 K resistor and 1.4V battery. Depending on the polarity of the battery, the Back Emf either added or subtracted 1.4 volts from the total voltage. With no current, the Back Emf read the voltage across the battery. The correct voltages were obtained for both the total voltage and Back Emf using both the a and b circuits shown in Figure 5.

Volts/Div scales of both channels of the Dual Trace Amplifier were calibrated with a d.c. signal from a Precision potentiometer

flipped to time = 0 position[1] and the run begins. The purpose of this additional loop is to put a load on the battery similar to the load it will feel when the actual run starts. R_1 serves the same purpose as it did in the fluctuation studies; it serves as a swamping resistor.

All runs were taken under identical conditions with the 11 K resistor in the circuit, and with the 11 K resistor out. The total voltage and Back Emf were also measured under identical run conditions but without the membrane in the cell. They were both found to be constant after the first time division of the oscilloscope graticule. The electrode values were found to be dependent on concentration and temperature. Thus runs were taken at all concentrations and temperatures, with the membrane omitted as well.

Response Check

The response of the system was checked by replacing the cell, solution and membrane with a reasonable facsimile, as shown in Fig. 5. With current running, both the total voltage and Back Emf were simultaneously read across the 2.8 K resistor and 1.4V battery. Depending on the polarity of the battery, the Back Emf eit[redacted]ubtracted 1.4 volts from the total voltage[redacted]he Back Emf read the voltage across the [redacted]ltages were obtained for both the t[redacted]using both the a and b circuits sh[redacted]

Volt[redacted]ls of the Dual Trace Amplifier w[redacted]ignal from a Precision potentiomete[redacted]

Figure 5

Voltage-Time Response Check

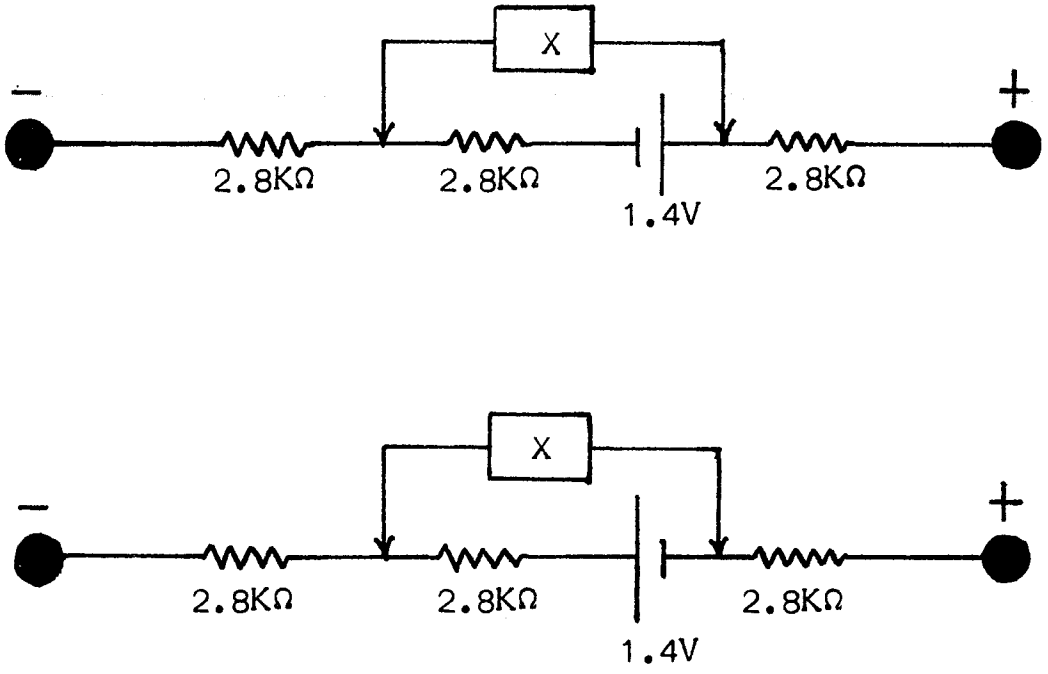

X - 610C Keithley Electrometer

Preparations of H_3PO_4 and Na_2HPO_4 Solutions

The water used in the preparation of all solutions was distilled from a Stokes still. Surfactant materials, that remained in the water after distillation, were then removed by a foaming process. The foam is created by placing the distilled water in a 600 ml medium porosity sintered glass funnel and sending N_2 gas through the filter and water. The foam formed, sits on the water surface and is removed several times by sweeping that surface.[39] The extra care taken to remove organic surfactant materials, as well as the scrupulous cleaning of the cell itself, was done to insure that the exchange sites on the membrane surface remain uncontaminated.

The NaOH pellets used were obtained from Amend Drug and Chemical Co., and the H_3PO_4 was obtained from J.T. Baker Chemical Co. (both were reagent grade). The Potassium hydrogen Phtalate, used in the calibration of solutions, was also obtained from J.T. Baker Chemical Co. (Primary Standard). All reagents were used without further purification. However, the KHPt was dried in a warm oven for two hours before it was used.

The procedure used in preparing the solutions is the following:

1) A concentrated NaOH solution was prepared by adding ~900g of NaOH to ~1000ml of boiled water. (The water was boiled to rid it of CO_2.)

2) The above solution was standardized with KHPt.

3) A titration curve was obtained by adding NaOH to H_3PO_4 acid and recording pH.

4) The concentrated H_3PO_4 solution was diluted to ~a 2.0M solution and standardized. This was done by adding standardized base to the acid and recording the pH, until one-third of the available H^+ ions were neutrualized. The end point was determined from the titration curve of step 3. The H_3PO_4 stock was found to be 2.192 M.

5) A stock solution of Na_2HPO_4 was prepared by adding standardized NaOH solution to standardized H_3PO_4 and recording the pH of the acid. Base was added until two-thirds of the acid's available H^+ ion was neutralized. The pH at the end point was determined from the titration curve in step 3. By knowing the amount of base added, the concentration of Na^+ ion in the Na_2HPO_4 was found to be 1.97 Molar.

6) All solutions used in our measurements were made from the above stock solution

Solutions .008M, .010M, .016M and .021M in H^+ion were prepared from the 2.192M H_3PO_4 stock solution. The pH of these solutions was determined with a Corning Model 5 pH Meter. The following table lists the concentrations of the H_3PO_4 solutions used, their respective pH's and H^+ ion concentrations calculated from pH, and H^+ ion concentration reported in the litera-

ture at these concentrations.

Table I

Check on Phosphoric Acid Concentrations

Conc. H_3PO_4 (molar)	pH	H^+ conc.	H^+ conc. from molarity
.008	2.08	.00834	.008*
.010	1.99	.0104	.00989
.016	1.80	.0159	.01588
.021	1.69	.0204	.02084

*extrapolated value

We shall assume that the only negative ion present in any non-negligible amount in these solutions is $H_2PO_4^-$. Thus we shall equate the concentration of this ion to that of H^+ ion. We shall present evidence to that fact that the concentrations of both $HPO_4^=$ and $H_5P_2O_8^-$ ions which are known to be present in H_3PO_4 solutions are present only in negligible amounts.

Nims reported the second ionization constant of phosphoric acid as 6.226×10^{-8}, which means that the ratio of $a_{H_2PO_4^-}/a_{HPO_4^=}$ is of the order of 10^6.[40] Thus we can neglect the concentration of $HPO_4^=$ ion in the above solutions. It has been shown that the first dissociation constant of phosphoric acid is a function of the concentration. This phenomenon is attributed to the presence in the acid of a species more acid than the monomer H_3PO_4. This species is assumed to be the dimer $H_6P_2O_8$ which ionizes to yield $H_5P_2O_8^-$.[41]

The concentration of $H_5P_2O_8^-$ decreases with molality and at 0.1m H_3PO_4 it is approximately 10% of the concentration of $H_2PO_4^-$. Therefore, it is reasonable to assume that it is negligible in all solutions used in this work.

Solutions .010, .020, .040 and .060 M in Na^+ ion were prepared from the 1.97M Na_2HPO_4 stock solution. The pH's are 7.19, 7.20, 7.12 and 7.02 respectively. The co-ion in these solutions is $HPO_4^=$.

RESULTS

Noise Measurements

The results of the fluctuation studies will be presented first. Voltage-time measurements will be presented later. Families* of power spectra were obtained at 10°C, 19°C and 36-45°C for .008M H^+, .01M H^+, .016M H^+ and .021M H^+ solutions of phosphoric acid. Families of curves were also obtained for solutions of Disodium hydrogen phosphate. The temperature at which these spectra were obtained are - 10°C, 19°C, 28°C and 40°C and the Na^+ concentrations were .01M, .02M, .04M and .06M.

The data were plotted as log V^2 vs log frequency. The measured total rms voltage represents a band of frequencies 40 Hz to 100 KHz and the fluctuations were studied in this frequency range. Two typical noise power spectra families can be seen in Fig. 6, 7 and 8. The total measured noise (total rms volts, integrated over the complete frequency range) increased with increasing flux in each family as did the voltage measured at any given frequency. Spectra were obtained over a total rms range of 4.0×10^{-3}mv to 17.0mv. When the flux was at or near the critical current density (C.C.D.), the total noise was only slightly above 4.0×10^{-3}mv. With dilute solutions, at fluxes

---

*The term family refers to the set of curves obtained by varying the flux at a given temperature and concentration.

Figure 6

Power Spectra of H_3PO_4 (.016M in H^+ ion) at 283°K

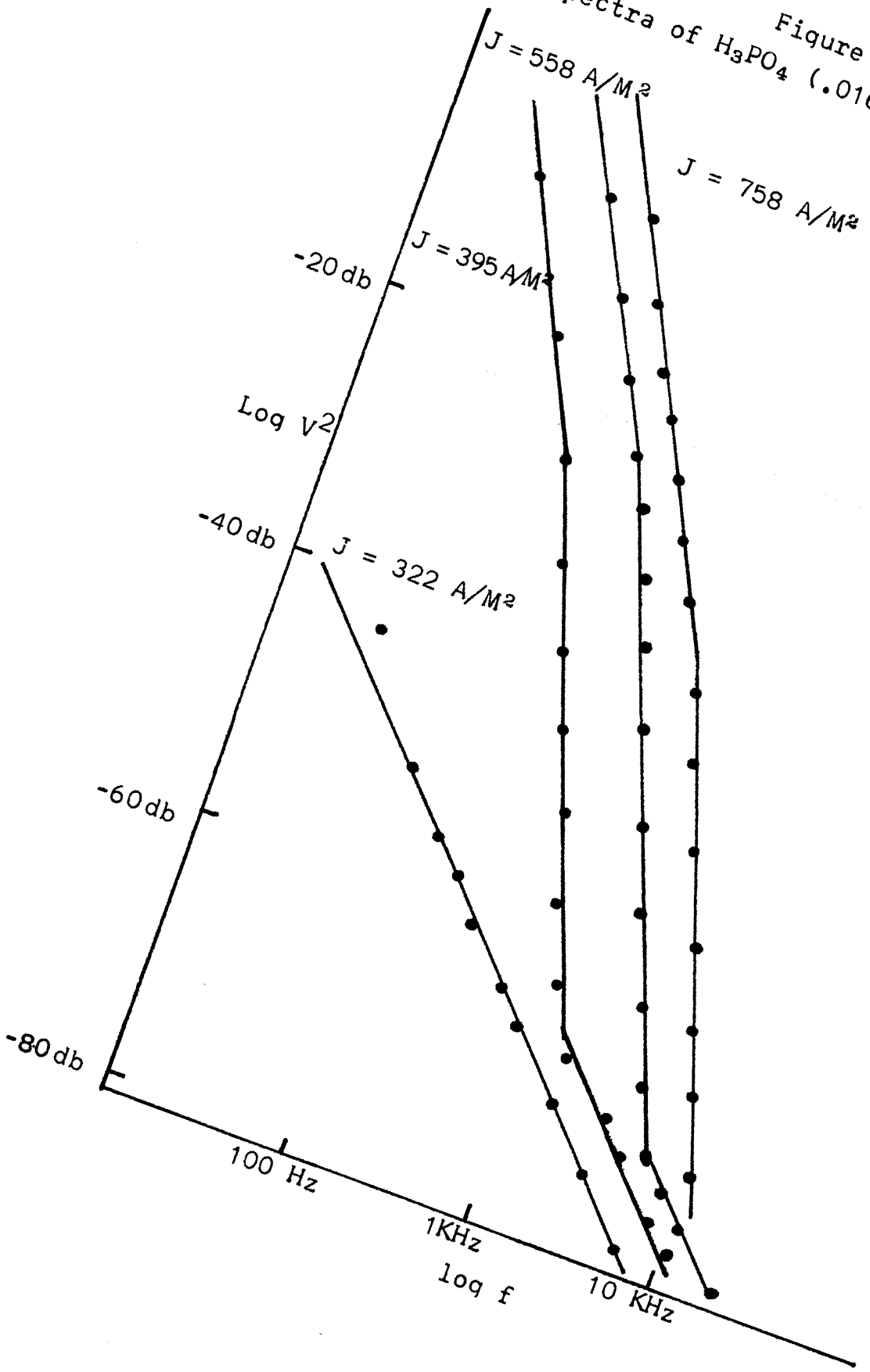

Figure 7

Power Spectra of Na_2HPO_4 (.060M in Na^+ ion) at 313°K

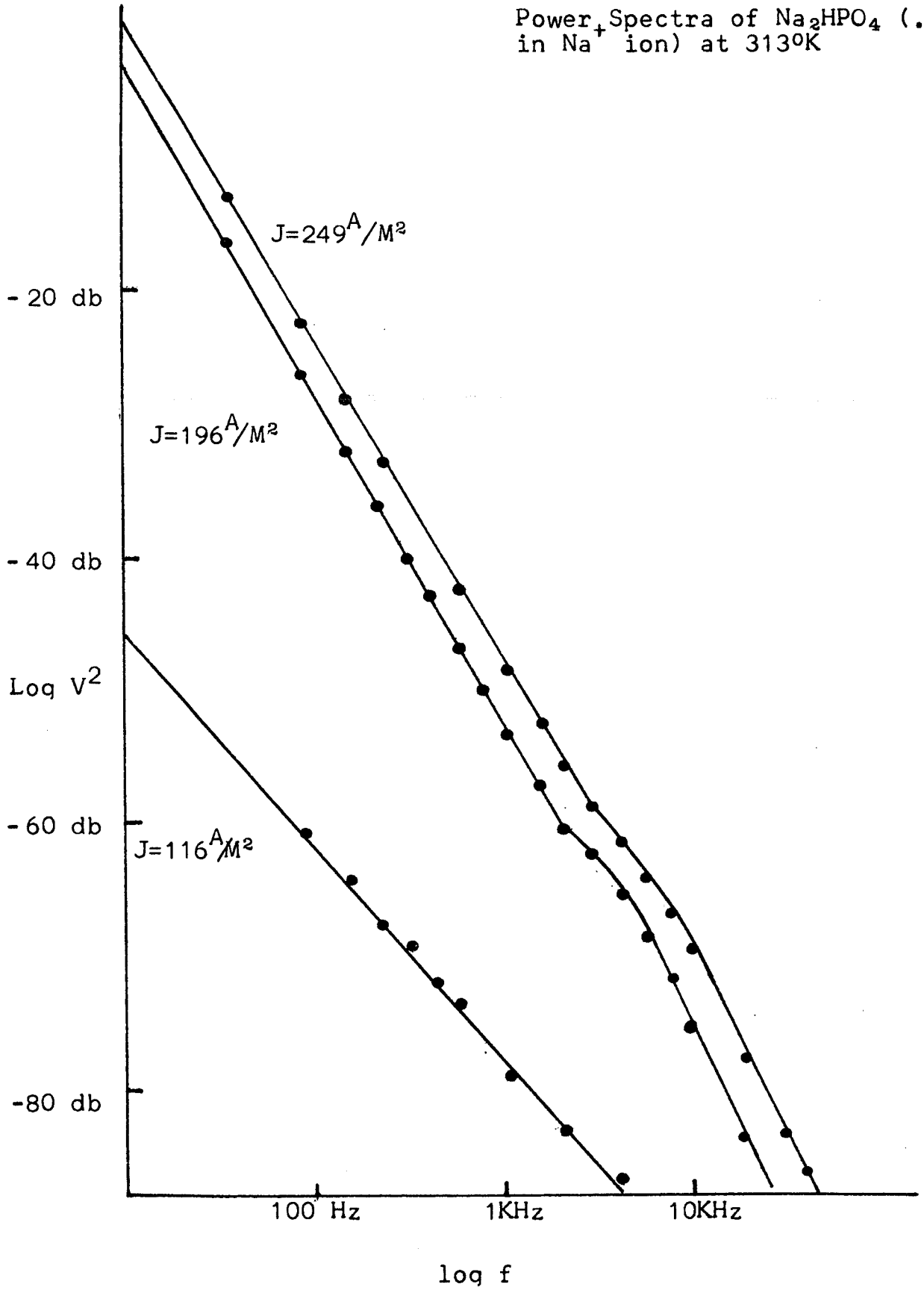

Figure 8

Power Spectra of Na_2HPO_4 (.020M in Na^+ ion) at 283°K

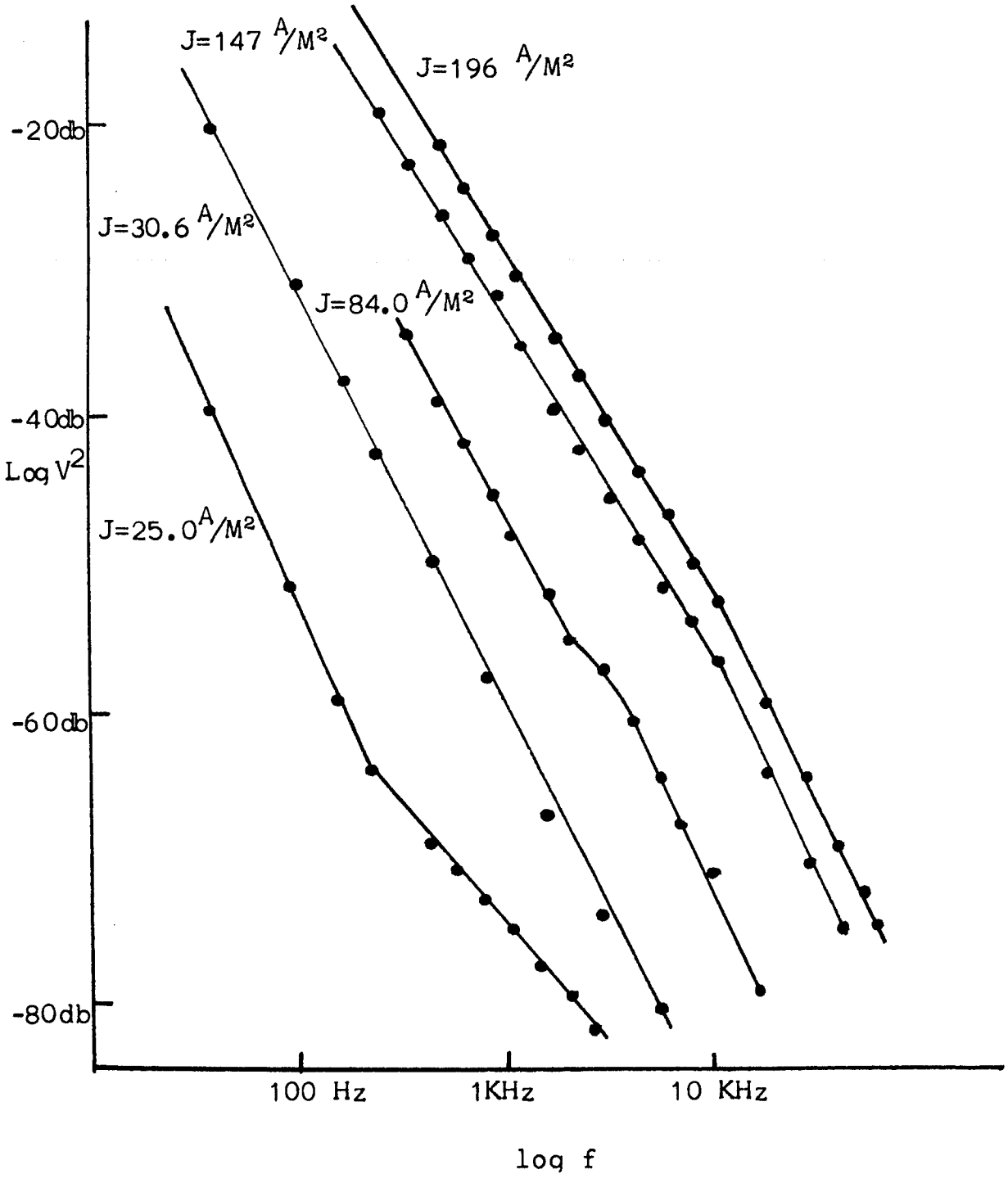

well above the C.C.D., the total noise approached 17.0mv. At this point it should be noted that in the absence of a membrane, even in dilute solutions and at quite high current densities, there is no measureable noise above background. Background noise is $3.0 \pm 0.3 \times 10^{-3}$mv.

If we ignore concentration, temperature and flux differences, a qualitative analysis reveals that the spectra will form distinct groups whose members have a similar shape and total noise. Table 2 (page 182) lists the concentration, temperature, flux and total noise for a number of spectra of both Na^+ and H^+ ion. The shape of each spectrum can be obtained by matching the total noise in Table with the figures in Fig. 9. We can modify Fig. 9 by combining the two lowest noise groups into one group in both the H^+ ion and Na^+ ion case. Aside from the different frequency dependence of "b" and "x", the only noteable difference in these newly formed composite groups is that in the Na^+ ion case we have more of the higher rms type and in the H^+ ion case we have more pure C spectra.

Tables 3a and 3b show the magnitude of the slopes as a function of concentration (C), temperature (T), and flux (J). At a given C and T, the magnitude of slopes "a", "b", "c", "x" or "y" shows no dependence on J. Thus variations in slope at a given C and T are due to experimental error. The slopes at each C and T were averaged over the flux. The results are shown in Tables 4 and 5. A parenthesis around a slope indicates that the number of runs used in the averaging process was small. The sigma

Figure 9

Representative Power Spectra of H^+ Ion and Na^+ Ion as a Function of Total Noise

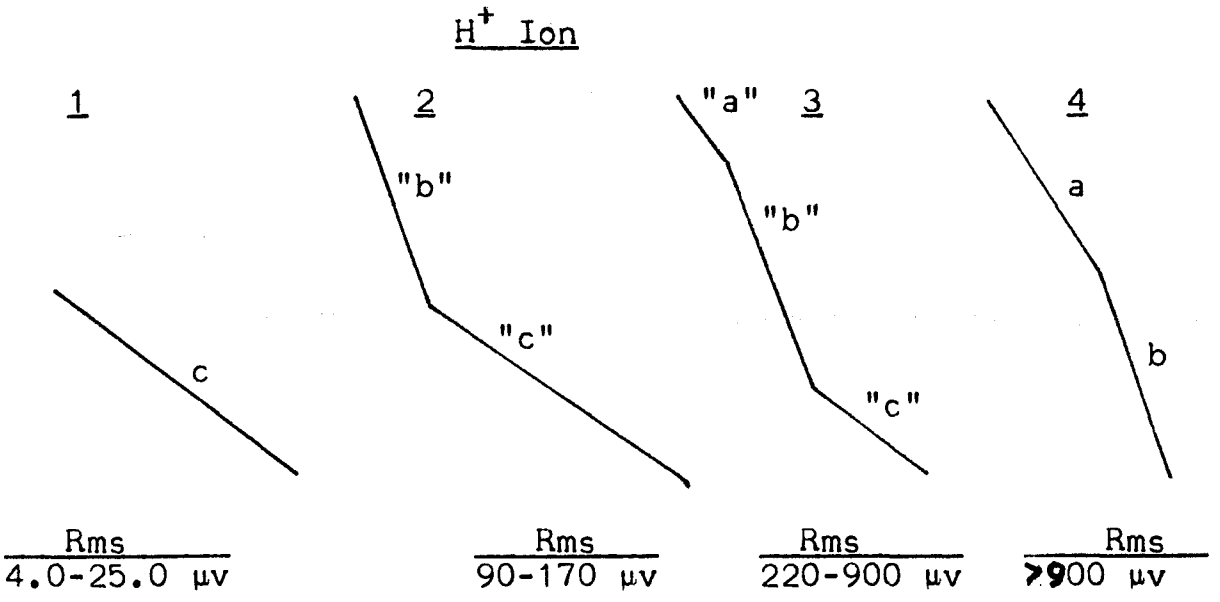

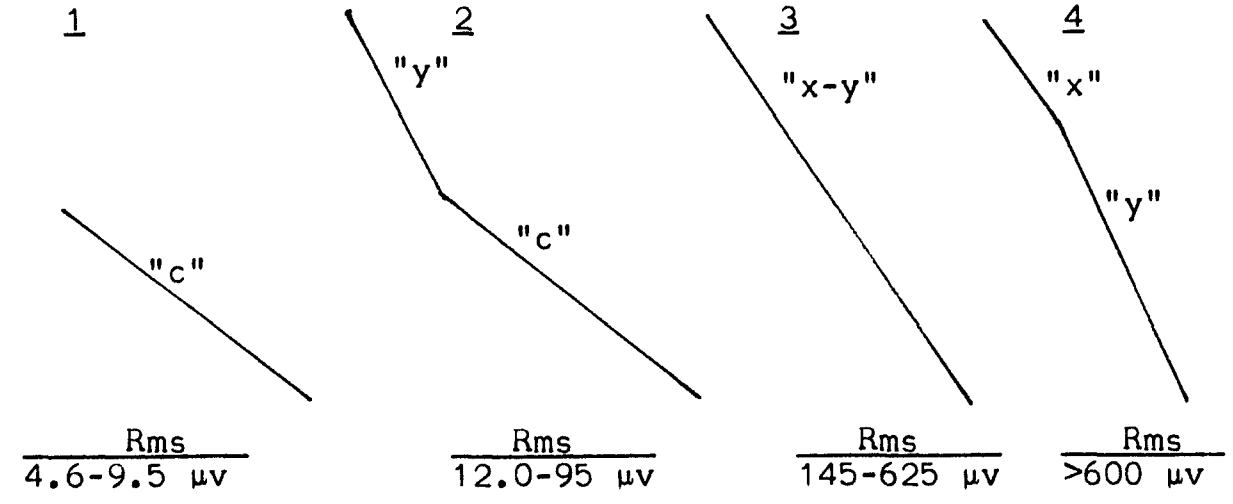

(only four examples found)

where "a" "b" "c" "x" "y" "x-y" represent the slopes

in Tables 4 and 5 is the standard deviation of these "average slopes" (averaged over flux at a given T and C) from a "new average" (the average over T of the "average slope" at a given C). This "new average" is the slope as a function of C only. For example, in .016 H^+ solution, the average "C" slope is 1.45. This means that there is an $f^{-1.45}$ frequency dependence in the "C" part of the power spectra. In the same .016 H^+ solution, $\sigma_C = .032$. This is the standard deviation. It represents the deviations of three "C" values of .016H^+, one at 10°C, one at 18°C and one at 40°C, from the average "C" value that is averaged over T. (1.45)

There are some obvious qualitative trends in slope that can be seen in Tables 4 and 5. They are listed below:

1) "b" and "y" get steeper with decreasing C of H^+ and Na^+ ion, respectively. (See Fig. 10 and 11)
b) "b" and "y" are independent of T at a given C of H^+ and Na^+, respectively.
3) "a" is independent of C in H^+ ion case.
4) "x" is independent of C for .02 Na^+, .04 Na^+ and .06 Na^+ ion solutions.
5) At a given C, "a" slope (dependence) gets shallower with increasing T (See Fig. 12).

Table 6 shows that slope "a" decreases with increasing T not only at constant C (No. 5 above) but also at constant total noise (or total flux).

Figure 10

Slope "b" of the H_3PO_4 Power Spectra as a Function of the Concentration of H^+ ion

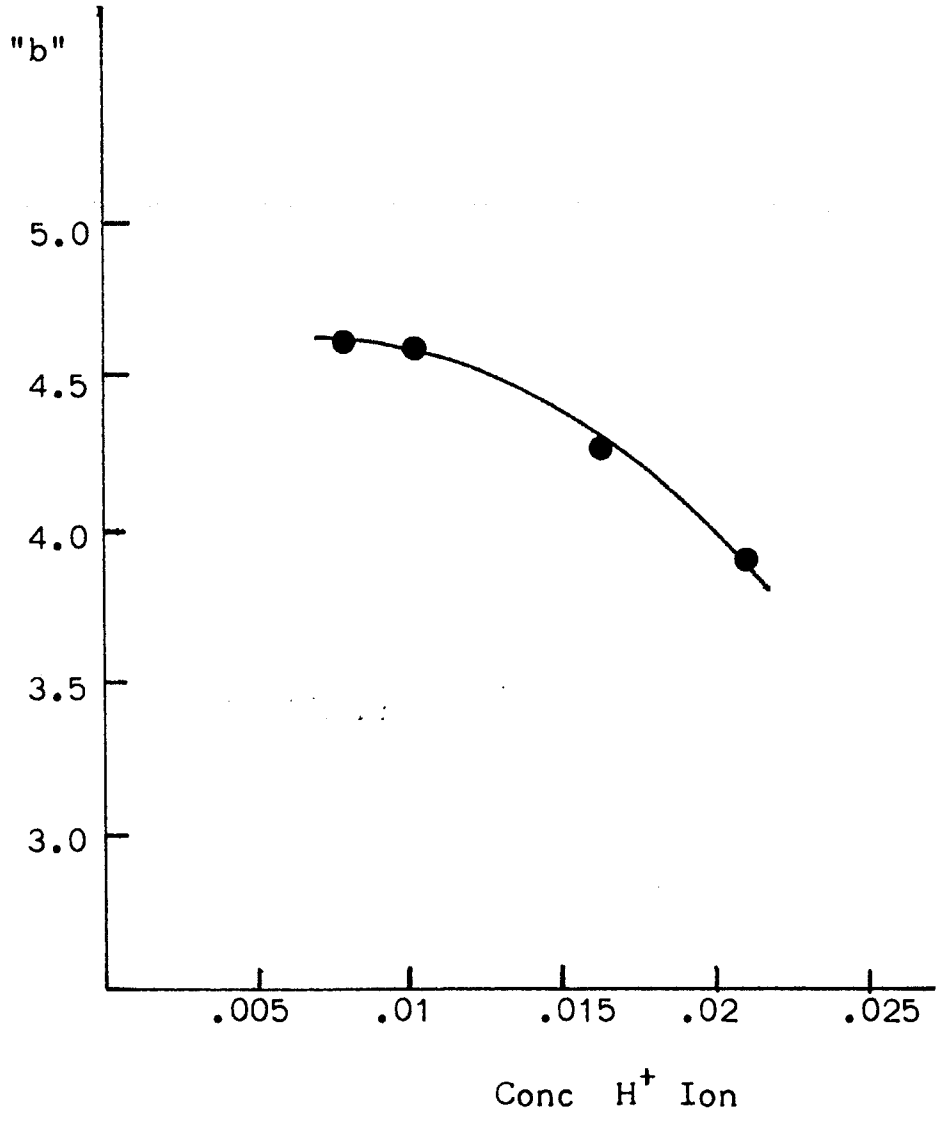

Figure 11

Slope "y" of the Na_2HPO_4 Power Spectrum as a Function of Concentration

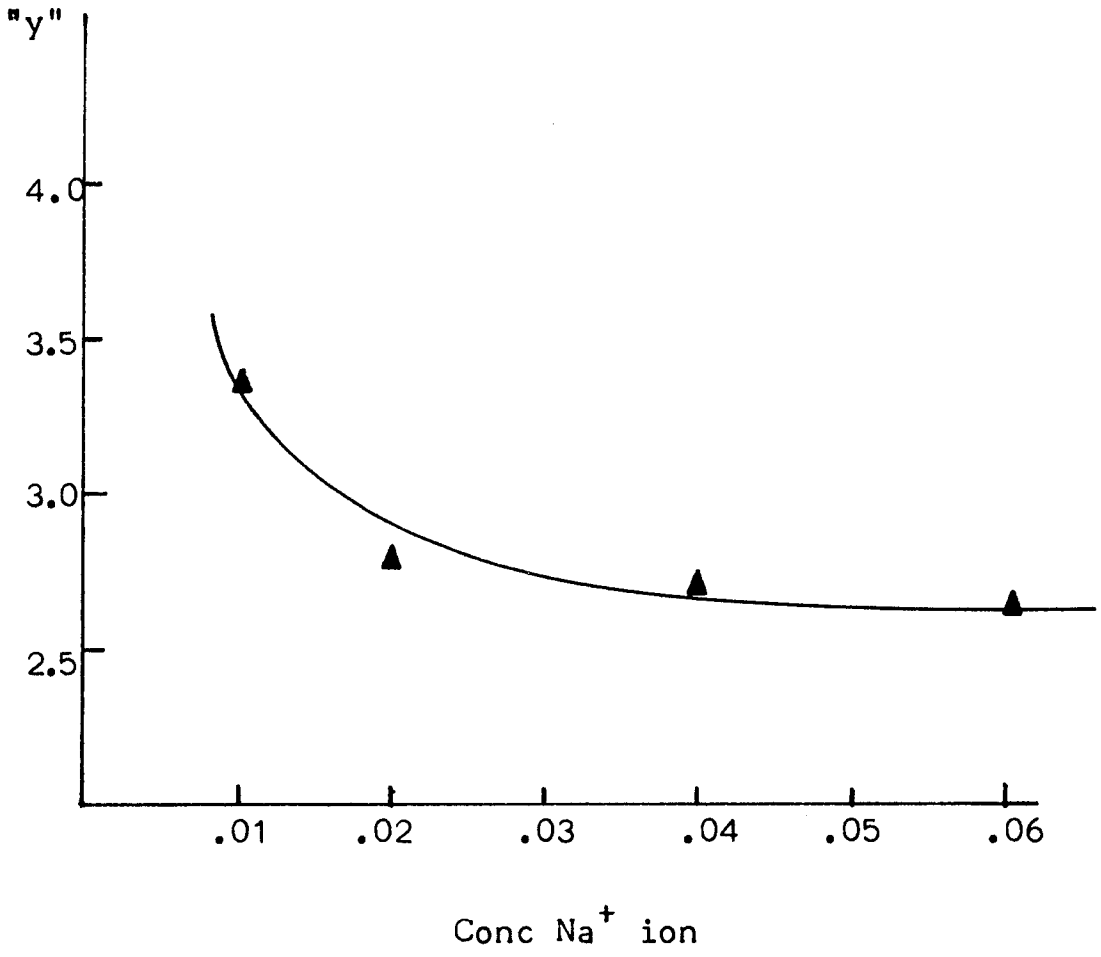

Figure 12

Slope "a" of the H_3PO_4 Power Spectra as a Function of Temperature

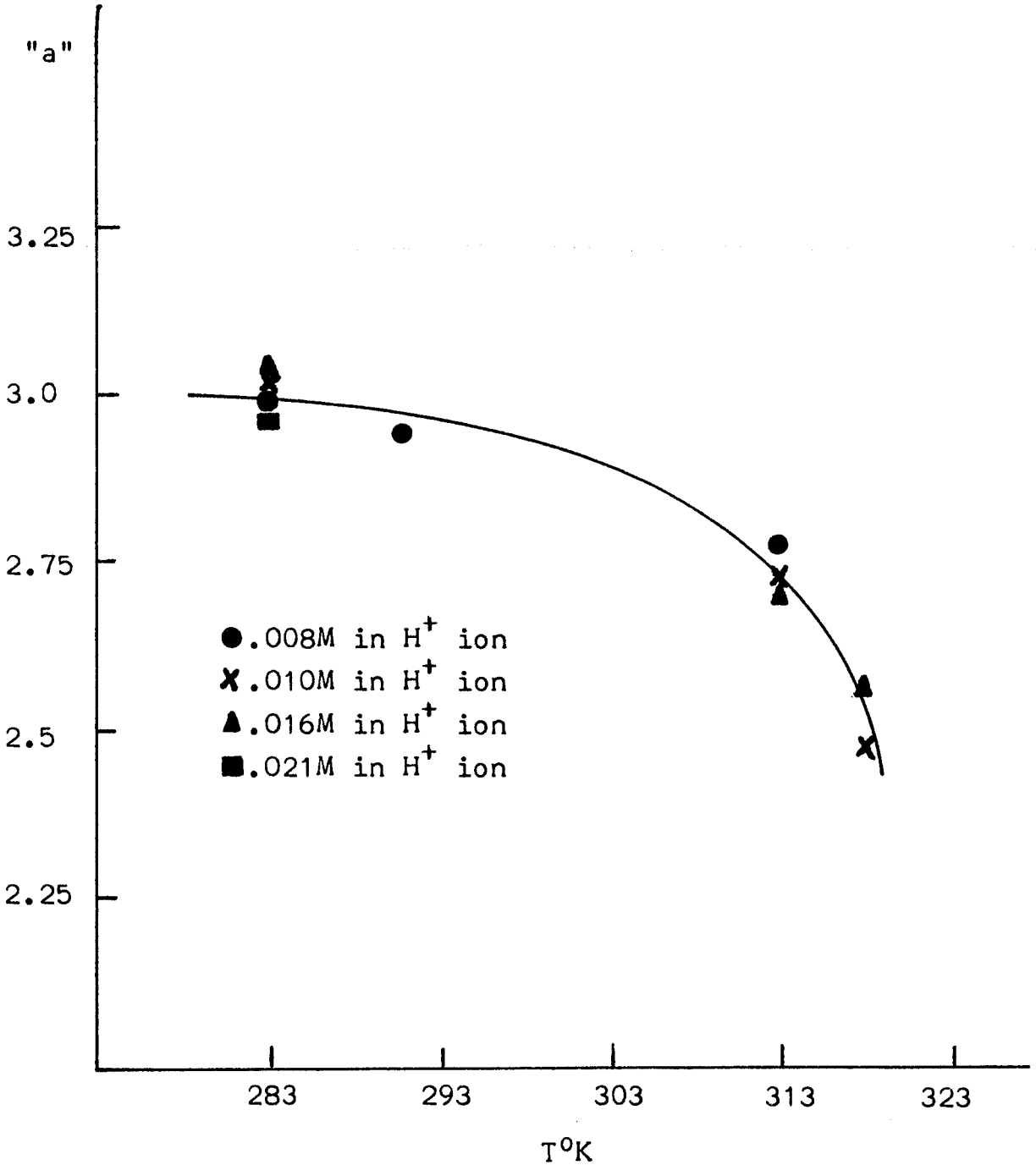

The H^+ ion spectra at high flux are characterized by a sharp shift from an f^{-a} dependence to an f^{-b} dependence. The frequency at which this sharp break occurs will be called the "break frequency", f_B. In the Na^+ ion case, the spectra shifts from an f^{-x} dependence to an f^{-y} dependence. Since f^{-y} is a good deal shallower than f^{-b}, whereas f^{-x} is only slightly shallower than f^{-a}, f_B is not always clearly defined in the Na^+ ion power spectra. The Na^+ ion spectra are, in fact, more often characterized by a "bump" rather than a break. This is particularly true at .02M Na^+, .04M Na^+ and .06M Na^+ concentrations (see Fig. 7 and 8). The .01M Na^+ power spectra are somewhat different from those found for the other concentrations of Na^+ ion. In this case $x \approx a$ and $y \rightarrow b$. Therefore, f_B is clearly discernable in this case. .01M Na^+ spectra are also very much "H^+ion-like" in character, in that the break frequencies are shifted down toward the region where break frequencies are found for H^+ ion spectra. Na^+ ion "bumps" are generally found approximately one full decade of frequency above H^+ ion breaks.

Table 7, lists break frequencies found in these noise measurements.

Yafuso and Green[11] found that a linear relationship existed between the break frequency and the flux. This relationship has been verified in this work (See Fig. 13, 14 and 15). They presented a linear equation to describe this dependence.

Figure 13

Plot of Break Frequency vs Flux for

Phosphoric Acid

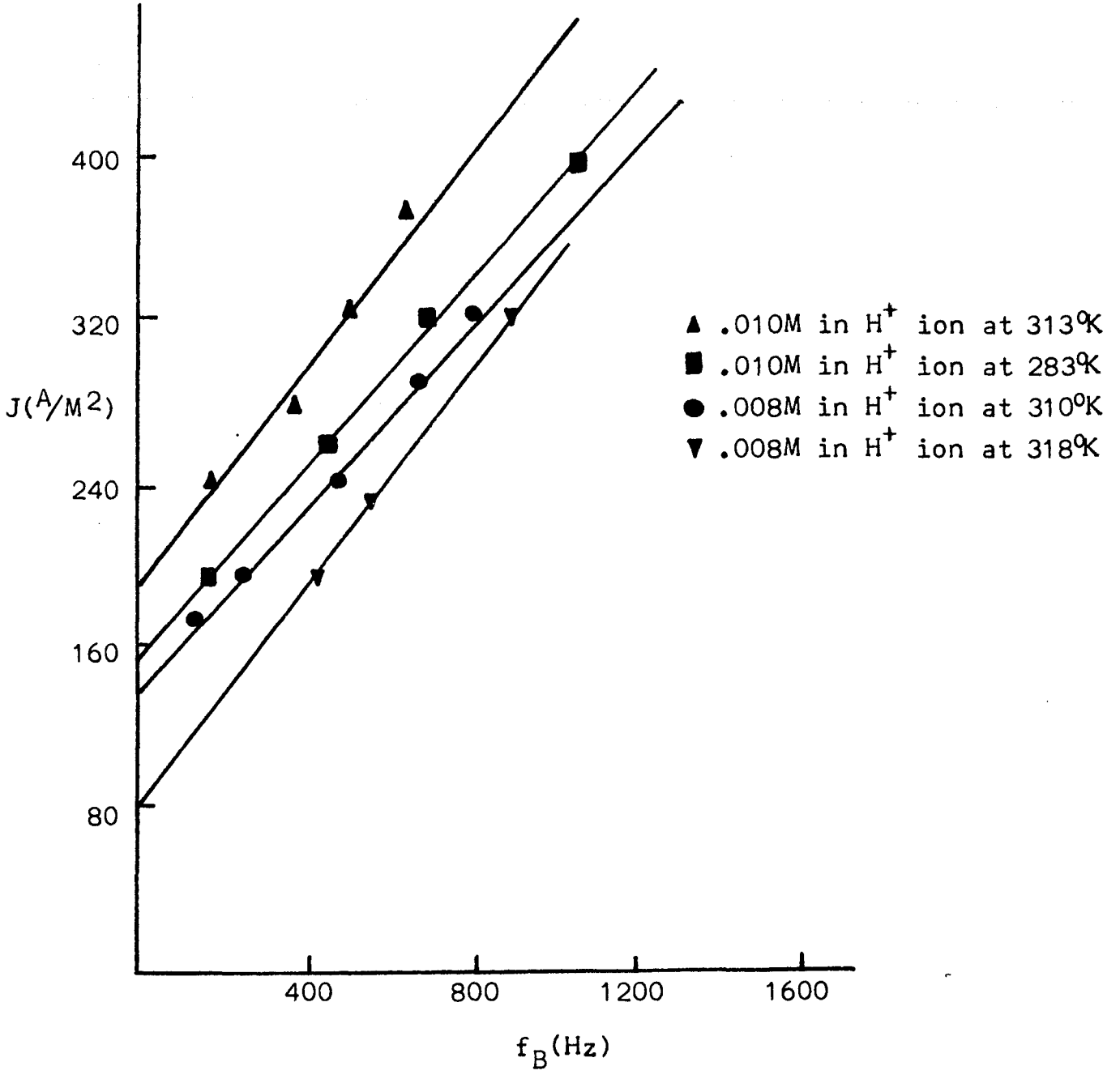

Figure 14 Plot of Break Frequency vs. Flux for Phosphoric Acid

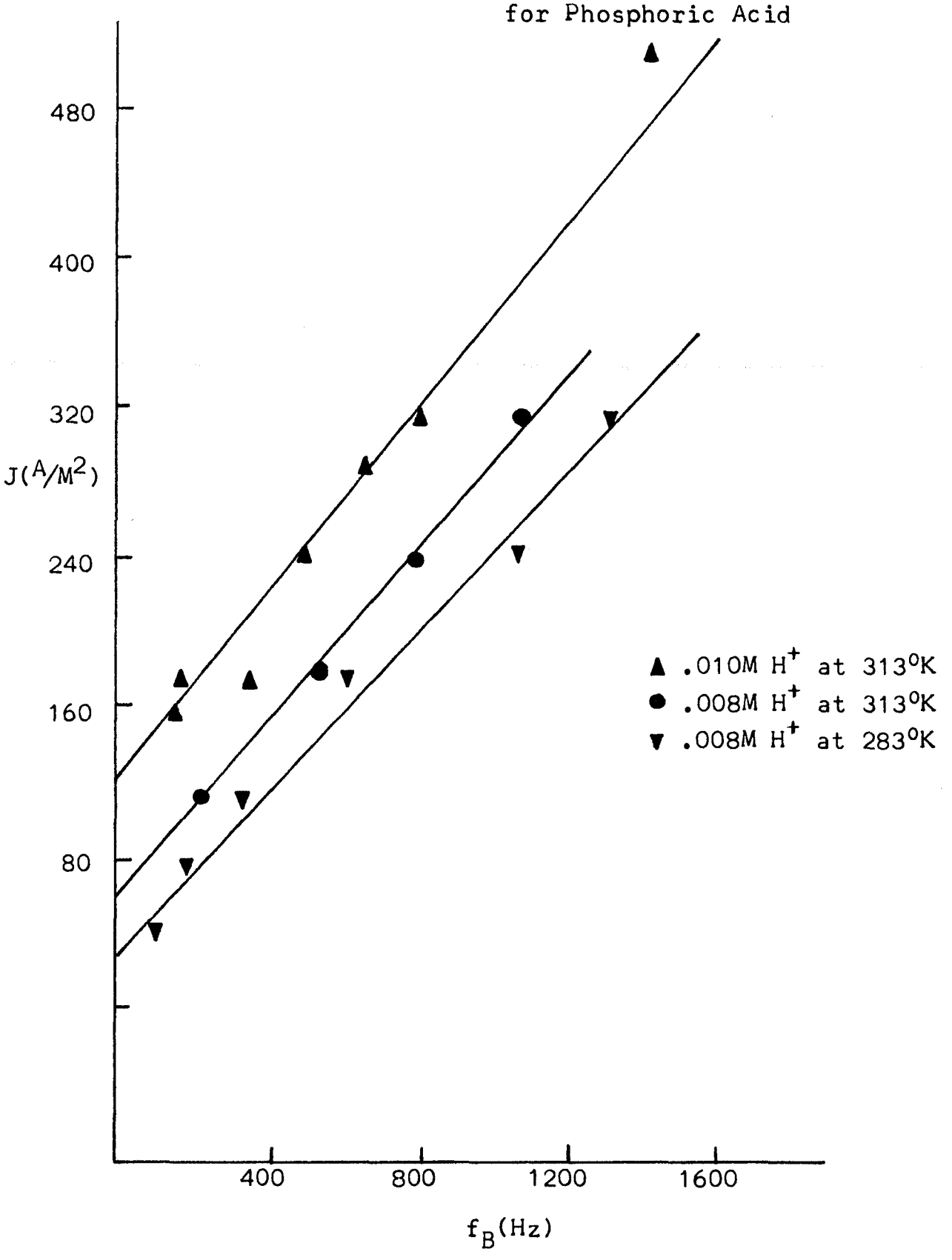

Figure 15

A Plot of Break Frequency vs Flux for

Na_2HPO_4 (.010M in Na^+ ion)

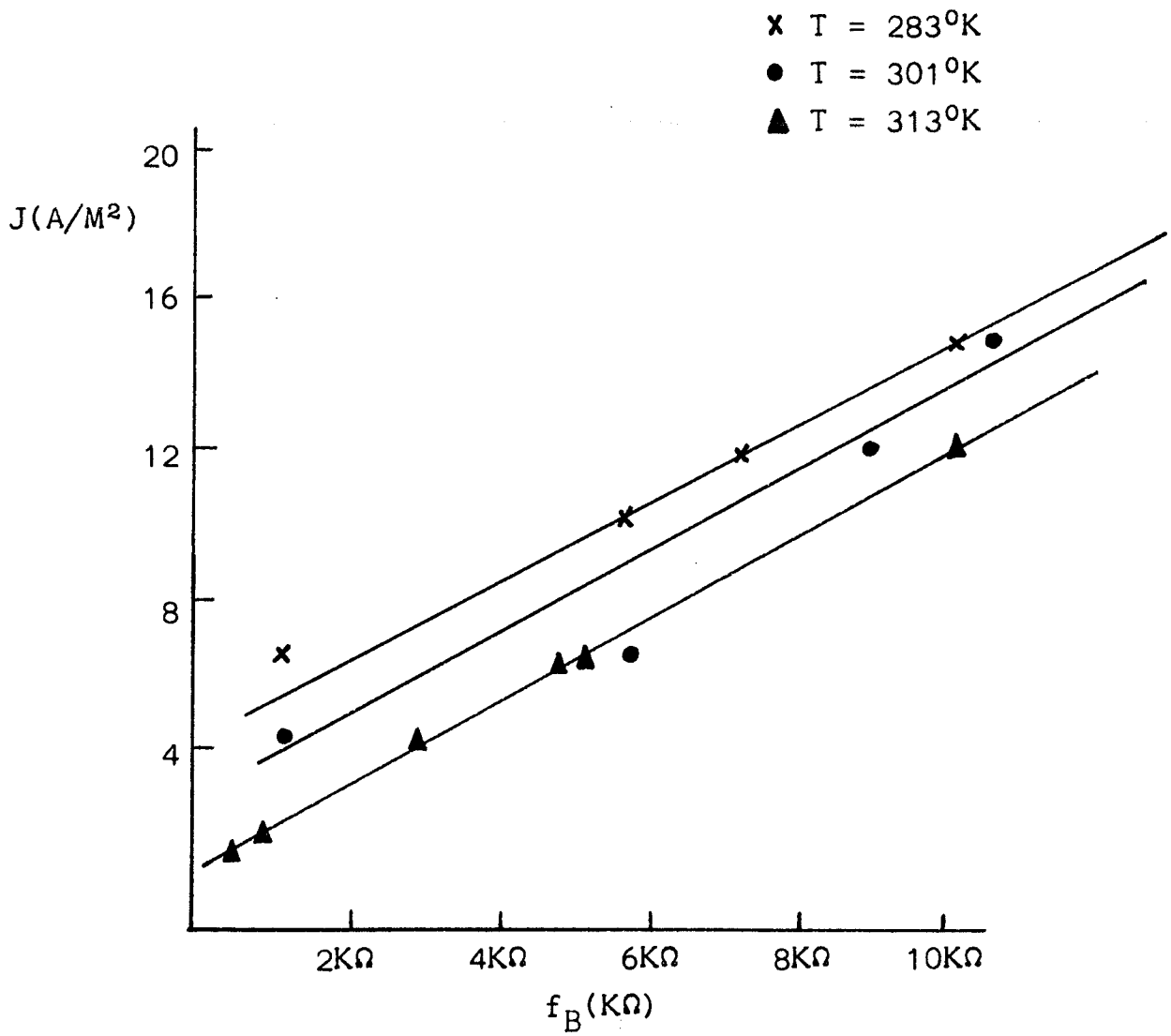

$$J = Kf_b + \beta$$

where

K = slope

β = intercept

J = flux

f_b = break frequency

Plots of total noise vs f_b were plotted for H^+ ion at 285°K and 313°K (Fig. 16 and 17 respectively). Table 7, and Figures 16 and 17 show that for H^+ ion, the break frequency is independent of C, dependent on T, and directly proportional to total noise. In the Na^+ ion case, no such independence of C is found (See Table 7). Except for differences in "a" and "b", two phosphoric acid spectrum will be almost identical, if the temperature at which they were obtained is identical and the total noise generated in transport is the same.

Figure 16

Total Noise vs Break Frequency for

Phosphoric Acid at 283°K

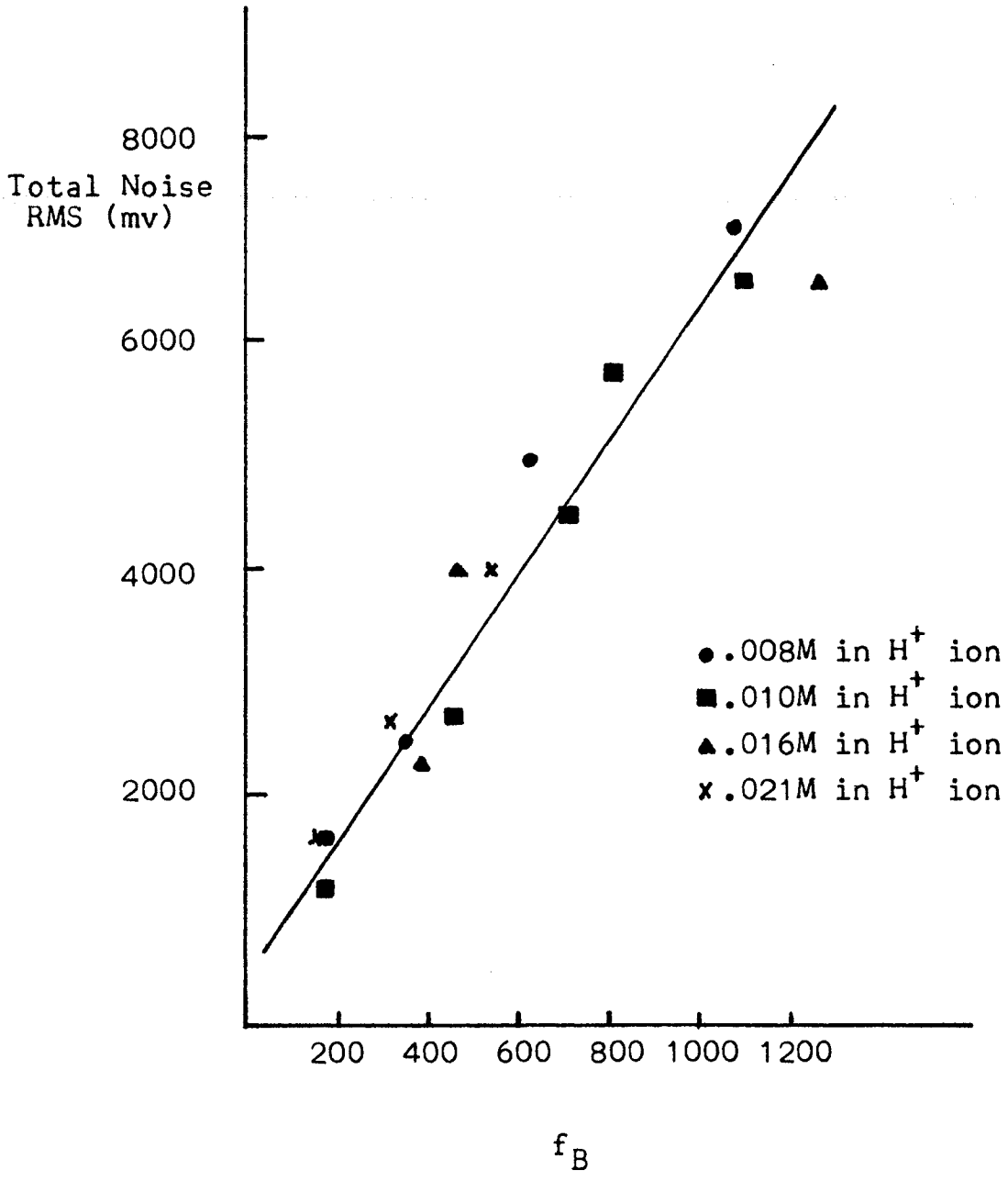

Figure 17

Total Noise vs Break Frequency for

Phosphoric Acid at 313°K

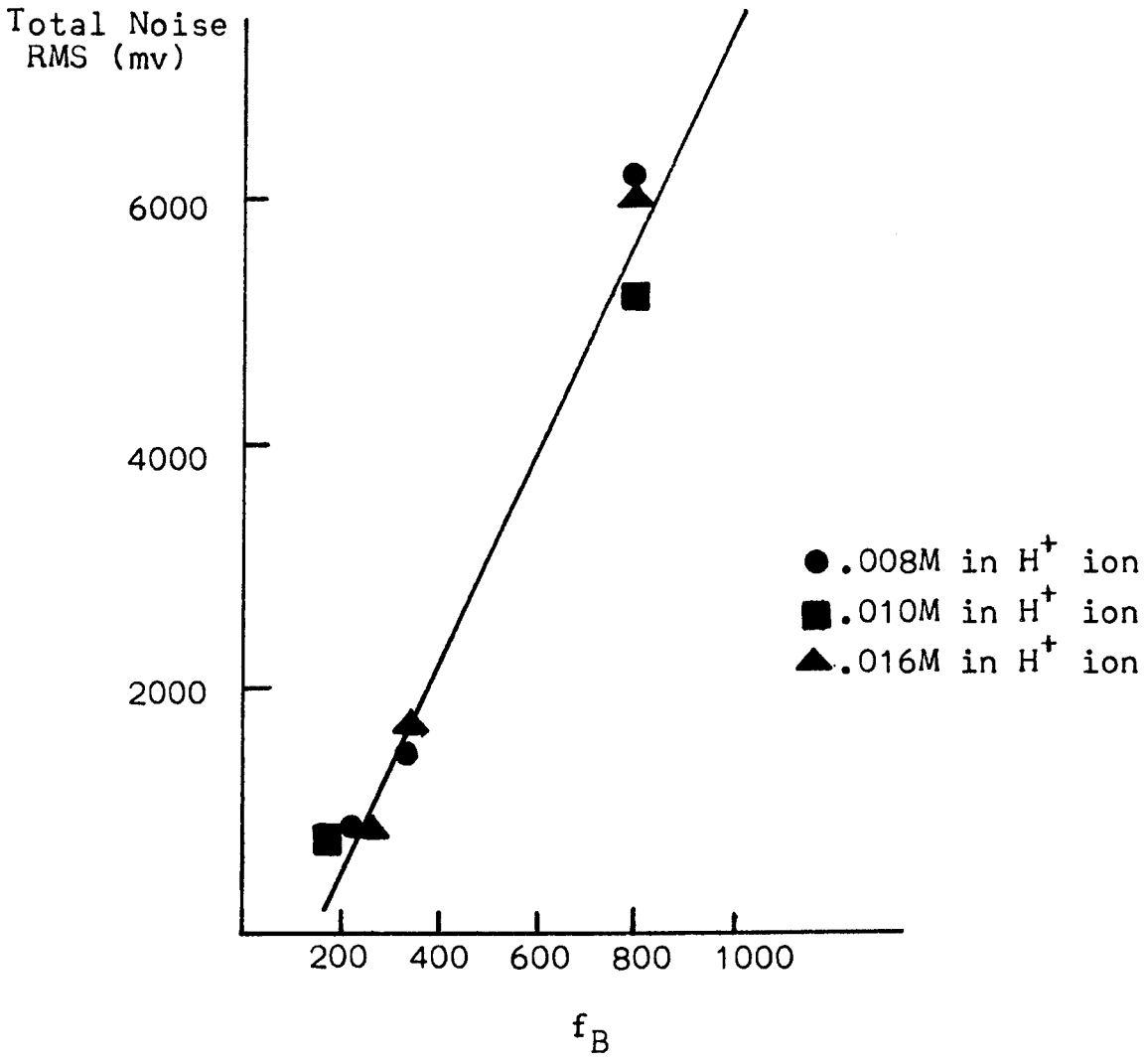

II Voltage-Time (t=0 to time equals steady state)

Chronopotentiometric data and Back Emf (defined as d.c. voltage across the membrane with the current off) measurements were recorded for Disodium hydrogen phosphate solutions, whose Na^+ ion concentration was .010M, .020M, .040M, and .060M, as well as phosphoric acid solutions .008M, .010M, .016M, .021M in H^+ ion at 285°K, 298°K and 313°K. Fig. 18 through 25 are typical of this data. In all of the photographs, the voltage increases as the curve moves toward the bottom of the graticule and decreases as the curve moves toward the top of the graticule (top of the photograph). With no membrane in the cell, the back voltage (V_B) and total voltage (V_T) were constant at all times. The electrode voltages were determined at all concentrations, temperatures and fluxes, and subtracted from the voltages found with the membrane in the cell so that absolute resistance and Back Emf values could be determined.

Voltage-Time Curves (From the time the current is first applied until steady state)

1) curves were obtained in H_3PO_4 and Na_2HPO_4 solutions

2) membrane used was Ionac MC-3142

3) In all photographs, the voltage increases as we move toward the bottom of the graticule and decreases as we move toward the top of the graticule.

4) 11KΩin - 11KΩ resister in parallel with membrane (Switch 1, Fig. 4, closed)

11KΩout - 11KΩ resister in parallel with membrane (Switch 1, Fig. 4 open)

11KΩin and out - indicates that both an "11KΩin" run and an "11KΩout" runs are found on the same photograph.

5) V_B - Back Emf with Switch in Fig. 4 closed.

V_T - Total voltage with Switch in Fig. 4 closed.

V_T' - Total voltage with Switch in Fig. 4 open.

i - flux change (the same for 11KΩ in and out) 0.010 $\frac{\text{volts}}{\text{Div.}}$ scale

6) $V_{B_{ss}}$, $V_{T_{ss}}$, $V_{T'_{ss}}$, and i_{ss} - steady state values

7) V_B' - zero under all conditions

Fig. 18 .016 H^+ at 12°C, 0.500 volts/div., 3.0 sec/div.

a) J = 334 A/M^2, 11KΩ in and out

b) J = 461 A/M^2, 11KΩ in and out

a)

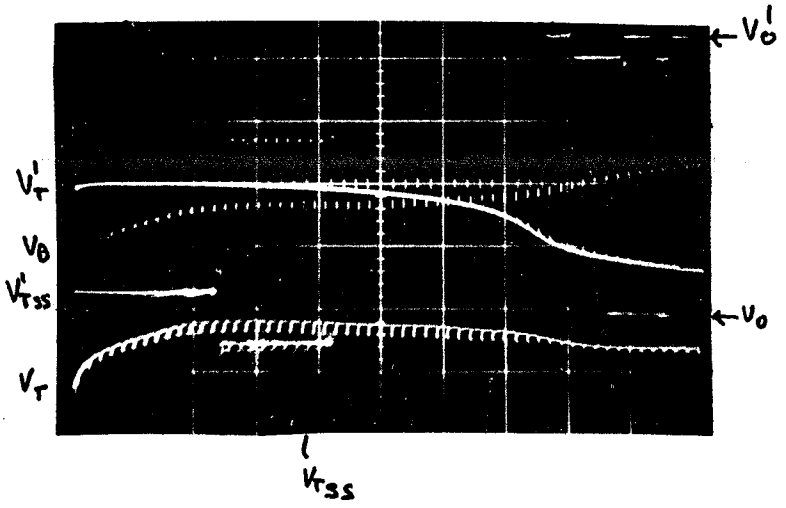

b)

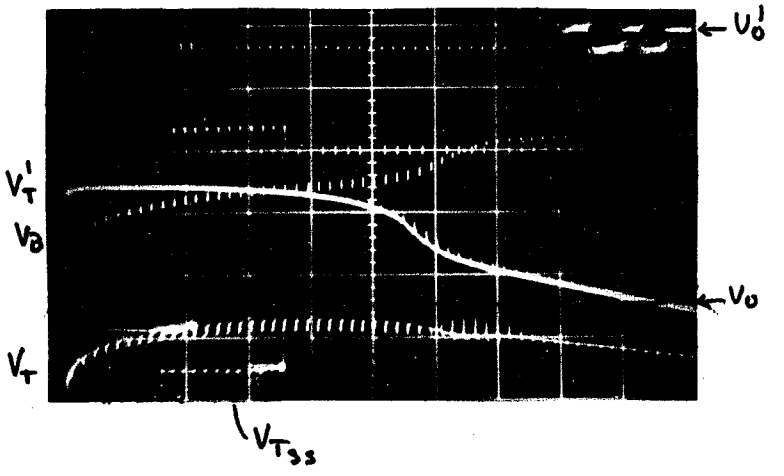

Fig. 19 .016 H^+ at 12°C, 0.500 volts/div. 1.5 sec/div.

a) J = 608 A/M^2, 11KΩ in

b) J = 608 A/M^2, 11KΩ out

a)

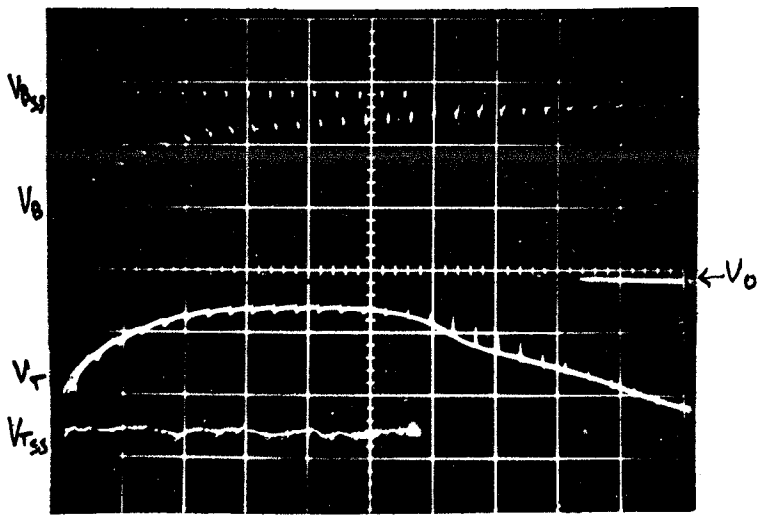

b)

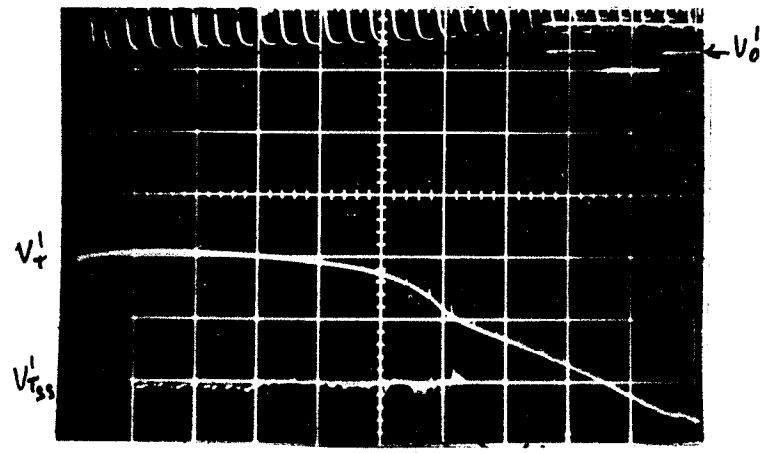

Fig. 20 .016 H^+ at 12°C, 0.500 volts/div, 1.5 sec/div.

a) J = 656 A/M^2, 11KΩ in

b) J = 656 A/M^2, 11KΩ out

a)

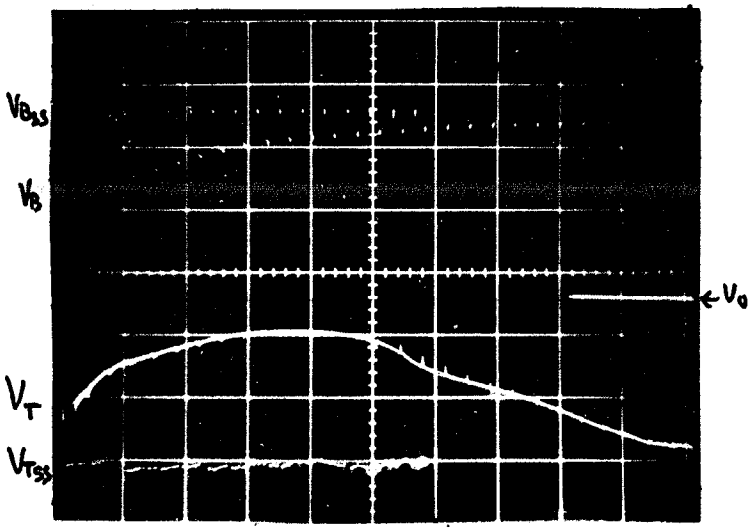

b)

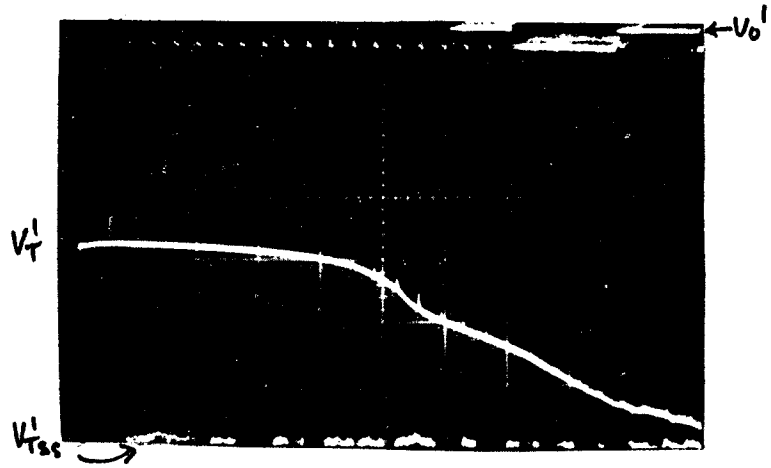

Fig. 21 a) .020 Na^+ at 25°C, 0.500 volts/div; 7.5 sec/div
J = 25.5 A/M^2, 11KΩ in and out
b) .060 Na^+ at 12°C, 0.500 volts/div; 1.5 sec/div
J = 127 A/M^2, 11KΩ in and out

a)

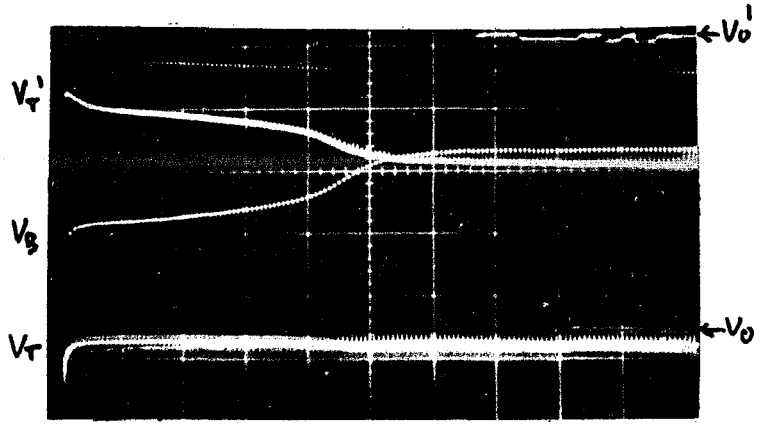

b)

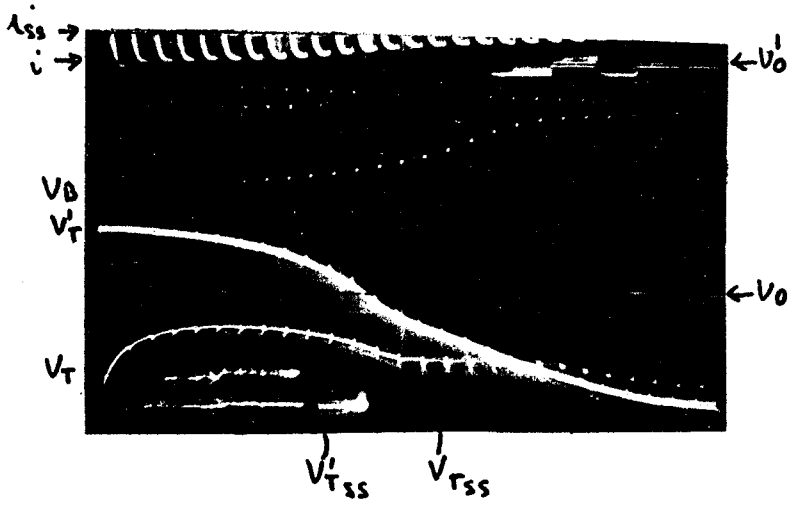

Fig. 12 .010 H^+ at 40°C, 0.500 volts/div; 1.5 sec/div

a) J = 350 A/M^2; 11KΩ in

b) J = 350 A/M^2; 11KΩ out

a)

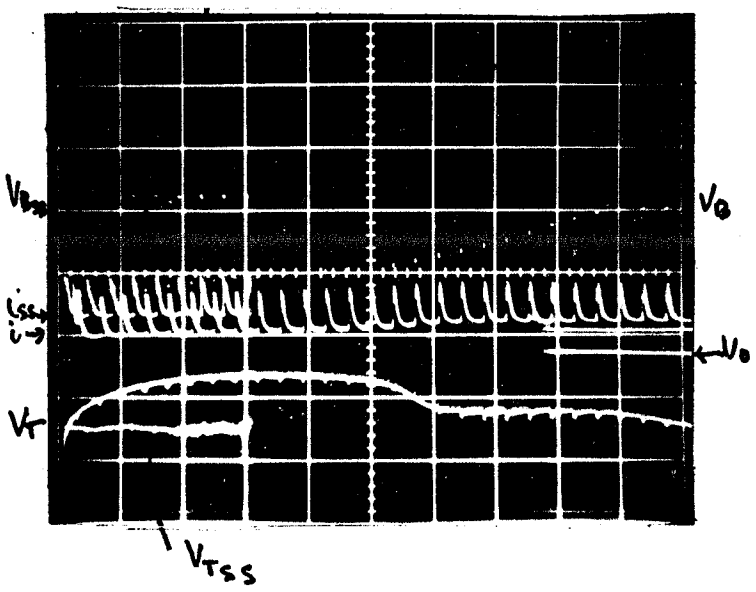

b)

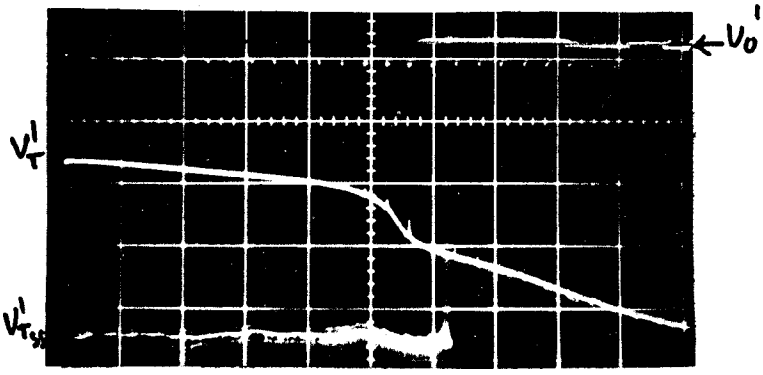

Fig. 23 a) .060 Na^+ at 25°C, 0.500 volts/div; 1.5 sec/div
J = 153 A/M^2; 11KΩ in and out
b) .016 H^+ at 25°C, 0.500 volts/div; 1.5 sec/div
J = 656 A/M^2, 11KΩ in and out

a)

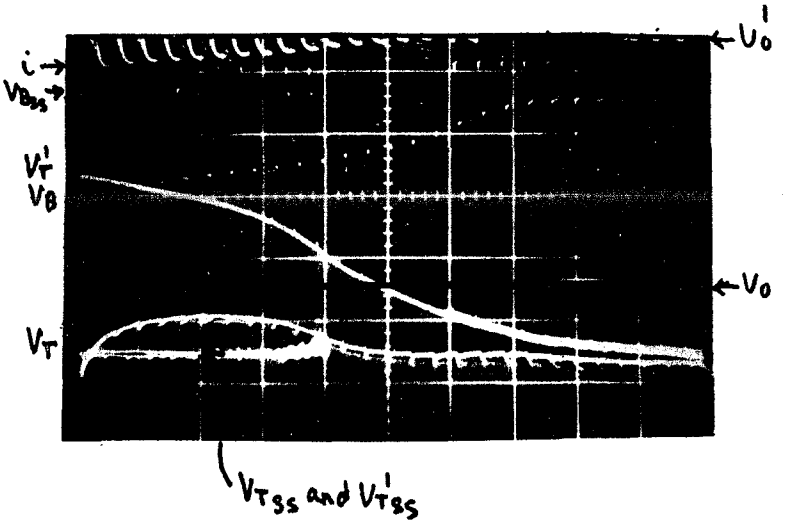

b)

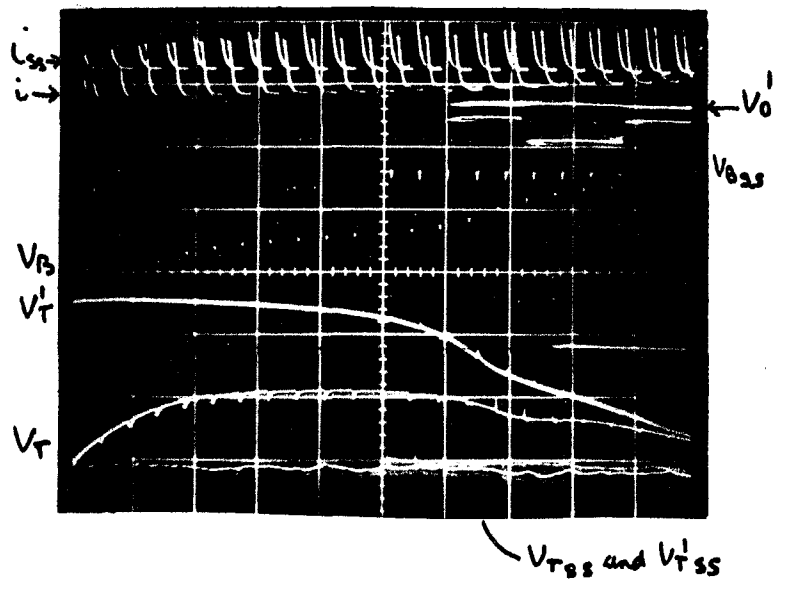

Fig. 24 .060 Na^+ at 25°C, 0.500 volts/div, 0.75 sec/div

a) J = 204 A/M^2, 11KΩ in

b) J = 204 A/M^2, 11KΩ out

a)

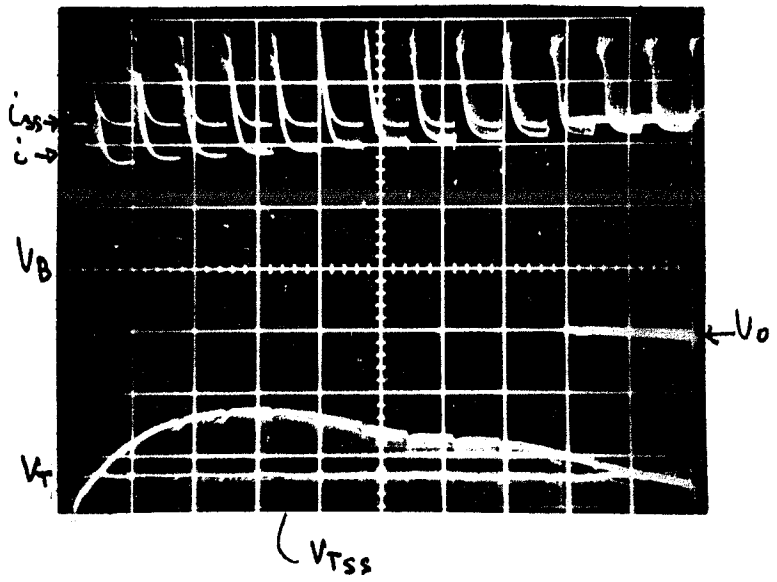

b)

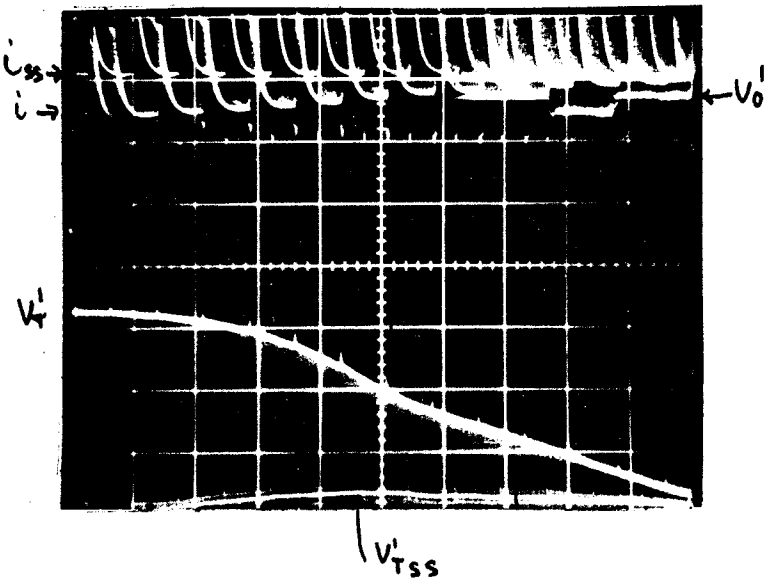

Fig. 25 a) .060 Na^+ at 12°C, 0.500 volts, 3.0 sec/div
$J = 102\ ^{A}/M^2$, 11KΩ in and out
b) .010 H^+ at 12°C, 0.500 volts, 1.5 sec/div
$J = 350\ ^{A}/M^2$, 11KΩ in and out

a)

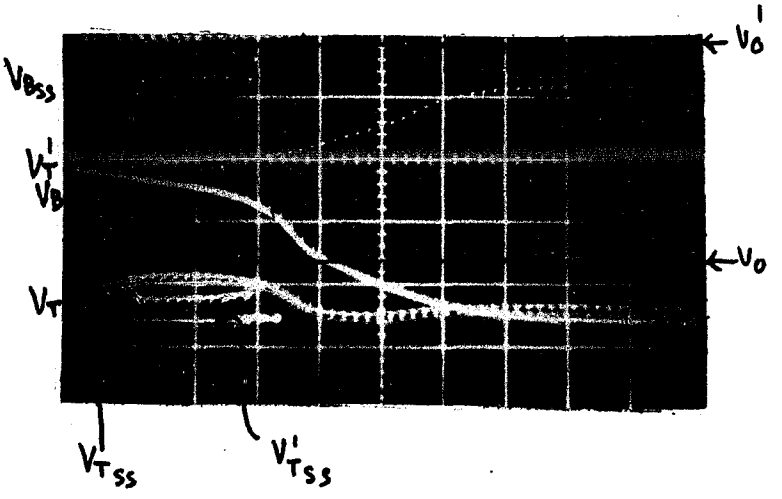

b)

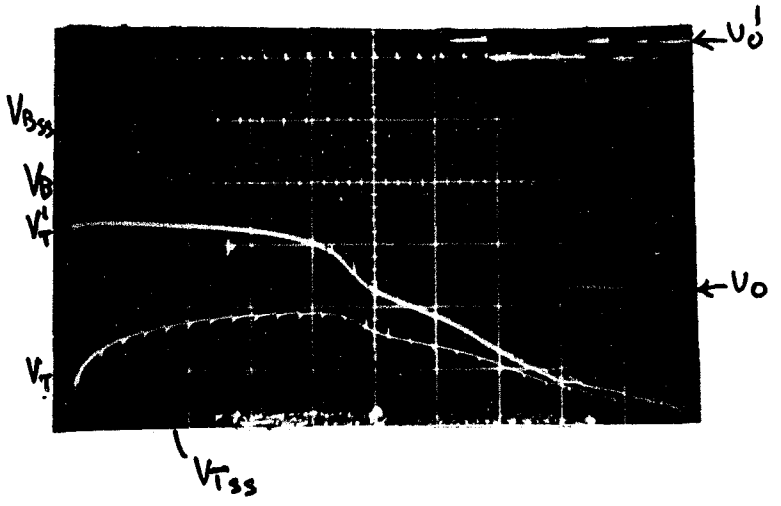

A series of curves for .016M H^+ at 298°K are shown in Figures 18-20. A careful examination of this series as well as other series (not shown here) reveals that the shape of both V_B and V_T (11K in) change with increasing flux and the shape or type of curve found is also dependent on temperature (T) and concentration (C). In comparing 11K in curves to those found in the 11K out case, we will ignore the initial voltage drop. (This voltage drop is discussed on page 99.)

We shall now describe three sets of conditions or three type curves. "Condition I" means that, at the same T, C and J, V_B(11K in) mirrors (the shape is the same but it is of opposite sign) V_T(11K out). This occurs at low C and.or high T and/or low J conditions (see Fig. 18 and 21a). V_T(11K in) remains almost constant until steady state (except for the initial voltage decrease). In some cases V_T(11K in) is almost a straight horizontal line; in other cases there is a perceptible valley in V_T(11K in). This valley occurs after the break and its maximum value is greater than V_T at steady state (see Fig. 25a).

"Condition III" occurs at high C and/or low T and/or high J. It means that at the same C, T and J, V_B(11K in) attains its steady state value well before V_T(11K in or 11K out). At times after which V_B(11K in) reaches a constant value, V_T(11K in) is identical in shape to V_T(11K out). This can be seen in Figs. 19a and b, 20a and b, 25b. "Condition II" is found at intermediate conditions of C, T and J. Here V_T(11K in and 11K out) and V_B(11K in) have features of both extreme conditions (I and III).

Note that after the transition time (the time it takes until the sharp rise in V_T - henceforth to be called τ) and before the time needed to reach steady state (t_{ss}): there is a "break" or "bump" in V_T(11K out) (see Fig. 20b). This break or bump is also visible at the same C, T and J in V_T(11K in) (see Fig. 20a). At the time the bump is found, V_B(11K in) reaches a constant value and at later times the shape of V_T(11K in) and V_T(11K out) will be the same until steady state is attained. This bump or break can also be seen in Figures 19a, 19b and 25b.

The intermediate condition (condition II) offers proof of two critical current densities (C.C.D.'s). This proof (to be discussed later) comes in the form of a "plateau" (see Figs. 21b, 22a and 23b) which is often found in V_T(11K in) i.e., after the transition time ( ), V_T(11K in) will remain constant for a period of time ($dv_T/dt = 0$). While V_T(11K in) is in the "plateau" portion of the curve ($dv_T/dt = 0$), V_B(11K in) is increasing at a rate equal to the rate of increase of V_T(11K out) over the same time interval, at the same C, T and J. Once V_B(11K in) reaches a constant value, then the plateau region is over and V_T(11K in) will now increase at the same rate as V_T(11K out).

The duration of the plateau is a function of flux. With decreasing flux, the time interval over which the plateau extends increases. For example, Fig. 23a and 24a show "plateaus" in .060 Na^+ and 298°K. In one case J = 153 A/M^2, in the other 204 A/M^2. V_T(11K in) is constant for 3.5 seconds at the lower

flux and 1.2 seconds at the higher one. It was mentioned earlier that the existence of the plateau is a function of C, T, and J. (See Fig. 22a and 25b; Fig. 19a and 23b)

Because the C.C.D's of H^+ ion are always higher than those of Na^+ ion at all values of C and T, any comparison of H^+ ion and Na^+ ion chronopotentiometric data is severely limited. There is no way to match the C, T and J values of the two ions.

One difference (although of secondary importance) between the chronopotentiometric data of the two ions, is that τ is usually clearly visible in V_B(11KΩin) of H^+ ion but always difficult to see in V_B(11KΩin) of Na^+ ion. Also this same τ found in V_B(11KΩin) is identical to the τ found on the same run in V_T(11KΩin) for H^+ ion, but in the Na^+ ion case the τ found in V_B(11K in) is often somewhat larger than the transition time found on the same run in V_T(11KΩin).

Steady State Resistance and Steady State Back Emf

Resistance values (R) were calculated using Ohm's Law from t = 0 to time equals steady state (t_{ss}).

$$R = \frac{V_T(11K \text{ out})}{i} \qquad (24)$$

Table 9 lists the steady state resistances (R_{ss}) as well as the steady state Back Emfs (V_B(11K in)) values as a function of C, T and J for both H^+ ion and Na^+ ion. V_B(11K out) values are 0 volts under all conditions and therefore not reported.

Figures 26-30 show how R_{ss} varies with flux (J) and Figures 31-34 how V_B varies with J for both H^+ ion and Na^+ ion at various concentrations and temperatures. The small arrows on Figures 31-34 indicate the V_B values at the lowest fluxes (J_m) at which the first breaks in the power spectra were seen. These V_B values are listed in Table 10. Table 10 reveals that a break in the Na^+ ion power spectra is dependent on attaining a V_B value of sufficient magnitude (between 500-900 mv). H^+ ion spectra, on the other hand, show a sharp break with V_B values as low as zero.

Figures 26-28 show that R_{ss} values of solutions .020, .040 and .060M in Na^+ ion are nearly independent of flux. These R_{ss} values were averaged and an average resistance found, (R_{ss}avg) at 285°K, 298°K and 313°K for .02, .04 and .06M Na^+ (see Table 11). An R_{ss}avg value is also reported in Table 11 for .010 Na^+ at 313°K.

Figures 29 and 30 show that R_{ss} values are nearly independent of flux in .016 H^+ and .021 H^+ at 285°K and 298°K and for .010 H^+ at 285°K. R_{ss} avg values for H^+ ion are reported in Table 10.

R_{ss} values were also obtained in the 11K in case using Ohm's Law. A correction was made for having the 11K resistor in parallel with the cell. The voltage used was obtained by adding V_B to V_T. These R_{ss} values were invariably less than those found in the 11K out case - usually by 8 - 16%.

Figure 16

The Total d.c. Resistance as a Function of Flux for Na_2HPO_4 at 285^0K

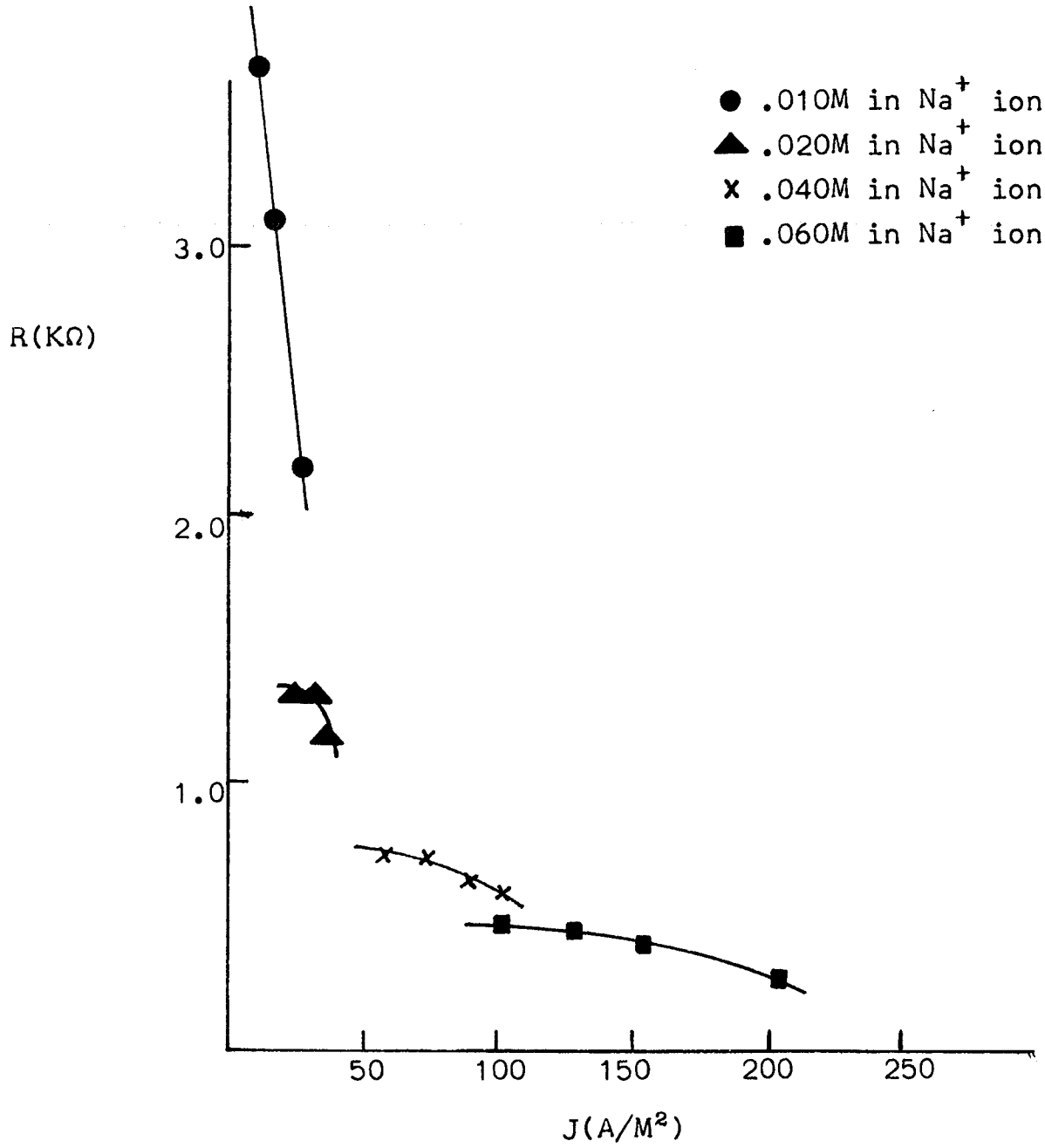

Figure 27

The Total d.c. Resistance as a Function of Flux for H_3PO_4 at 298°K

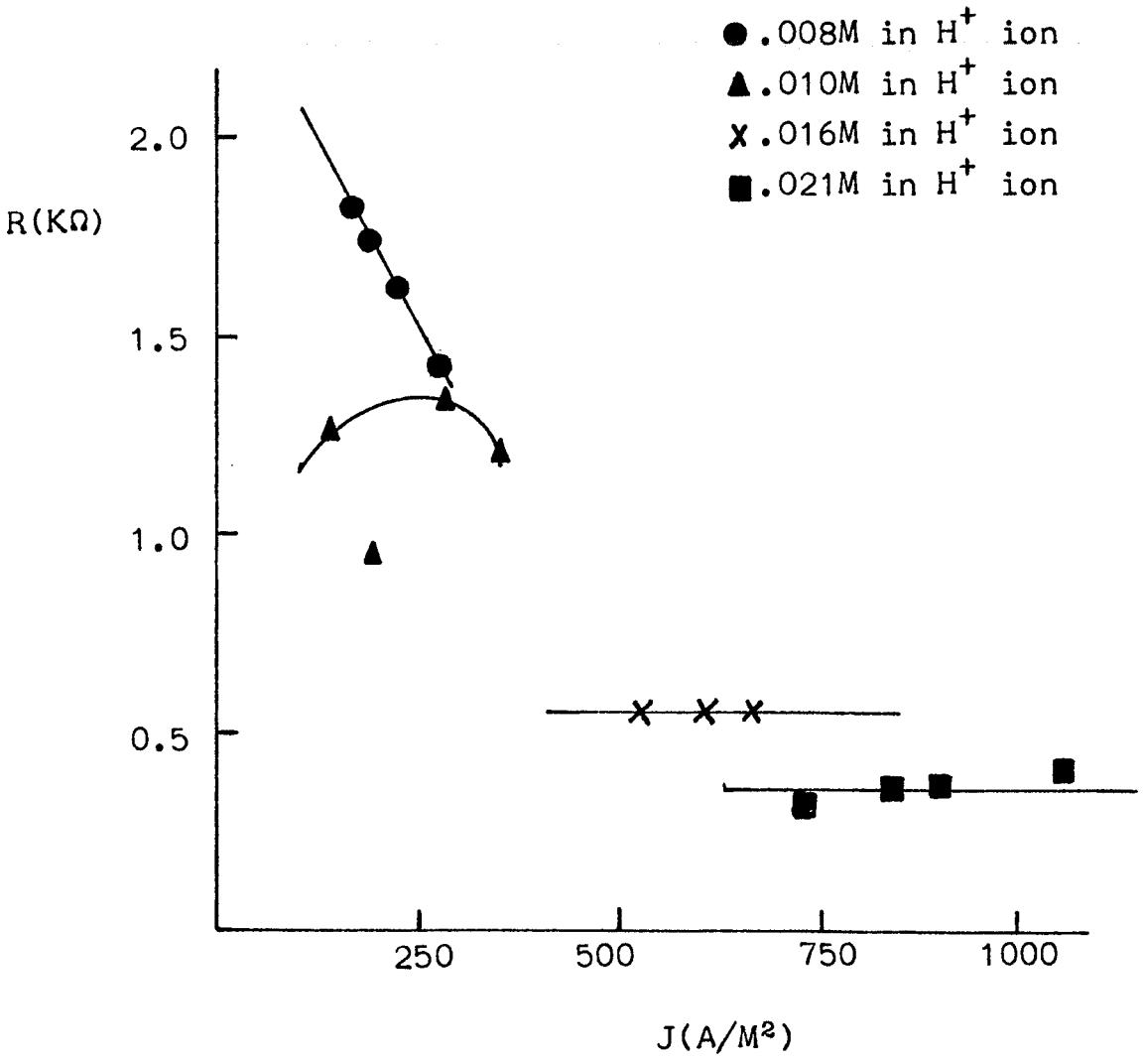

Figure 18

The Total d.c. Resistance as a Function of Flux for Na_2HPO_4 at 313°K

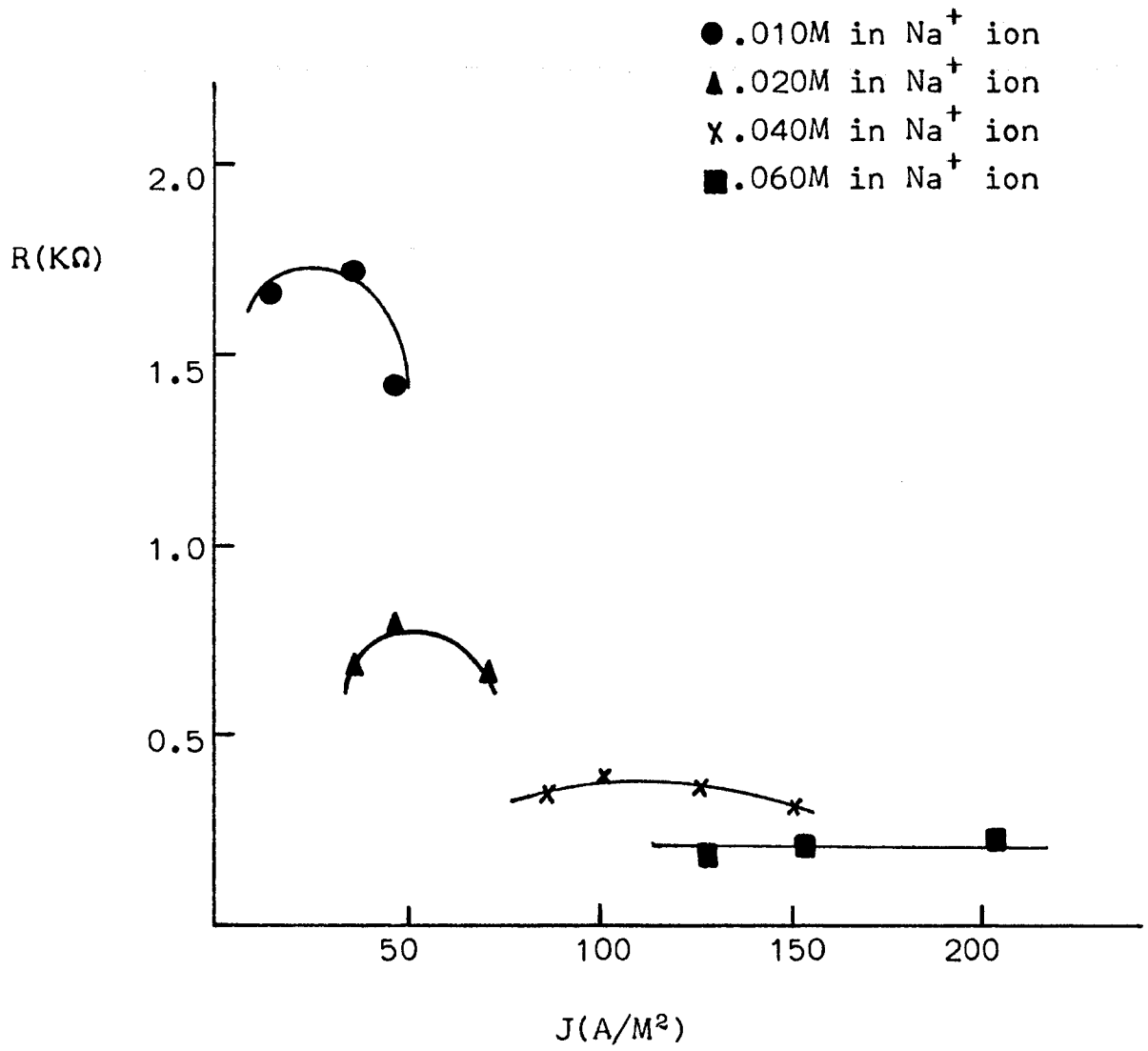

Figure 29

The Total d.c. Resistance as a Function of Flux for H_3PO_4 at 285^0K

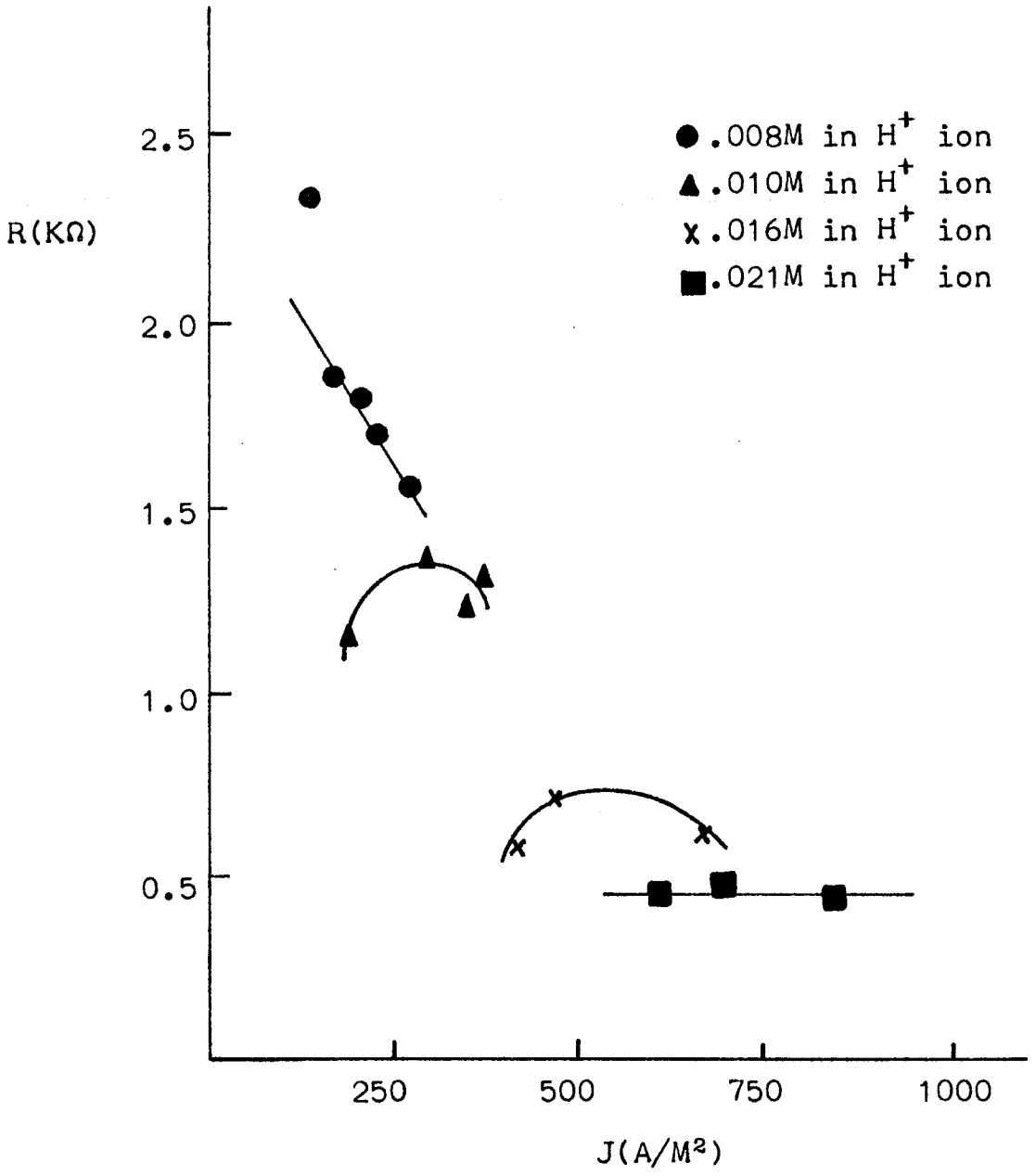

Figure 30

The Total d.c. Resistance as a Function of Flux for Na_2HPO_4 at 298°K

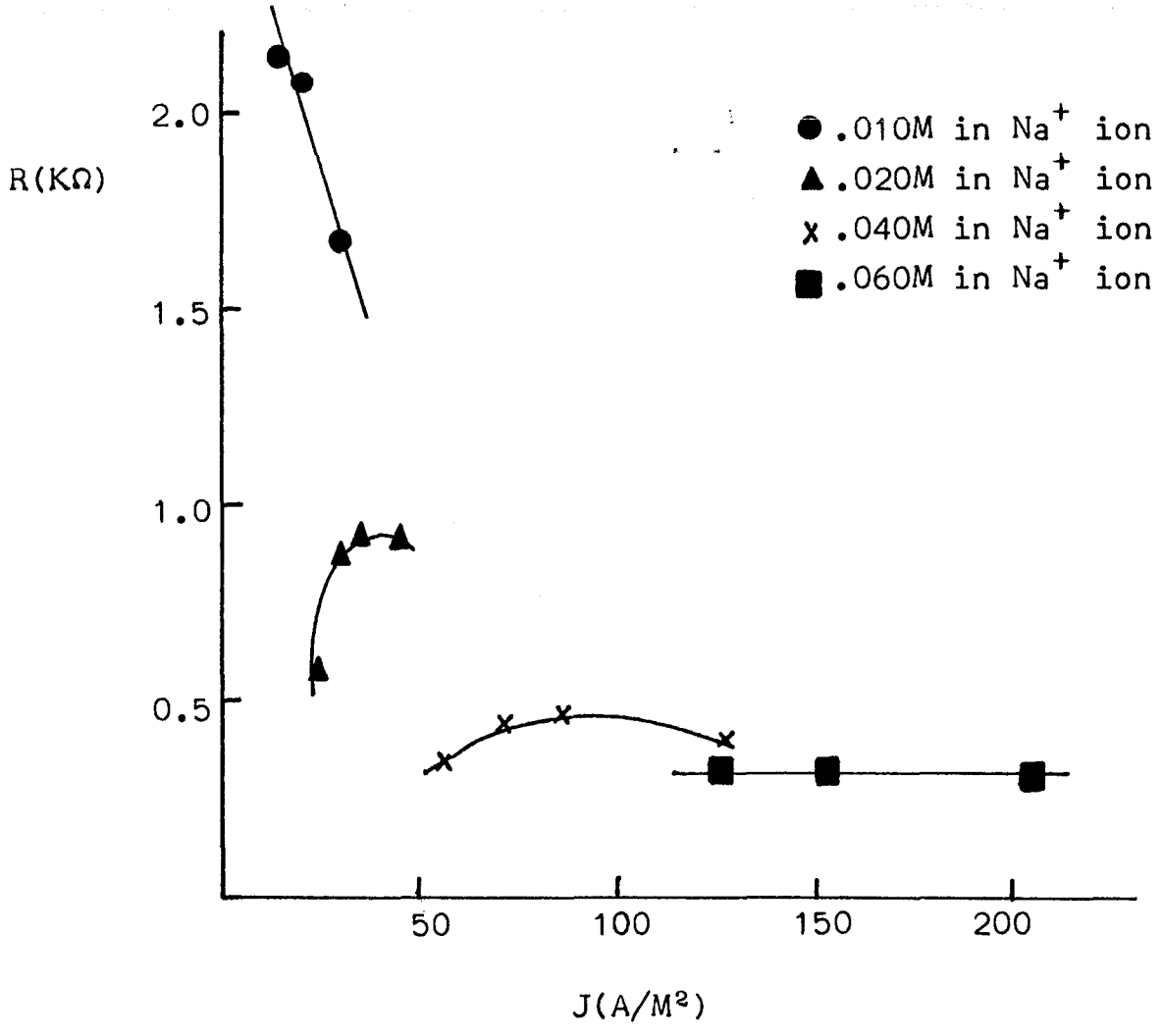

Figure 31

Plot of Back Emf vs the Flux for Na_2HPO_4 at 285°K

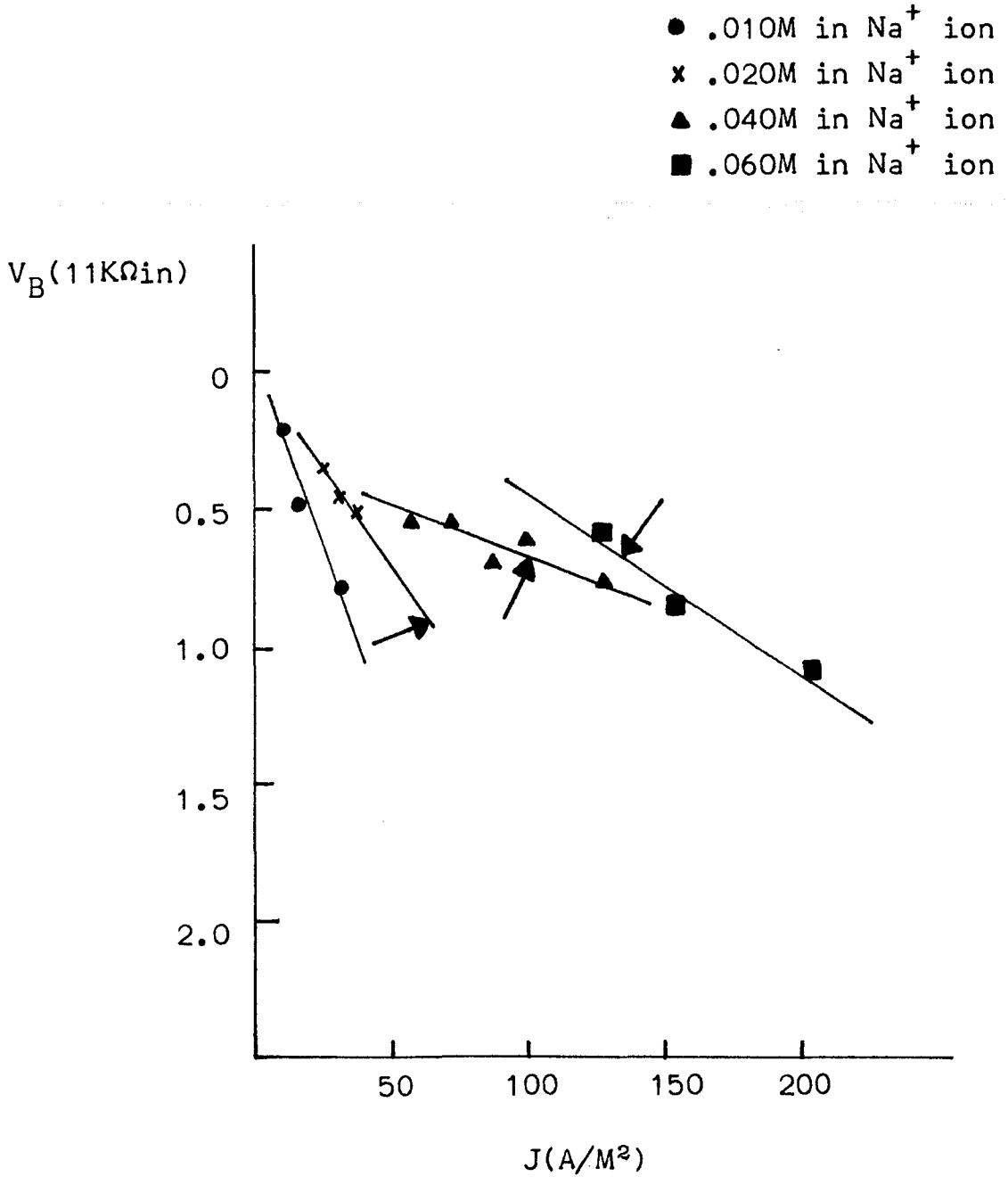

Figure 3a

Plot of Back Emf vs Flux for Na_2HPO_4 at 298^0K

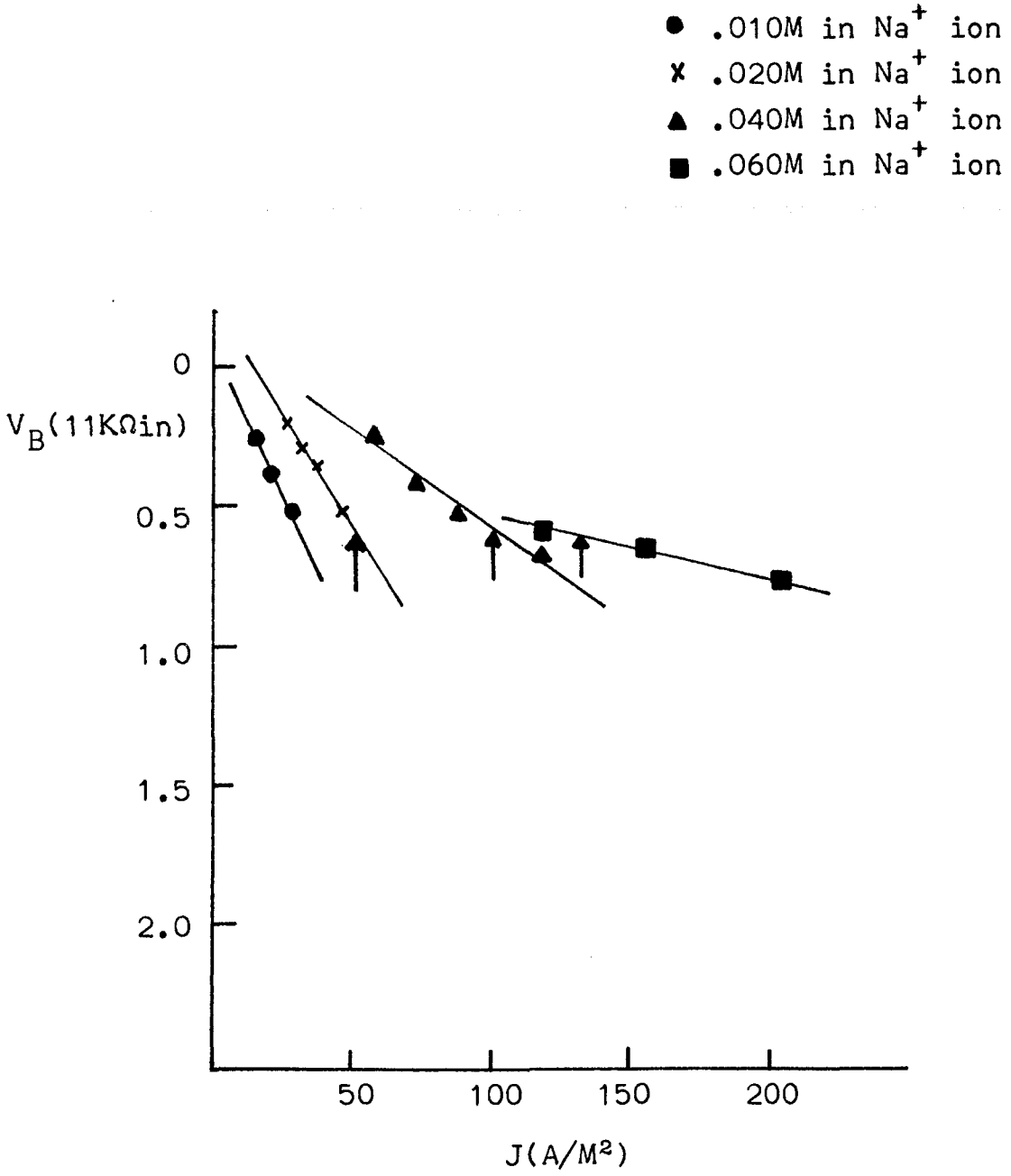

Figure 33

Plot of Back Emf vs Flux for Na_2HPO_4 at 313°K

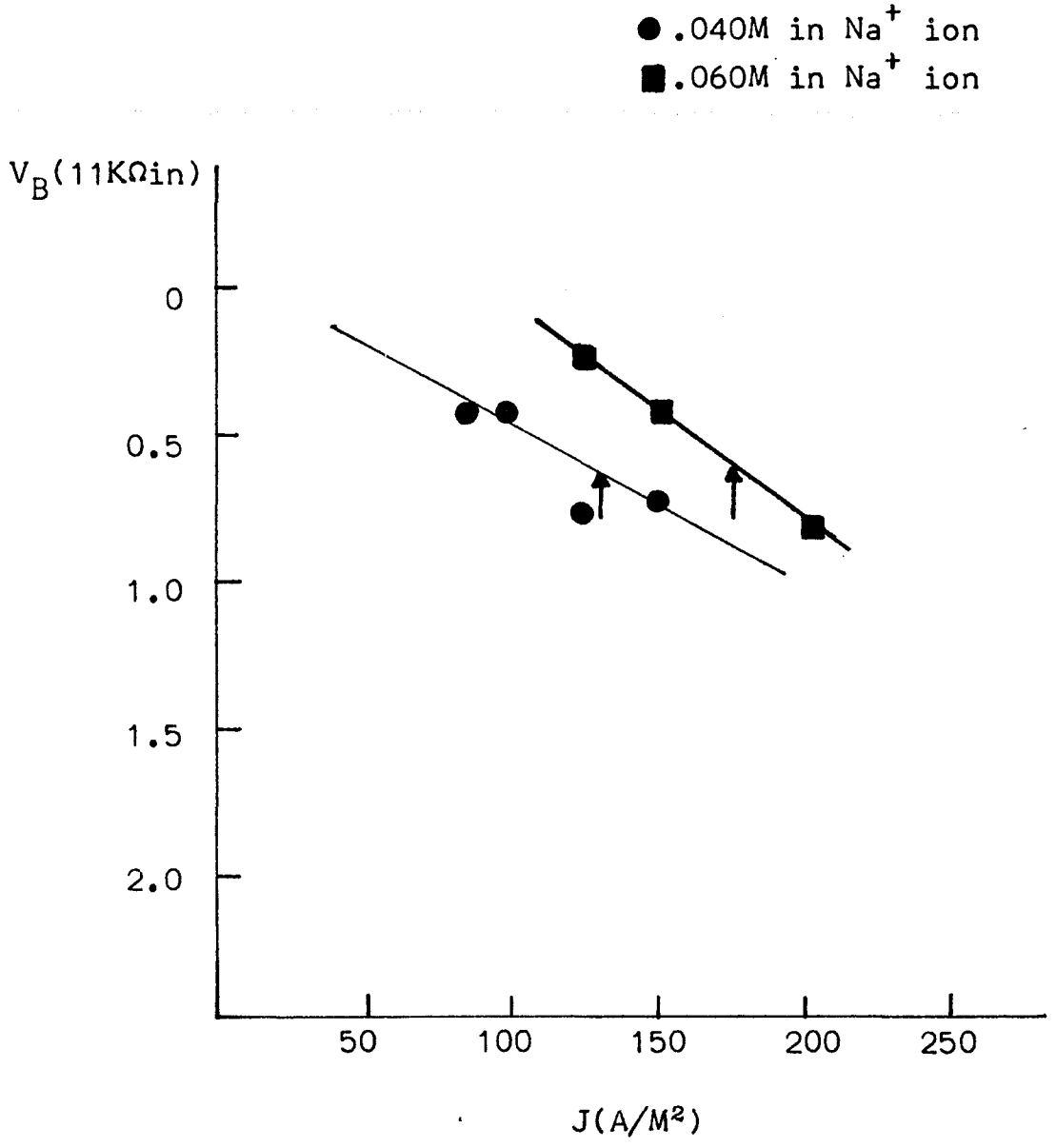

Figure 34

Plot of Back Emf vs Flux for H_3PO_4 at 298°K

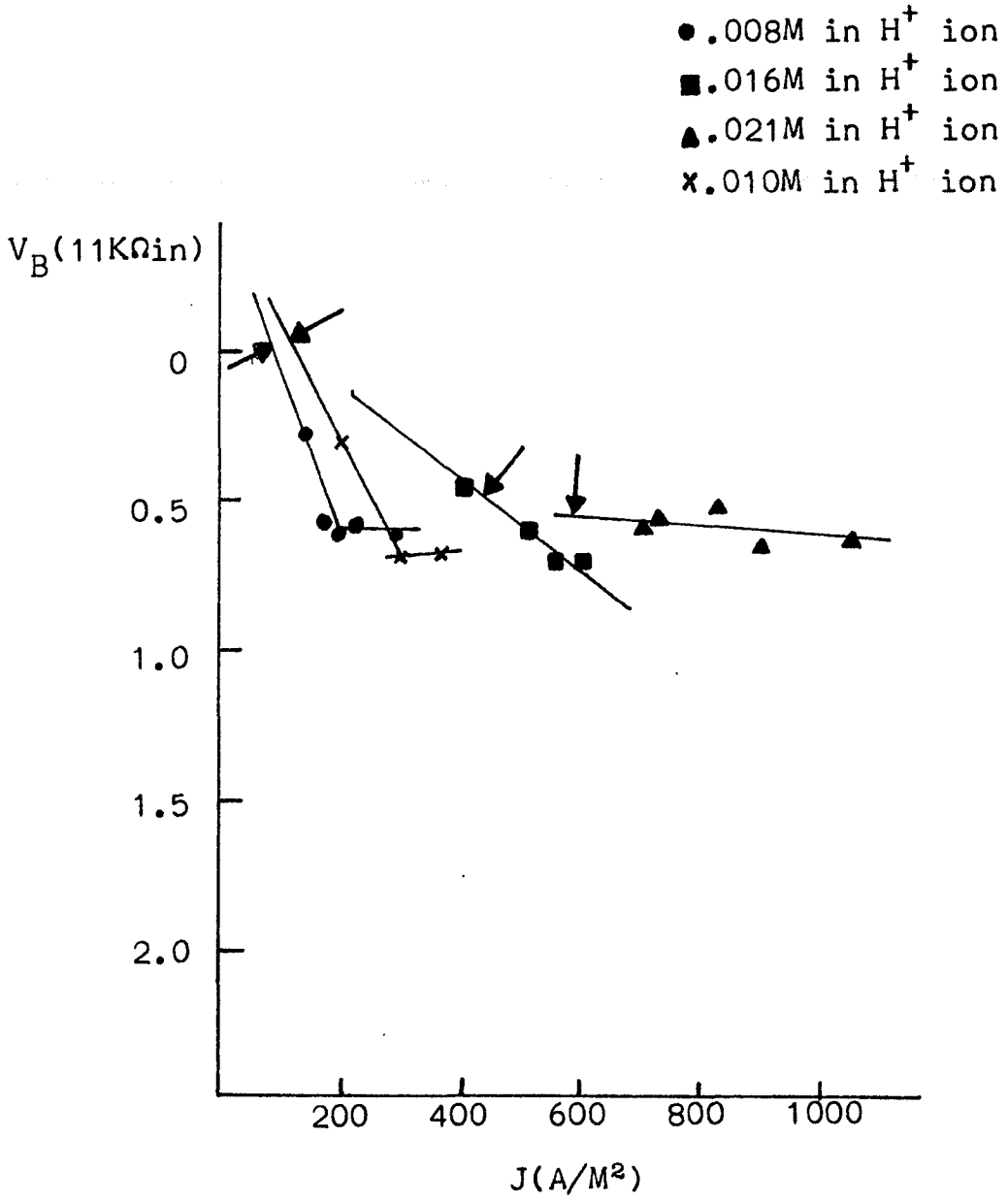

The initial voltage drop

The chronopotentiometric data reveals that V_T(11KΩin) decreases in magnitude from the time the current is first applied (t = 0) to a time t", which is always less than τ. It is only after t" that V_T(11KΩin) begins to increase. This initial voltage decrease is listed as ΔV in Table 12. Plots of J vs ΔV are shown in Figures 35 and 36. These plots show that there is a linear relationship between the flux and the initial voltage drop in the Na^+ ion case.

This initial voltage drop is mirrored in V_B(11KΩin) where it is identical in shape to the drop in V_T(11KΩin), $0 \leq t' \leq \tau'$. The 11KΩout case is quite different. For one thing, as has been previously mentioned $V_B \simeq 0$. For another $V_T(t) \quad 0$, $0 \leq t' \leq \tau$.

Figure 35

The Voltage Drop in the Na_2HPO_4 Voltage-Time Curves (.010M and .020M in Na^+ ion) vs the Flux

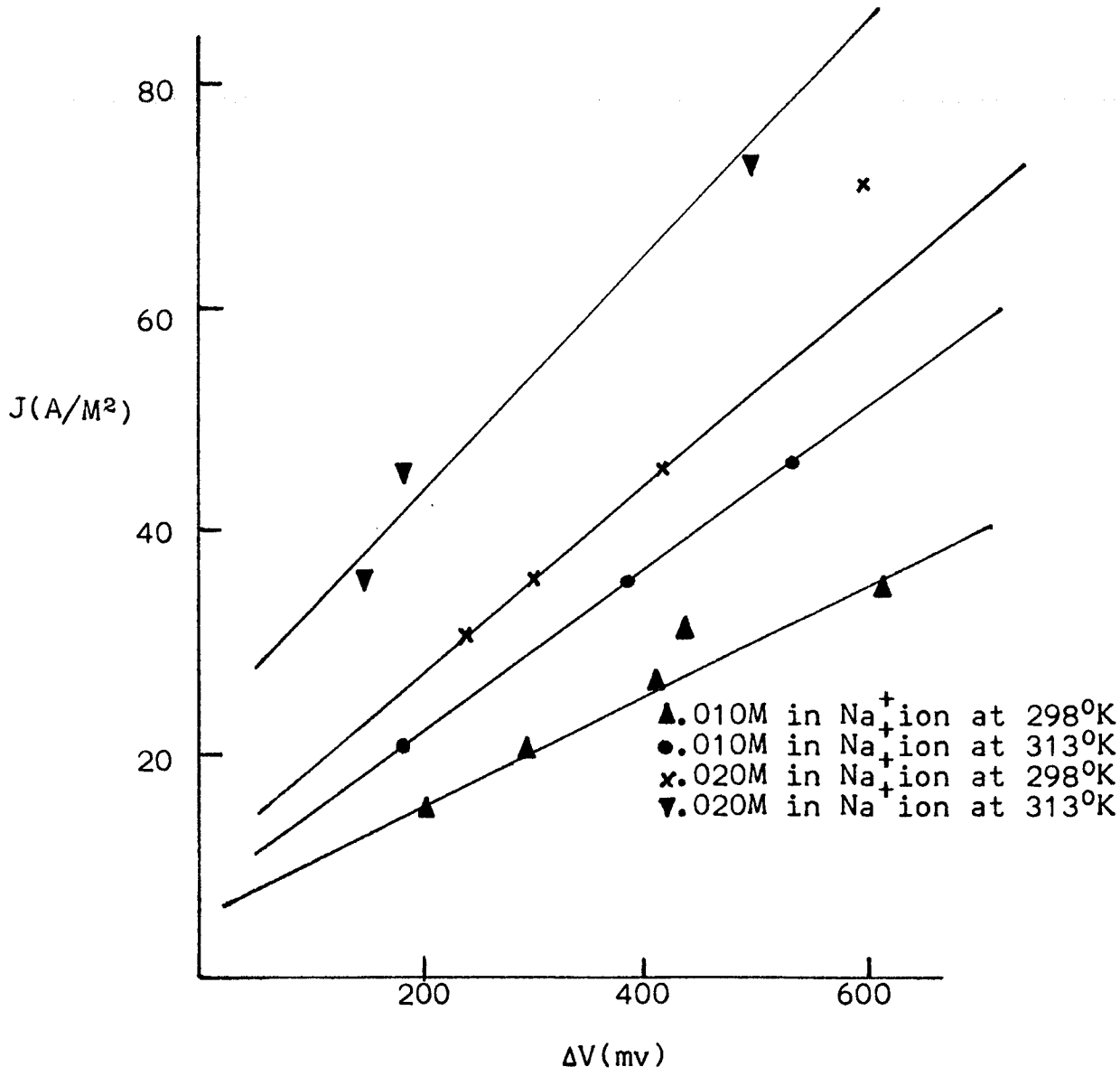

Figure 36

The Voltage Drop in the Na_2HPO_4 Voltage-Time Curve (.040 and .060M in Na^+ ion) vs the Flux

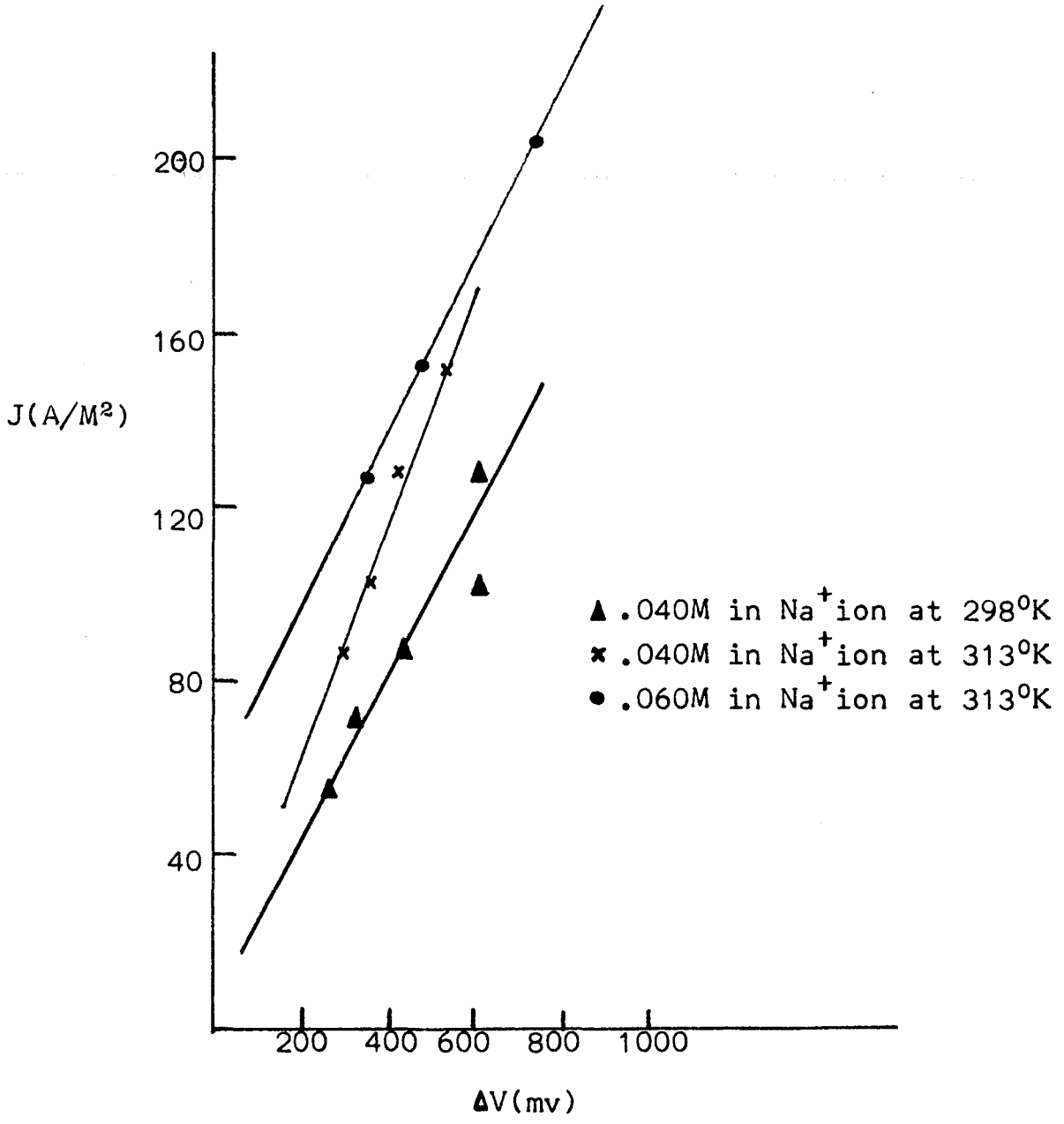

Transition times

Transition times obtained from chronopotentiometric data with no 11KΩ resister between the measuring electrodes, at all C, T and J values, are shown in Table 13. The transition times obtained with an 11KΩ resister in the circuit were identical within experimental error to those found in the 11KΩout case.

If both the diffusion coefficient and the counterion transport number are assumed to be independent of T, then Sands equation reduces to

$$\frac{1}{\tau} = \frac{k}{C^2} J^2$$

where k includes other constants.

Plots of J^2 vs $1/\tau$ are given in Figures 37 - 43. The slopes of these plots are listed in Table 14.

Table shows the expected slope ratios determined experimentally and the expected slope ratios determined from the concentration ratios. The difference between the experimentally determined and theoretically determined ratios are also listed in Table 15.

Figure 37

A Plot of Flux Squared vs Reciprocal Transition Time for Na_2HPO_4 (.010M in Na^+ ion)

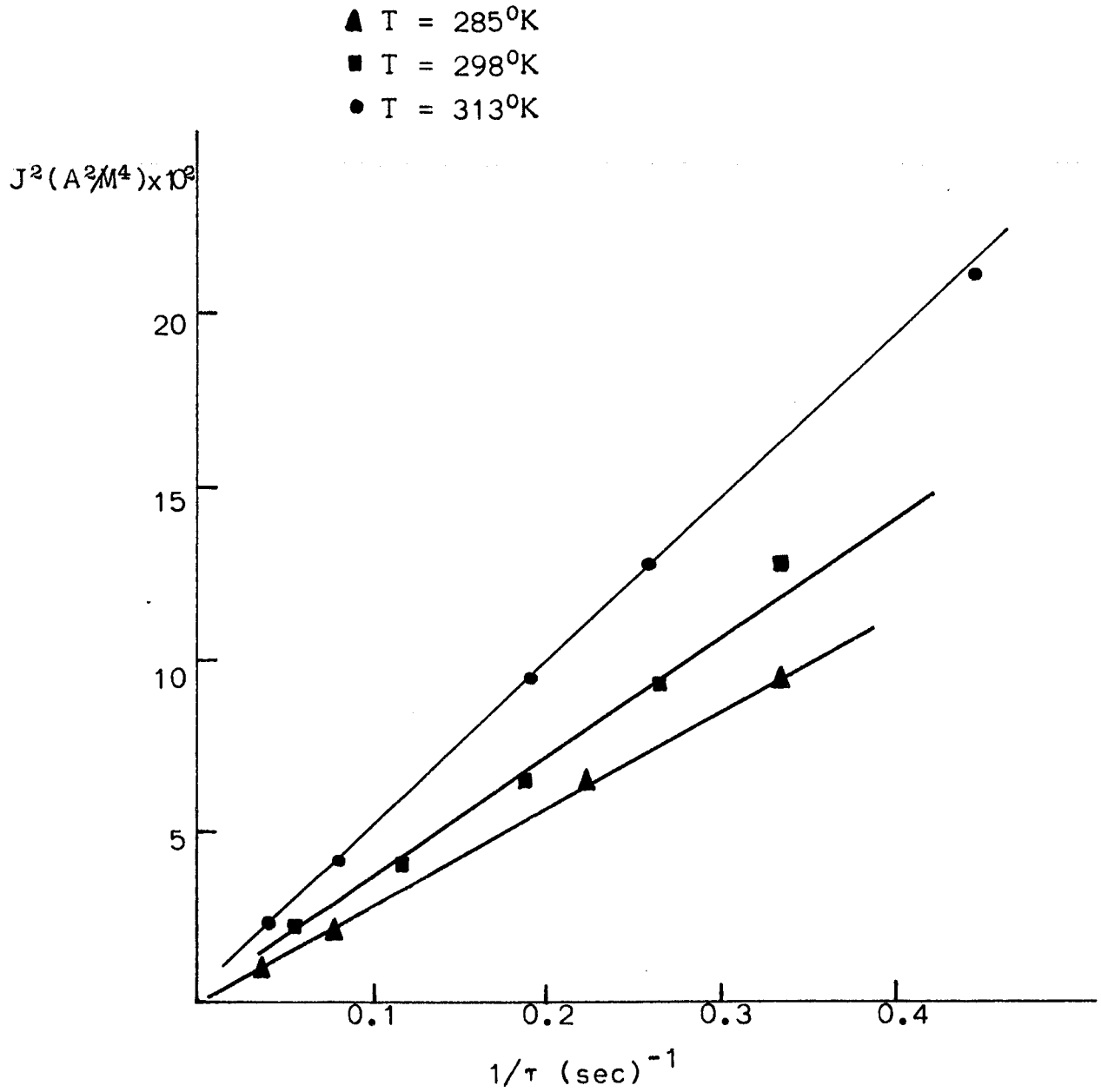

Figure 38

A Plot of Flux Squared vs Reciprocal Transition Time for Na_2HPO_4 (.020M in Na^+ ion)

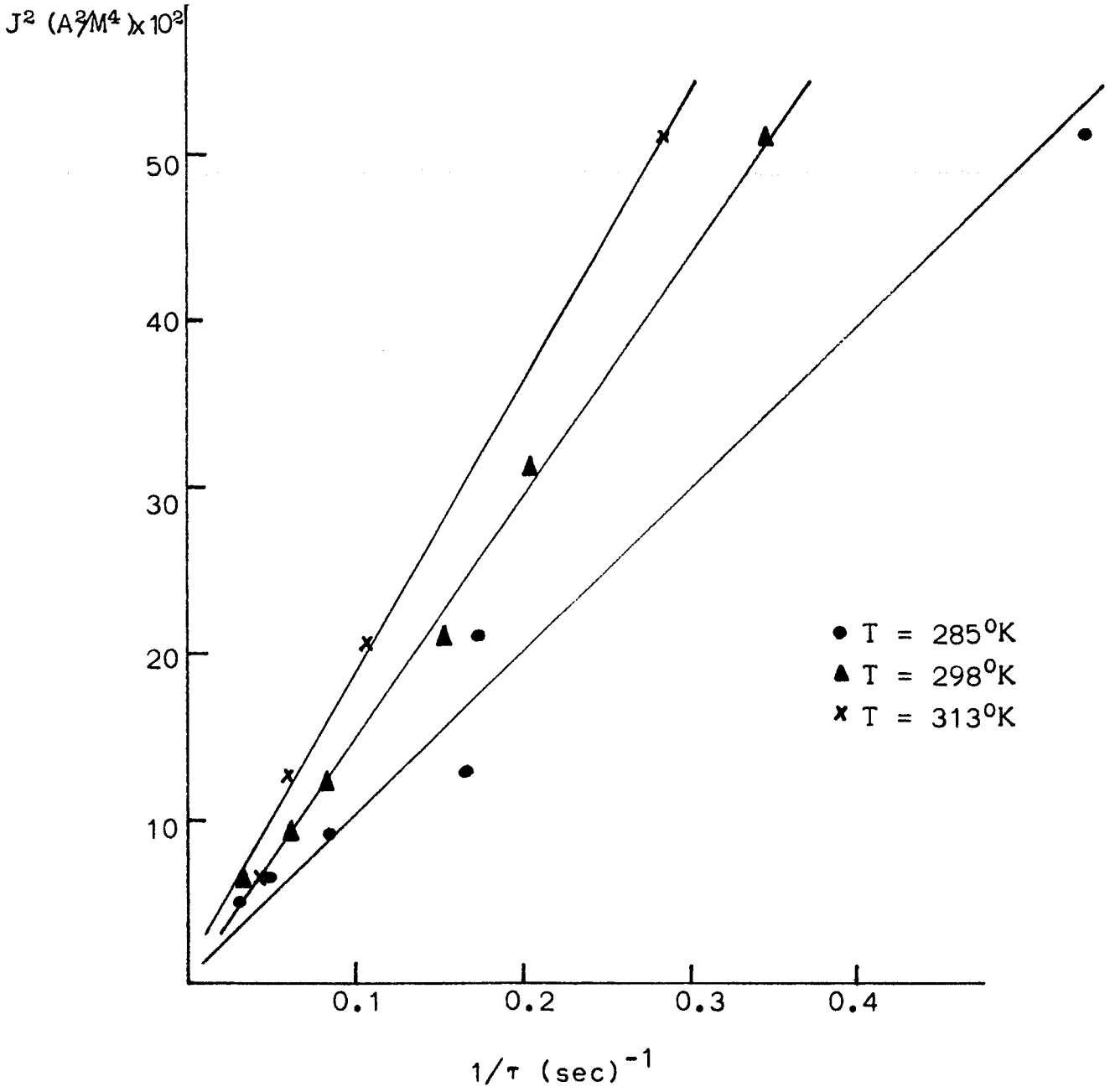

Figure 39

A Plot of Flux Squared vs Reciprocal Transition Time for Na_2HPO_4 (.040M in Na^+ ion)

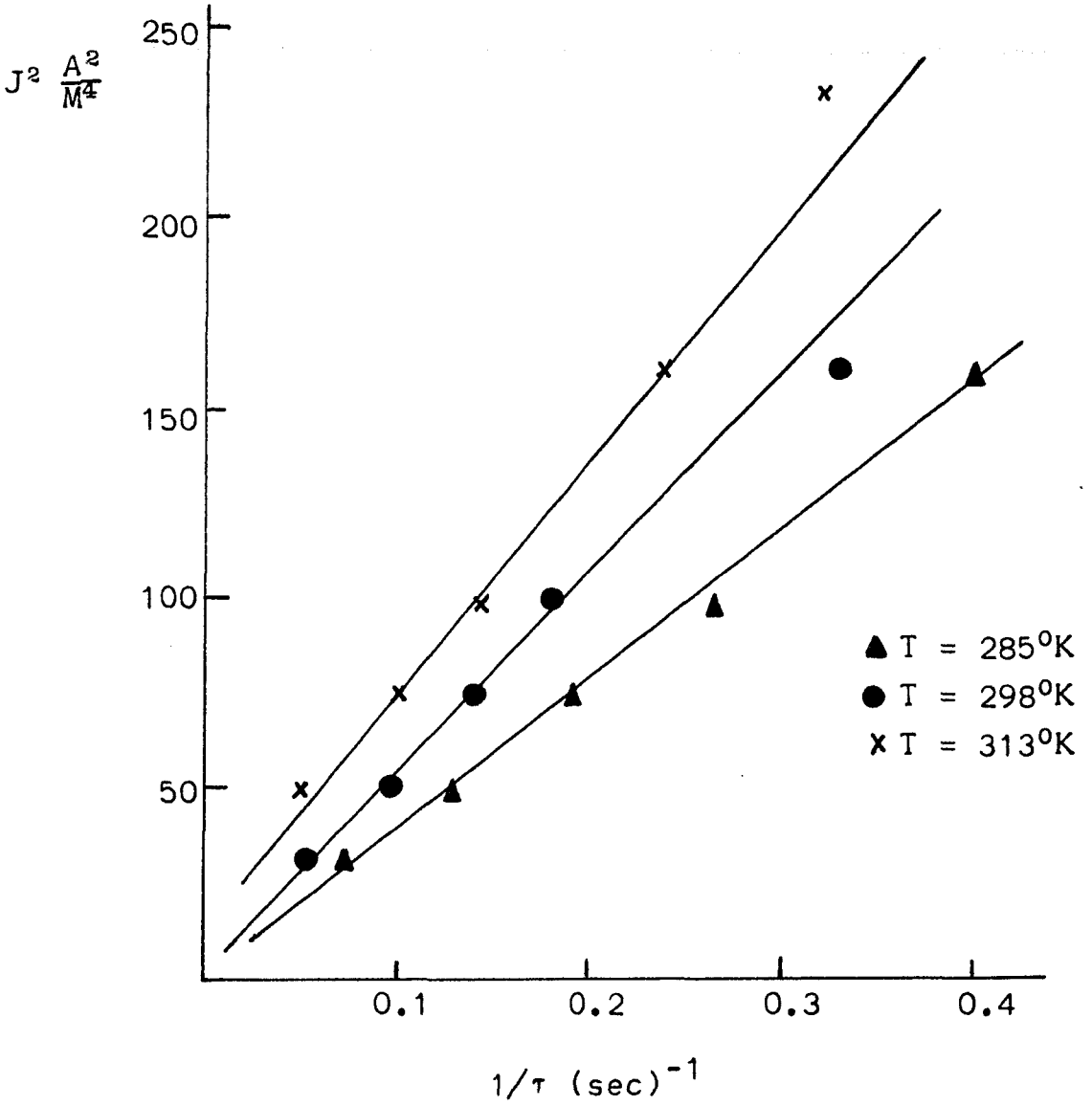

Figure 40

A Plot of Flux Squared vs Reciprocal Transition Time for Na_2HPO_4 (.060M in Na^+ ion)

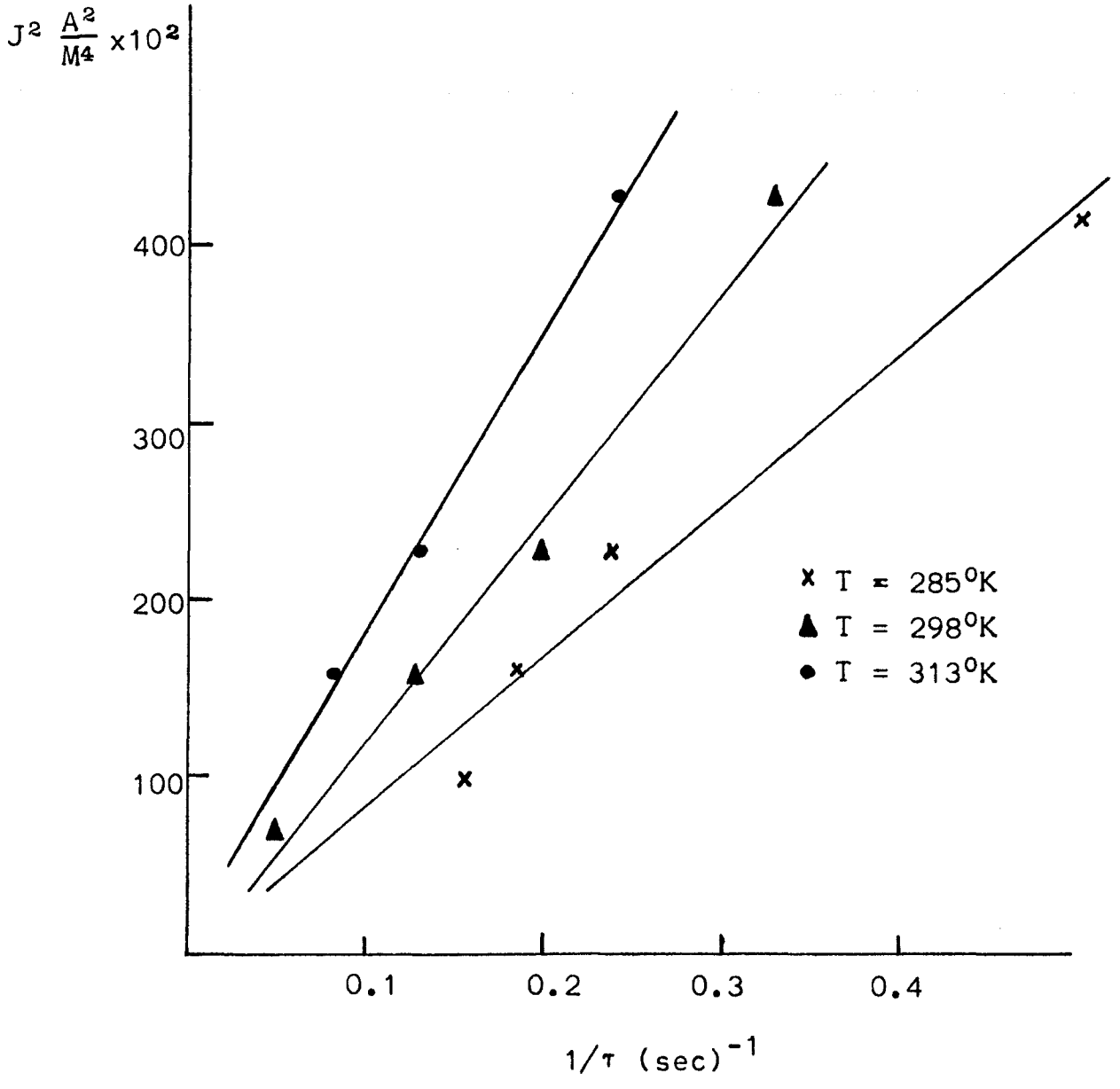

Figure 41

A Plot of Flux Squared vs Reciprocal Transition Time for H_3PO_4 (.008M in H^+ ion)

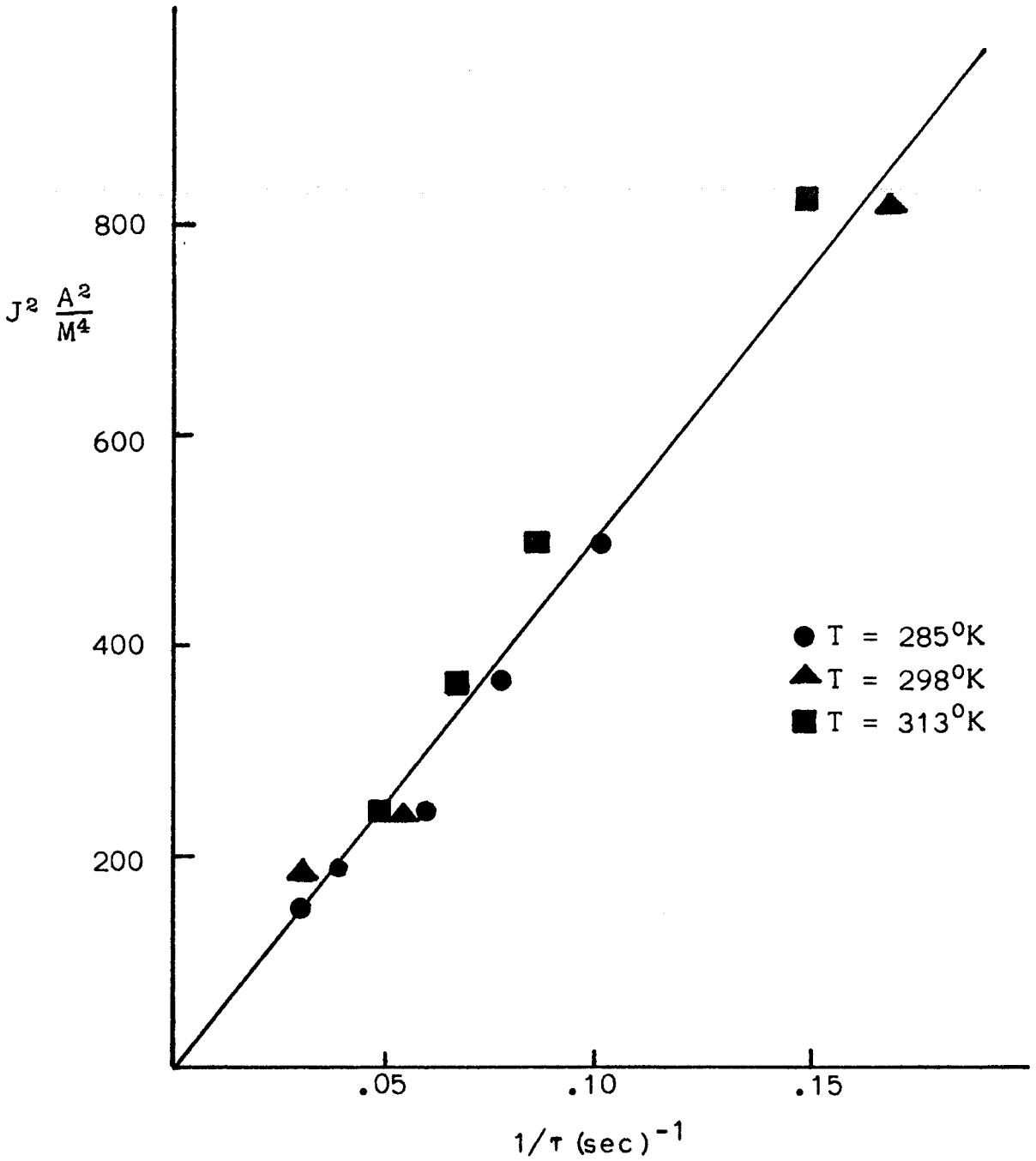

Figure 42

A Plot of Flux Squared vs Reciprocal Transition Time

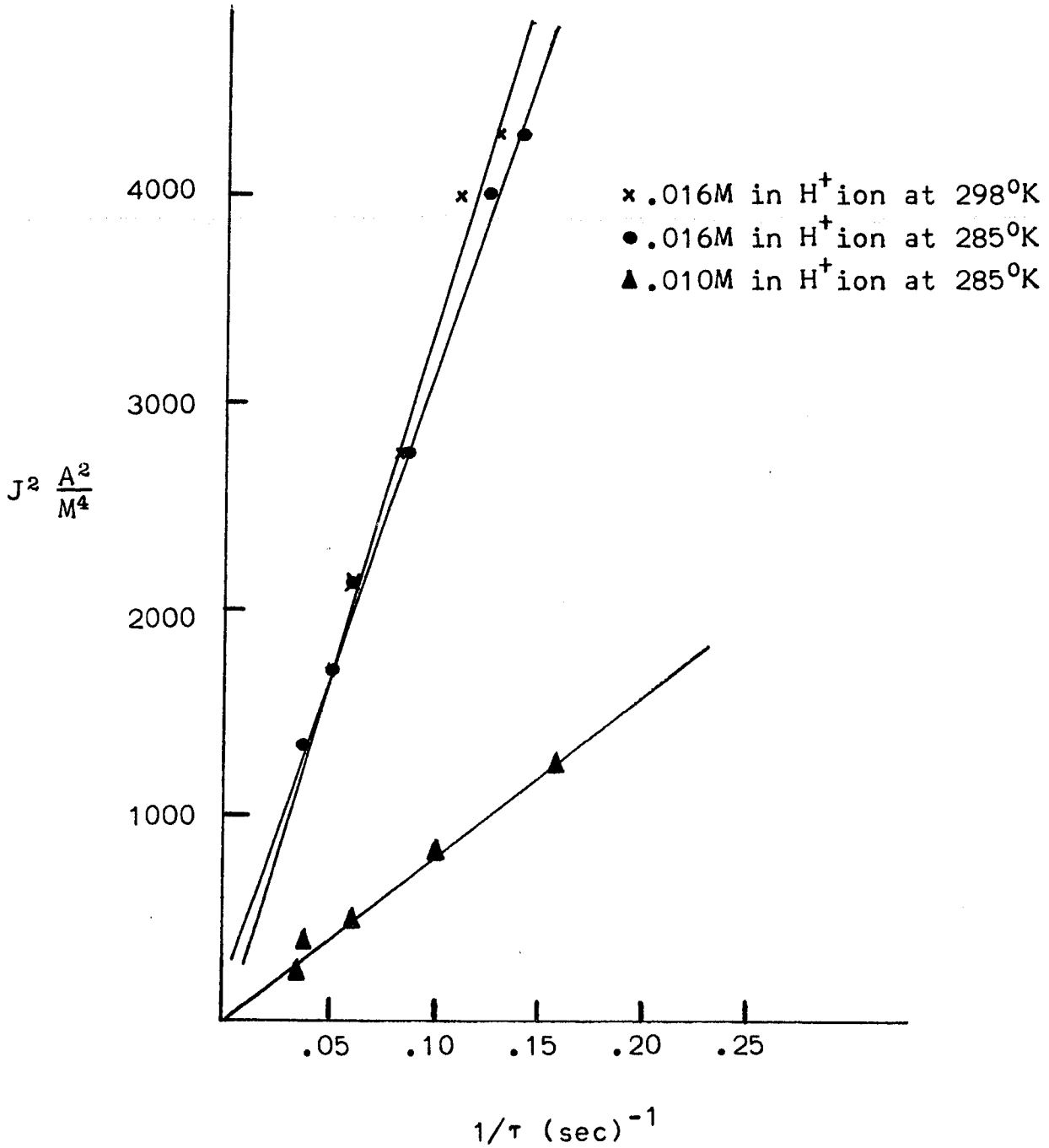

Figure 43

A Plot of Flux Squared vs Reciprocal Transition Time for H_3PO_4 (.021M in H^+ ion)

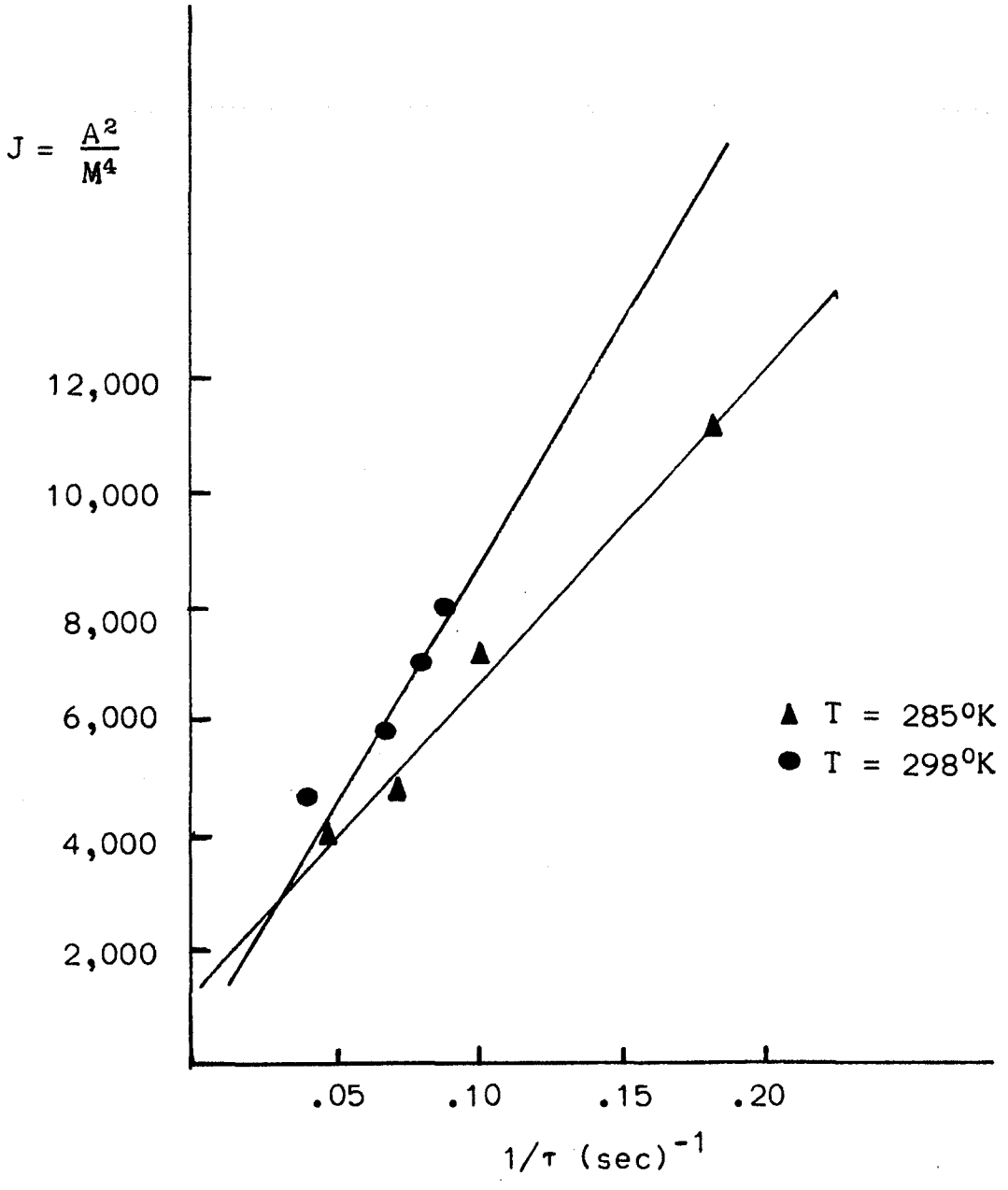

III Voltage-Time (at steady state)

When steady state is reached with the 11KΩ resistor between the two measuring electrodes (see Fig. 4- switch I closed), removing this resistor results in an increase in voltage until a new steady state associated with having no 11KΩ resister between the measuring electrodes is obtained (Fig. 4- switch S 1 open). Similarly, if we reinsert the 11KΩ resist r between the electrodes, the voltage will decrease until the steady state associated with having no 11KΩ resistor is attained. Measurements of these voltage changes were made over all concentrations of Na^+ ion and H^+ ion at 285°K, 298°K and 313°K. There is often an initial, sharp voltage found - at times ~0.5 sec after the current is applied. This is due to the measuring electrodes themselves and is, therefore, ignored. After this short time interval (~.5 sec), the voltage remains constant if no membrane is in the cell.

All the fluxes used were above the C.C.D. Figures 44-46 show a number of runs at various ionic concentrations and temperatures. In all photographs, as the voltage moves toward the bottom division it is increasing, as it moves toward the top it is decreasing.

At the same C, T and J, the voltage decrease is always more rapid than the voltage increase. An example of this can be seen in Fig. 44. Figures 45a and 45b show a series (all the

Voltage-Time Curves at Steady State

1) curves were obtained in H_3PO_4 and Na_2HPO_4 solutions
2) membrane used was Ionac MC-3142
3) In all photographs, the voltage increases as we move toward the bottom of the graticule and decreases as we move toward the top of the graticule.
4) Increasing voltage means that switch1 in Fig. 4 is opened at time zero.
5) Decreasing voltage means that Switch 1 in Fig. 4 is closed at time zero.

Fig. 44 .010 Na^+ at 25°C, 0.500 volts/div, 1.5 sec/div

Run No.	J(A/M^2)	
1	15.3	} 11K Ω in → 11K Ω out
2	25.5	
3	15.3	} 11K Ω out → 11K Ω in
4	25.5	

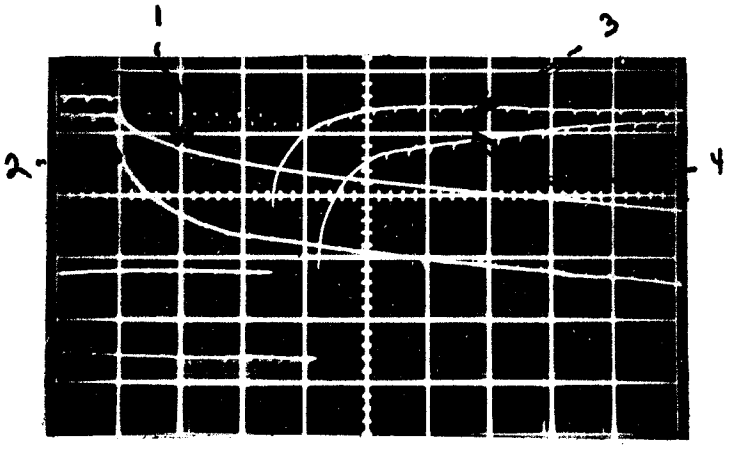

Fig. 45 .021 H^+ at 12°C, 0.500 volts/div

a) 1.5 sec/div

Run No.	J(A/M^2)
1	84.0
2	71.3

b)

Run No.	J(A/M^2)	Time(sec/div)
1	96.8	3.0
2	120.	7.5
3	153.	7.5

a)

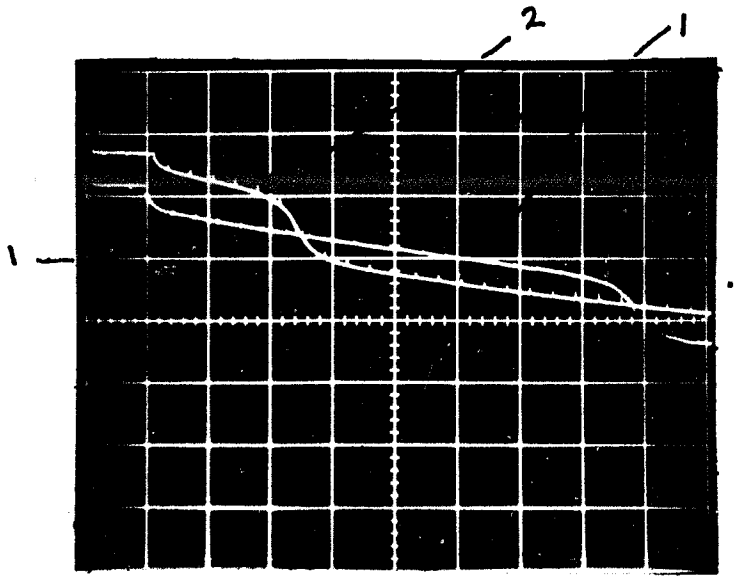

b)

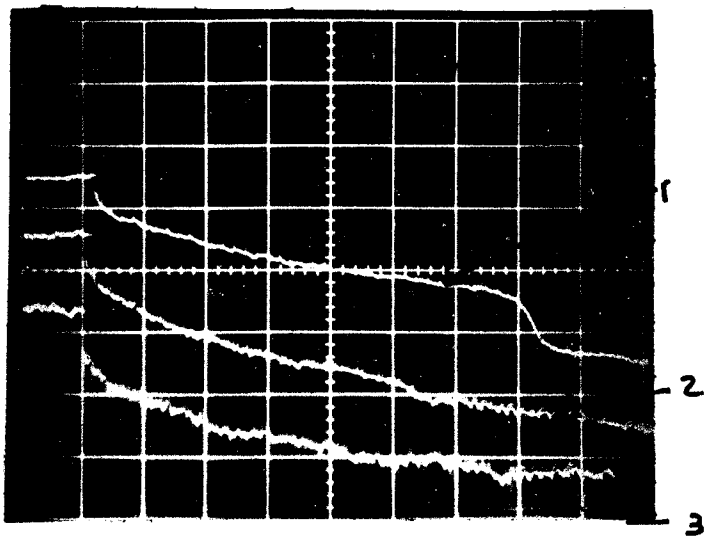

Fig. 46 .040 Na^+ at 25°C, 0.500 volts/div, 1.5 sec/div

a) Run No	$J(A/M^2)$	b) Run No	$J(A/M^2)$
1	86.6	1	127
2	56.0	2	102
3	56.0		

a)

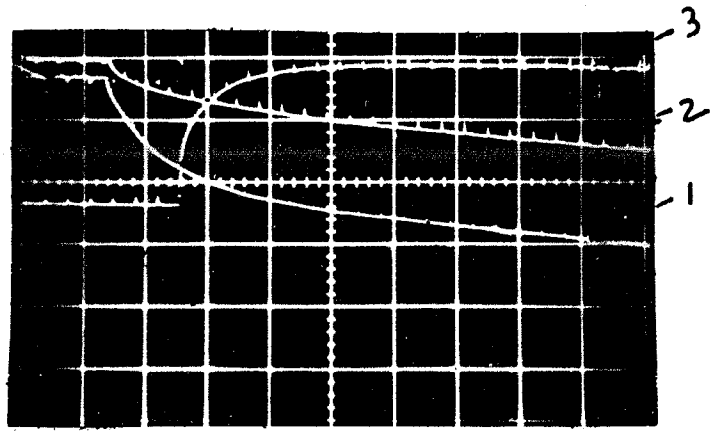

b)

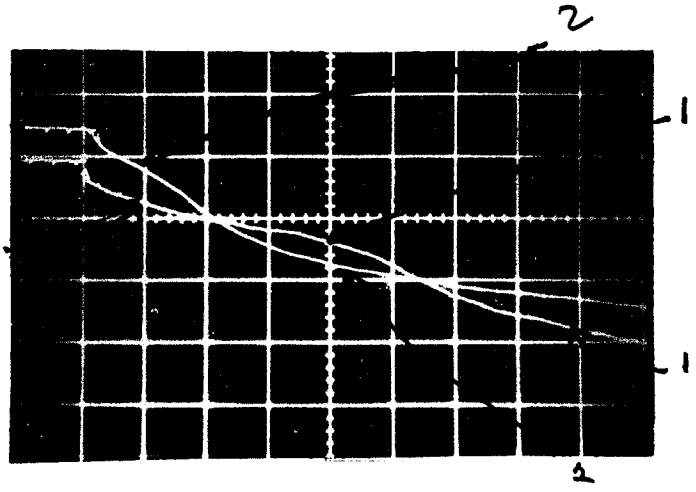

runs were taken at the same C and T) of voltage-time curves that were obtained when the 11KΩ resistor was removed from the system. In each run the voltage increases. At fluxes of 71.3 $^{A}/_{M^2}$, 84.0 $^{A}/_{M^2}$ and 96.8 $^{A}/_{M^2}$, the voltage increases in three stages. We shall refer to this type of three-stage curve as an "S-shaped" curve. Each of these "S-shaped" curves characteristically shows a slow increase in voltage followed by a rapid increase in voltage which is, in turn, followed by a slow increase, until steady state is reached. The time at which the sharp voltage increase takes place will henceforth be called t_B. With increasing flux, it takes more time until the rapid voltage increase begins (t_B increases). Eventually, if the flux is large enough, the "S-shaped" curve is lost and the voltage increases at the initial rate until steady state is reached. "S-shaped" curves can be found for all concentrations of both Na^+ ion and H^+ ion at all temperatures. Fig.46a shows that the magnitude of the flux can be too small to obtain an "S-shaped" curve (see fluxes 56.0 and 86.6 $^{A}/_{M^2}$). It is only at the larger fluxes of 102 and 127 $^{A}/_{M^2}$ (see Fig.46b) that the "S-shaped" curve appears. However, with a still larger increase in flux, the "S-shaped" curve is lost once again. The attainment of an "S-shaped" curve at a given ionic concentration and at a given temperature depends on finding a flux above the critical current density that falls in an appropriate flux range. The Na^+ ion and H^+ ion "S-shaped" curves

differ in that the change in the rate of voltage rise at the break time is sharper in the H^+ ion case.

Table 16 lists the break time (t_B) found in the "S-shaped" curves at various concentrations, temperatures and fluxes. Plots of t_B vs J (Figures 47 through 51) show that a linear relationship exists between flux and break time. The slopes of these plots increase with T but appear to be nearly independent of C.

Figure 47

Break Time vs Flux in Na_2HPO_4 (.010M in Na^+ ion)

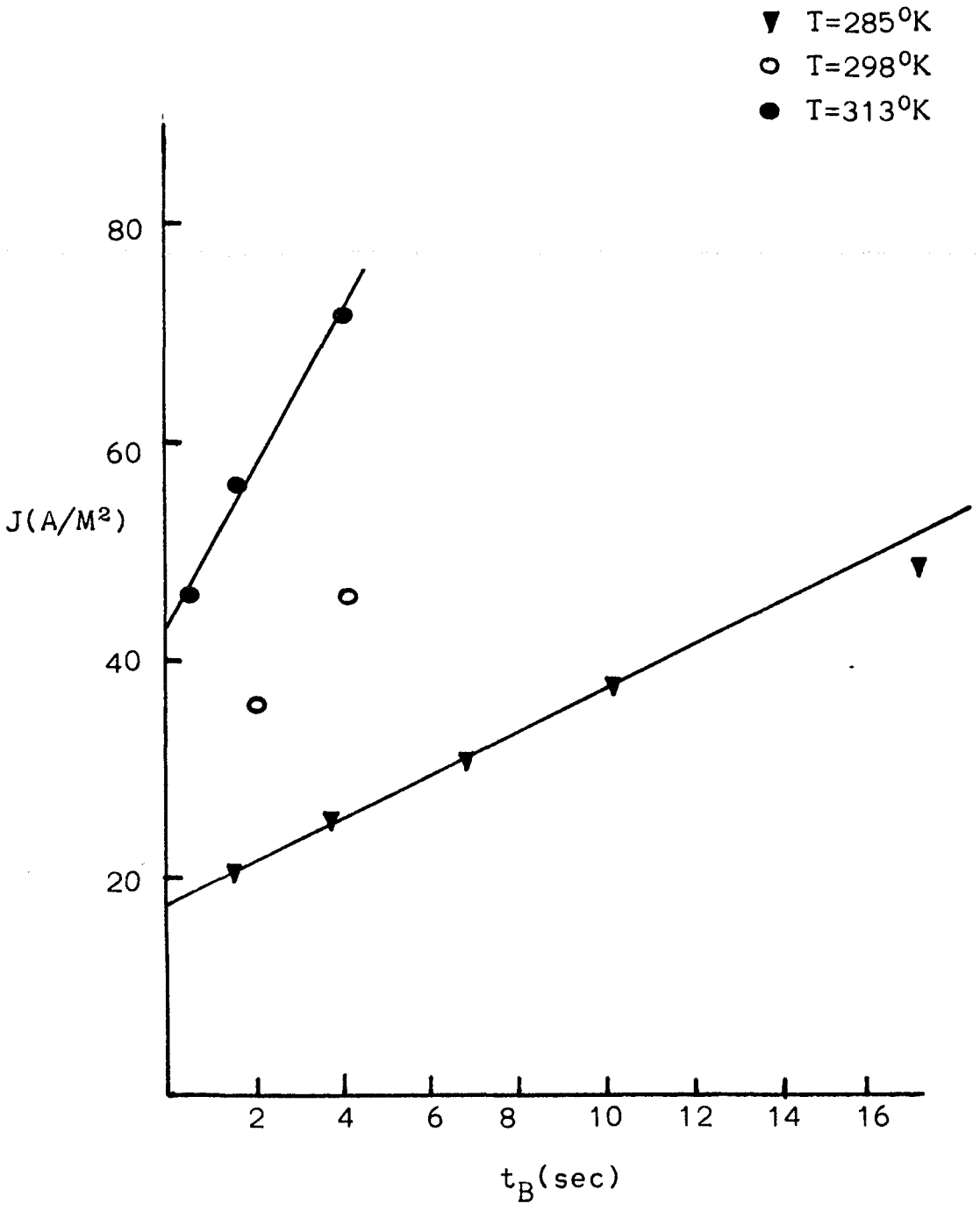

Figure 48

Break Time vs Flux in Na_2HPO_4 (.020M in Na^+ ion)

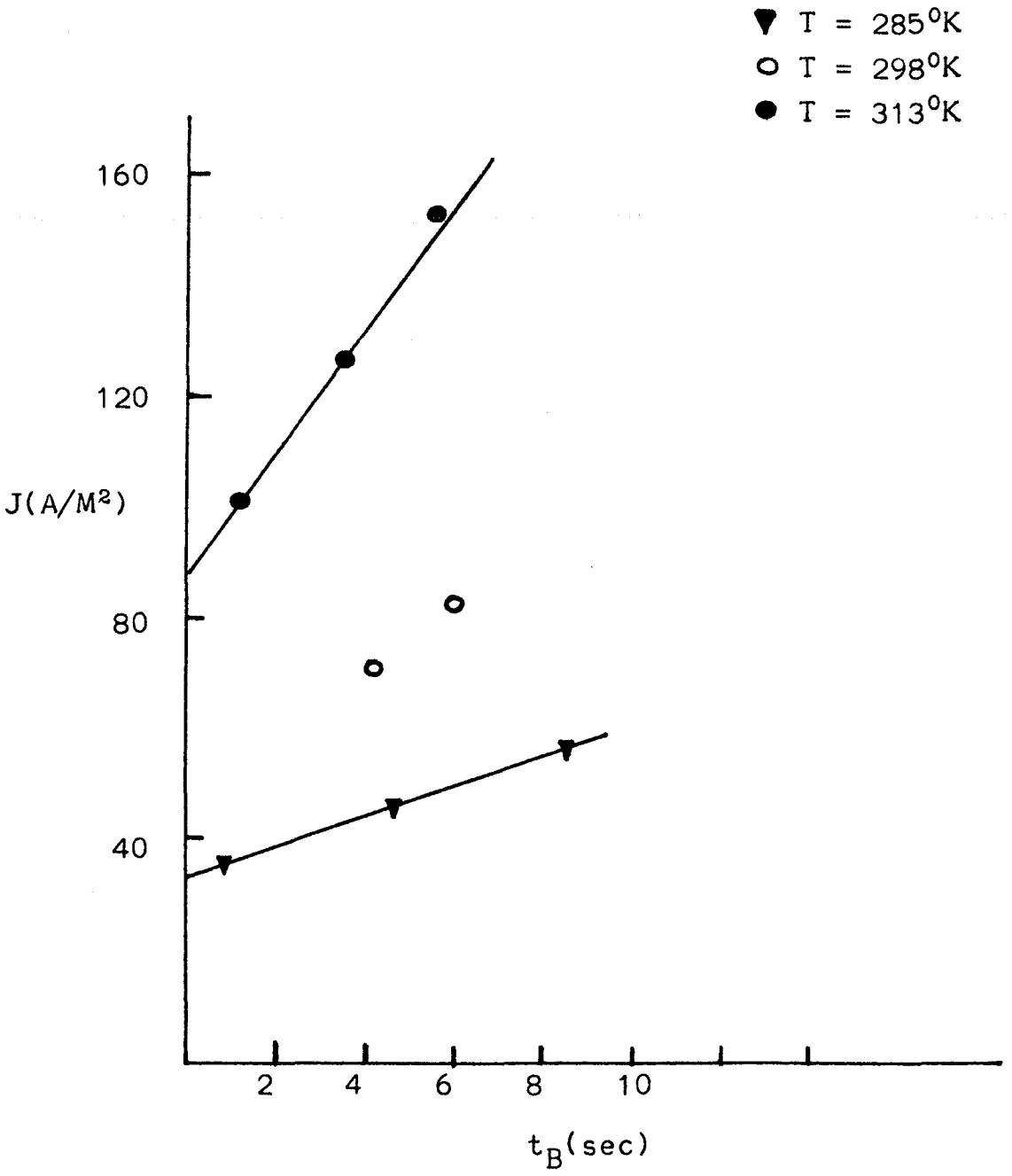

Figure 49

Break Time vs. Flux in Na_2HPO_4 (.040M in Na^+ ion)

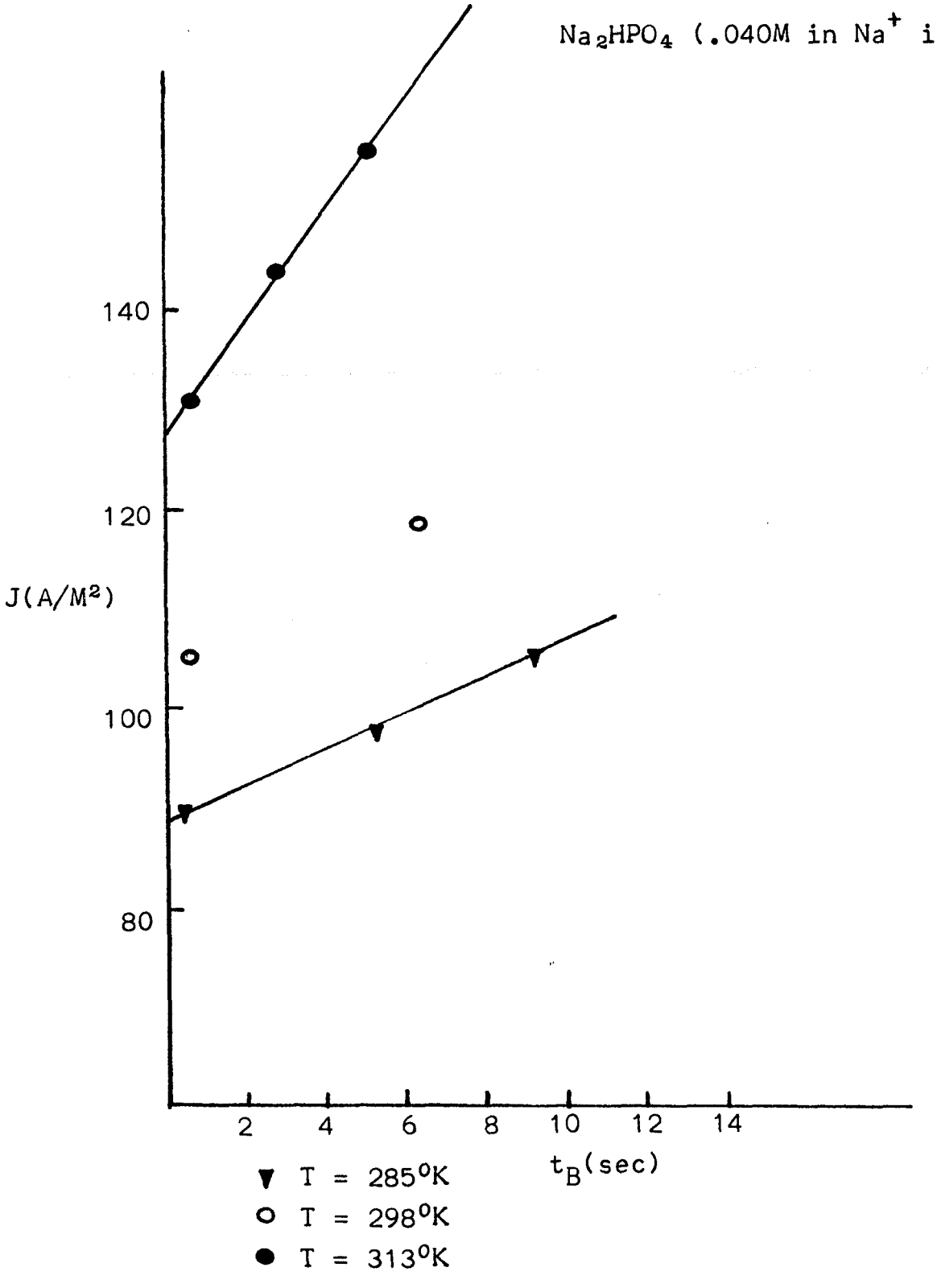

Figure 50

$\frac{dJ}{d(t_B)}$ as a Function of the Concentration of H^+ ion in H_3PO_4 at 285°K

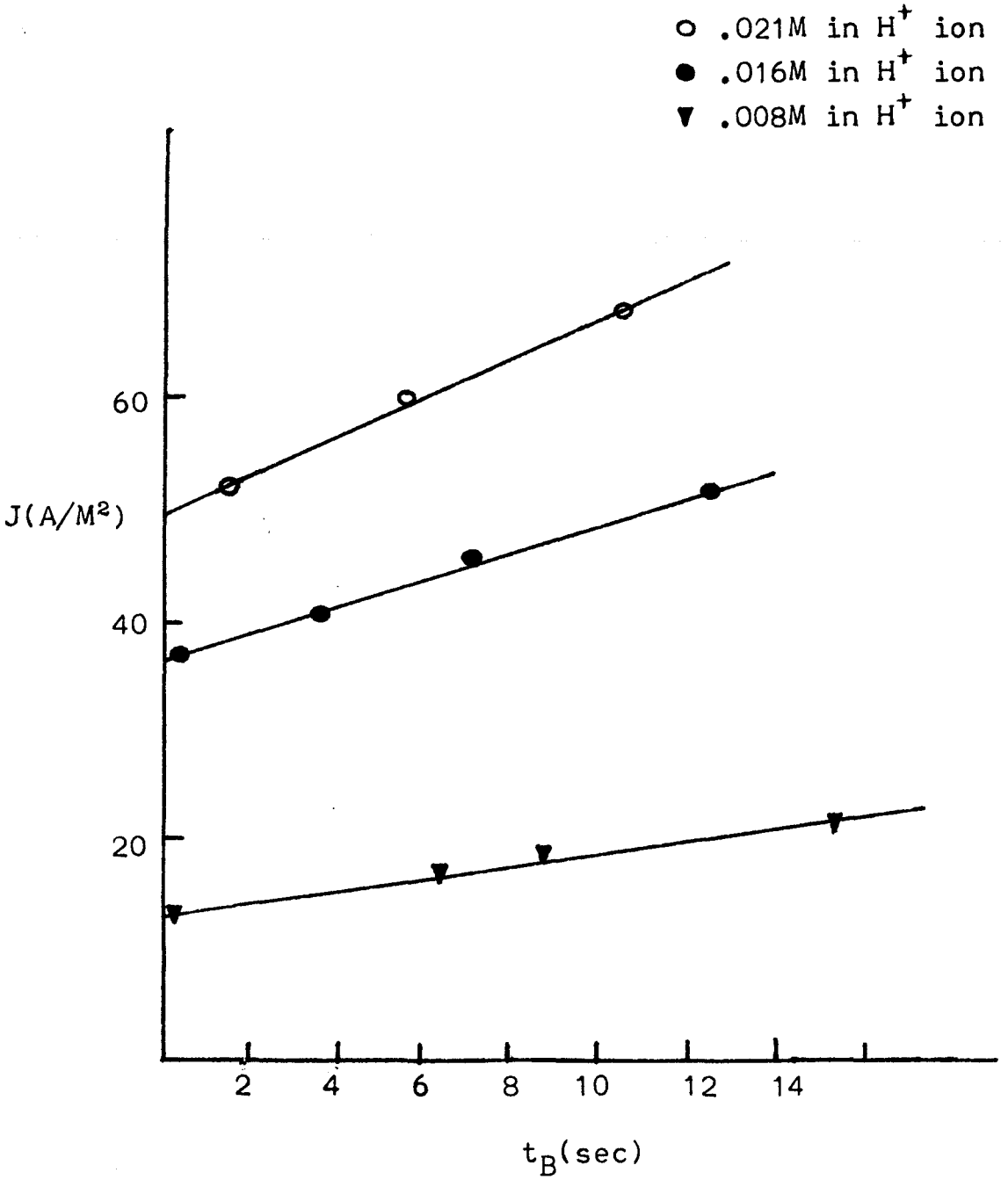

Figure 51

$\frac{dJ}{d(t_B)}$ as a Function of the Concentration of Na^+ ion in Na_2HPO_4 at 285°K

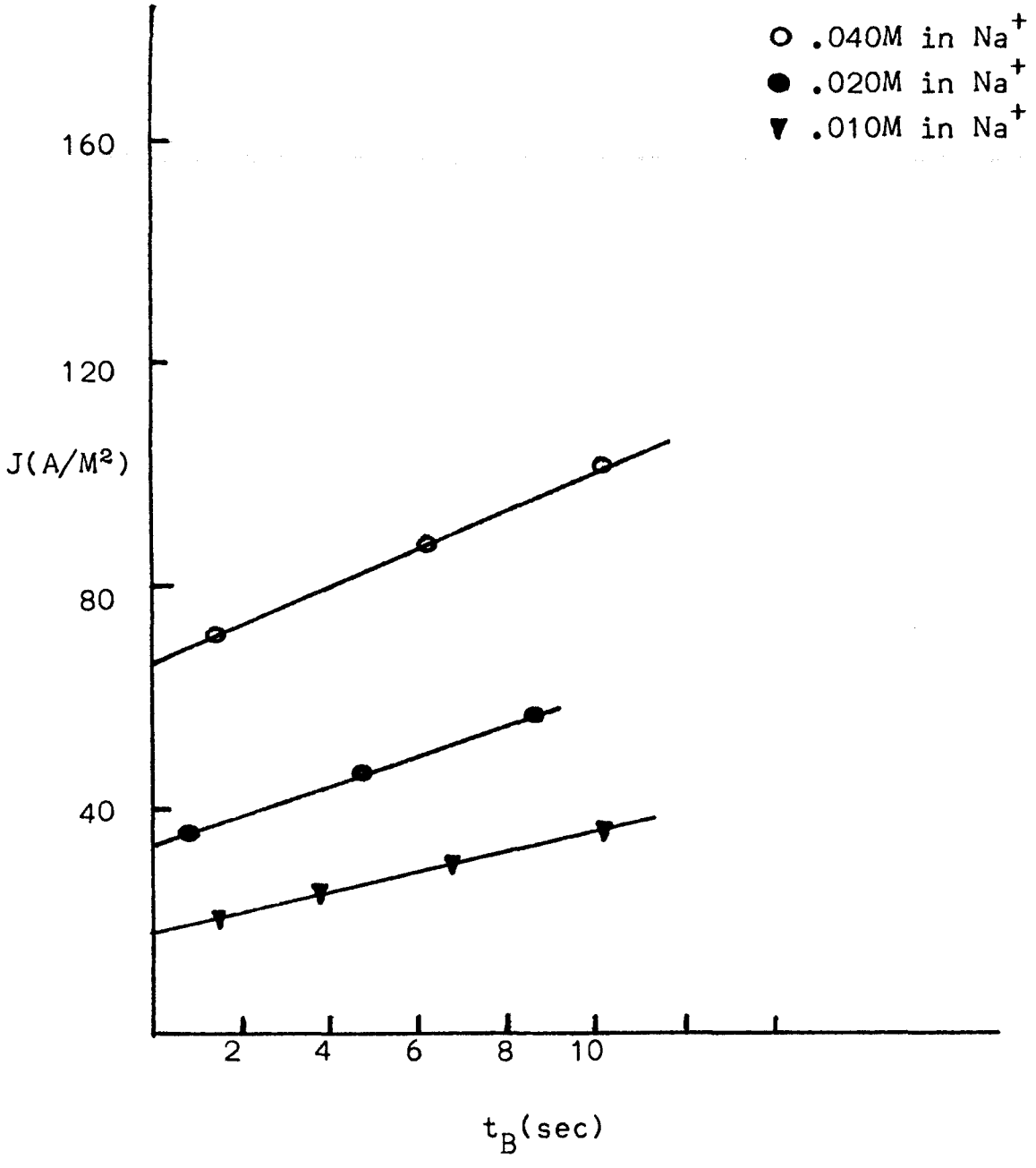

DISCUSSION

Two C.C.D.'s - Two Noise Sources

Earlier work published by Yafuso and Green presented considerable evidence that the attainment of a measureable amount of noise is dependent on the formation of the depletion layer.[10,11] They were able to show that the time needed to form the depletion layer, at a given flux, was the same time that was needed (after the current was turned on) until a measureable amount of noise was obtained. They further showed that a large increase in noise with increasing flux took place directly above the C.C.D., the C.C.D. being the lowest flux at which the depletion layer is formed.

Yafuso and Green were aware of only one noise source, that noise source being dependent on the formation of the depletion layer. They were also aware of only one C.C.D. This investigation has shown that there are, in fact, two distinct noise sources and two distinct C.C.D.'s.

The accepted definition of the C.C.D. would be that it is the lowest steady state flux at which the concentration of counterion at the membrane surface on the diluate side of the external solution will reach its minimum, perhaps 10^{-7}m H^+ or OH^-. This definition assumes that the concentration of counterions at all points on the membrane surface are always identical.

This investigation has shown that there is a flux region below the accepted C.C.D. at which only part of the membrane will be fully depleted. We shall refer to the lowest flux at which the entire membrane surface concentration of counterions is ~zero as the 2nd C.C.D. Our "new" or first C.C.D. will be the flux at which any part of the membrane surface is fully depleted. Support for this has been found in the work of Cooke.[7,8] He found that the counterion concentration at the outer circular edge of the membrane could be ~zero, while the inner portion is still not fully depleted. Cooke's work was published in 1961. Since that time, other published work in electrodialysis (with the exception of Sata et al in 1969[6]) seems to have ignored the possibility of having two C.C.D.s.

Voltage-time data (Figures 18 to 25) show that the membrane resistance remains constant until time τ. At time τ there is a sharp increase in V_B(11Kin), V_T(11KΩin) and V_T(11KΩout). (See pages 77-84). It appears that the increase in V_T(11KΩin and out) is due to the formation of a partially depleted region at the membrane surface. That is, the interfacial concentration reaches a value of ~zero at the outer circumference of membrane surface with the resultant creation of a depleted region in the external solution. The increase in V_B(11KΩin) at times after τ suggests that charge is beginning to leak off the membrane surface.

In many problems in interfacial phenomena, one encounters charged species near an interface.[42] The initial negative voltage drop in the 11KΩin case suggests that such a charge layer is built up during the time interval t = 0 to t = t" where $0 < t" < \tau$ (see page 99). The field intensity outside of any charged conductor is given by the equation:

$$E = \frac{\sigma}{\epsilon} \qquad (26)$$

where:

E - the field outside the charged conductor

σ - the charge per unit area on the surface of the conductor.

ϵ - permittivity of the dielectric

The field outside an infinite plane charged conductor is perpendicular to the surface and its intensity is independent of distance from the plane of surface charge.[43] This approximation (∞ surface) is adequate here.

The dielectric coefficient of material between two charged plates is:

$$K = \frac{C}{C_o} \qquad (27)$$

where K - dielectric coefficient

C - capacitance with the dielectric between the plates

C_o - capacitance with a vacuum between the plates

The permittivity is given by the equation

$$\epsilon = K\epsilon_0 \qquad (28)$$

where

ϵ_0 - permittivity of free space

Equation 26 can now berewritten as

$$E = \frac{\sigma}{K\epsilon_0} \qquad (29)$$

The field in the bulk solution will be

$$E_{BULK} = \frac{\sigma}{78(8.85 \times 10^{-12})\ f/m} \qquad (30)$$

The dielectric constant of 78 (25°C) is that of pure water. The water in this region is characterized by a high degree of cooperative orientation among neighboring molecules. The dielectric constant of water right at the membrane surface is quite different, however. The membrane surface can be considered to be made up of long chain polymers which have numerous charged sites on them. If the charges are in a configeration such that only water could be between them, then at most a few water molecules will be able to squeeze between the two negative charge sites. Any such water molecules would be unable to orient in an electric field. In view of this situation, Rice and Nagasawa[44] chose a value of 5.5

for the local dielectric constant. Thus we shall say that the field at the surface is:

$$E_{SURFACE} = \frac{\delta}{5.5\,(8.85 \times 10^{-12})\ f/m} \qquad (31)$$

The distance from the surface to the positive measuring electrode in the bulk solution is ~ 1mm. The measured voltage drop divided by this distance will give us the difference in field between the surface and the bulk solution. Therefore, we can write

$$E_{SURFACE} - E_{BULK} = \frac{\Delta V}{1\,mm.} \qquad (32)$$

where

ΔV = measured initial voltage drop

Subtracting equation 30 from equation 31

$$\delta = \Delta V\left(-52.2 \times 10^{-9}\right) \frac{COUL}{METER^2} \qquad (33)$$

Table 12, gives the relationship between the flux and the voltage drop measured at the inner electrode in the Na_2HPO_4 case. The values for H_3PO_4 are not shown since it was difficult to measure accurate ΔV values from the photographs. Plots of J vs ΔV in Figures 35 and 36 show that a linear relationship exists between the voltage drop during charging

and the flux. This tells us that at a given concentration of Na^+ ion and at a given temperature a constant increase in flux results in a constant increase in the charge on the membrane surface. Because a net asymetry charge exists in solution before the current is turned on, what we have actually measured is a difference between surface charge and this charge. The charge due to the depletion of ions need not be considered since there is no significant depletion before time τ. Surface charge calculations taking both the net asymetry charge and a non-infinite surface into consideration would be a complicated and difficult problem if not an impossible one. Nevertheless, the simple Gaussian Theory employed in our charge calculations does give us a rough order of magnitude of surface charge and more importantly, it does tell us how the surface charge depends on the flux.

Apparently, the initial negative charge built up on the membrane surface can not be maintained with an 11KΩ resistor between the measuring electrodes. As positive ions are depleted from the membrane surface, the large negative charge leaks through the 11KΩ resistor. V_B (11KΩ in) will continue to increase, i.e., charge will leak off the surface, until such time as the entire surface has an interfacial counter-ion concentrate of ~ zero after which V_B (11KΩ in) remains constant.

We mentioned earlier (page 85-87) that "in condition II", while V_B(11KΩ in) increases after time τ, V_T(11KΩ in) increases for a short period of time only and then goes into a "plateau" region. At the same time that V_B(11KΩ in) attains a constant value, V_T(11KΩ in) begins to increase once again and does so until steady state is reached. This suggests that the end of the "plateau" (page 86) marks the second C.C.D.(i.e., the entire membrane surface is fully depleted). The increase in voltage from this point to its steady state value would then be due to further depletion in the external solution, not on the membrane surface. As the number of ions decreases, the voltage and resistance increase. The V_T(11KΩ in) voltage increase between time τ and the beginning of the plateau is due to surface depletion over part (the circular edge) of the membrane. Thus the plateau has separated in time the first and second C.C.D. The beginning of the plateau marking the end of the first C.C.D., the end marking the end of the second C.C.D.

At the same C, T and J values, the beginning of the "plateau" in V_T(11KΩ in) occurs at the same time as the formation of a "bump" in V_T(11KΩ out). After the "bump" and "plateau" have both ended V_T(11KΩ in) and V_T(11KΩ out) increase at the same rate until steady state is reached. The "bump" is completed more rapidly than the "plateau", however. This indicates that the time interval between the first C.C.D. and second C.C.D.

is larger in the 11KΩin case. This happens because depletion of ions at the membrane surface is limited by the rate at which the charge can leak off the membrane. In the 11KΩ out case, there is initial charge buildup before time τ on the membrane surface and no resistor of value comparable to 11KΩ for charge that might be on the surface to leak through. The fact that $\frac{dV_T\ (11K\Omega in)}{dt} = 0$ for a portion of the V_T(11KΩ in) curve suggested that the voltage increase due to the depletion of ions at the surface is balanced by the voltage decrease due to charge leakage.

At low C, high T and low J, the V_T(11KΩout) curves have a smooth transition between times τ and steady state. Under these conditions ("condition I"), a second C.C.D. is hardly noticeable. At high J, low T and high C, V_T(11KΩin) resembles V_T(11KΩout) from time τ until steady state. The plateau becomes increasingly shorter as J increases, T decreases and C increases, and eventually disappears and the time span between initial and complete counterion concentration of ~ zero at the surface approaches zero in both 11KΩin and 11KΩout case.

Green and Yafuso's[10,11] power spectra were recorded at fluxes above the second C.C.D. The spectra they obtained for HCl solutions had a similar frequency dependence to those found for H_3PO_4; however, the f_B values extended almost a full decade higher, at comparable fluxes above the second C.C.D., in the HCl case. The "new" noise source, with its $f^{-1.5}$

dependence was never seen in the HCl spectra. The possible reasons for this are:

1) It could have been overlooked. The "new" noise source is of very small magnitude just above the level of background noise and exists in a very narrow total noise region. This would make it somewhat difficult to find if one weren't looking.
2) In their investigation, elaborate shock mounting was not undertaken. In this work, a great deal of care was taken to "shock mount" the box when the phosphoric acid and Disodium hydrogen phosphate power spectra were taken. Without this "shock mounting" mechanical oscillations in the system which result from walking or talking in the laboratory would have interfered with the measurement of the low-noise spectra to the point that the measurement of such spectra would have been impossible.
3) The "new" noise source may be dependent on having phosphoric acid or Disodium hydrogen phosphate in lieu of hydrochloric acid. The major difference between the phosphoric acid or sodium hydrogen phosphate system and the hydrochloric acid system is that hydrochloric acid can depend only on the dissociation of water (equilibrium constant $\sim 10^{-14}$) for an additional source of ions.

In contrast, the phosphoric acid system has its first and second equilibria as sources of ions and the Disodium hydrogen phosphate has the first, second and third equilibria of phosphoric acid as sources of ions. The equilibria constants of phosphoric acid are:[45]

1) $H_3PO_4 \rightleftarrows H^+ + H_2PO_4^-$ $\quad K_1 = 7.25\times10^{-3}$ moles/l

2) $H_2PO_4 \rightleftarrows H^+ + HPO_4^=$ $\quad K_2 = 6.28\times10^{-8}$ moles/l

3) $HPO_4^= \rightleftarrows H^+ + PO_4$ $\quad K_3 = 2.2\times10^{-13}$ moles/l

The existence of two C.C.D.'s was first noticed when it was found that the lowest J values at which noise appeared at each C and T (J_N) were always slightly less than the flux (J_{VT}) needed to see depletion at the same C and T on the voltage-time curves (see Table 17). This is good evidence that our first noise source exists in a flux region below which the membrane is not fully polarized at all points. Although the "new" noise is small compared with the second noise source at fluxes above the second C.C.D., it remains essentially unchanged at these fluxes in both phosphoric acid and Disodium Hydrogen Phosphate solutions. For example, in .060 Na^+ at 313 ^oK, J = 116 A/M^2 (Fig. 7) and in .016 H^+ at 283^oK at J = 395 A/M^2 and 332 A/M^2 (Fig. 6), the slopes at high frequency still have $f^{\sim1.5}$ frequency dependence. This suggests that the noise processes originating at the first and second C.C.D. are independent of each other. Fig. 52 is a schematic representation of this fact. This suggests two possible transport schemes;

Figure 52

A Representation of the Two Noise Sources and Two C.C.D.'s - Total Noise as a Function of Flux

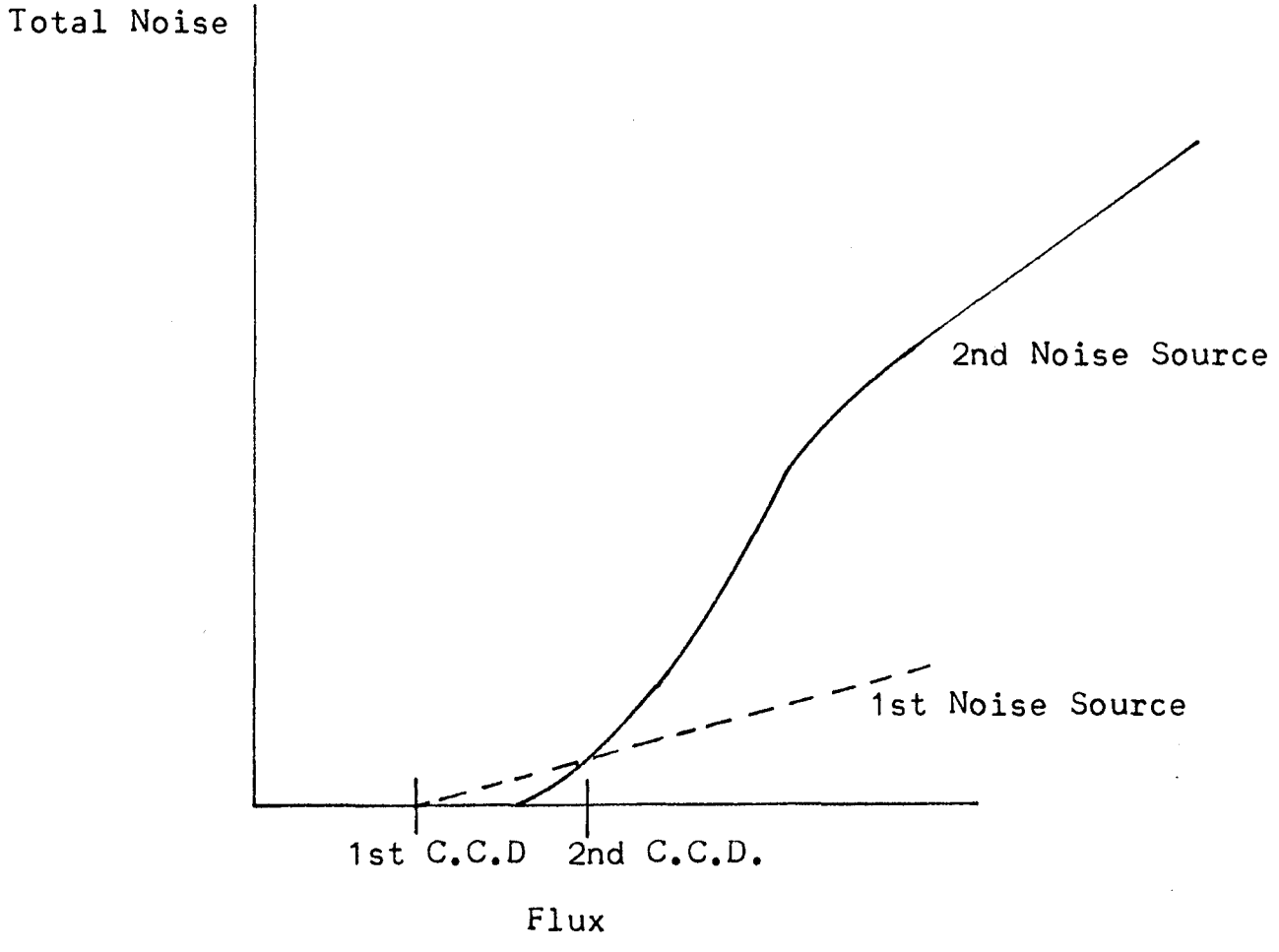

The noise at J_N, although only a few dB above background is sufficient to measure a spectrum; it is inevitably a diffusion spectrum. (See Fig. 9). At fluxes greater than or equal to J_{VT}, the break in the chronopotentiometric curve occurs and high density type spectra are clear; then the total noise is at least two orders of magnitude greater than background. There is a dramatic increase in total noise with increasing J when J is greater than J_{VT}.

Further analysis of the effect of flux on total noise (Table 2 and Fig. 9) reveals that there are only a few cases where the total noise falls between 25 uv and 200 uv. Spectra in this intermediate region are rarely found with H^+ ion. The Na^+ ion shows fewer representatives of pure diffusion spectra, but there are more Na^+ ion spectra in the intermediate region. In both cases there is a clear transition between high and low noise spectrum. This type of transition is strong evidence for the existence of two kinds of noise sources and therefore, two mechanisms of flux maintenance. One is diffusion, at the lower values of flux, the other is almost certainly associated with bulk flow of solution. We shall present considerable evidence, which will be discussed in detail, as to why we believe that bulk flow of solution is our second noise source. Our argument shall be based on the following:

1) "Abnormal Effects" at high flux that can only be explained by bulk flow of solution.
2) The inadequacy of the present theories of high flux maintenance.
3) The existence of enough energy in solution to create a turbulent situation.
4) Observations of solution turbulence in electrodialysis with Schlieren optical equipment.
5) Tchen's theory of plasma turbulence.
6) Bulk flow of solution can account for high flux maintenance.

The power spectrum of total noise above 200×10^{-3} is dominated by the second noise source. For H^+ ion we find f^{-a} to f^{-b} frequency dependence, for Na^+ ion an f^{-x} to f^{-y} dependence. In Fig. 7 (.02 Na^+ at 283°K) at a flux of 25 A/M^2, we see that the second noise source completely dominates the power spectra, yet the total noise is only 8×10^{-3} mv. In both H^+ ion and Na^+ ion spectra, particularly the latter, the power spectra show some dependence on the second noise source at fluxes below the second C.C.D. (that flux characterized by a dramatic increase in total noise). For instance, a f^{-b} or f^{-y} dependence at low frequency is not uncommon at total noise values near 25×10^{-3}mv (see Table 2 and Fig. 9). This indicates that the second noise source is not directly dependent on having a completely depleted membrane surface but that when such is the case, a dramatic increase in noise occurs.

Alternative Theories of Flux Maintenance

It is known that in high fields the equilibrium constants of weak electrolytes will shift so that more ions are formed.[46] Water dissociation in the high field region in the diluate solution external to ion-exchange membranes is often the most accepted mechanism for maintenance of high flux currents. It is assumed in this theory that additional H^+ and OH^- ions will form with increasing flux and carry the additional current. Sata et al[6] rule out water dissociation as an important part of flux maintenance by pointing out that in an electric field of 10^4V/cm, the dissociation constant of water will increase by only 1%. Yafuso and Green,[10,11] on the other hand, showed that if the electric field is as high as 10^6V/cm there would be a significant increase in the dissociation constant. They argue that fields of such magnitude do exist in the external solution.

The basic argument against the water dissociation theory is that the expected pH change resulting from having the newly formed H^+ ions carry the current is not found in cation-exchange membrane electrodialysis.[5,6,7,8,9,47,48,49] With anion-exchange membranes, the transport of OH^- would produce an opposite pH change. It is found that for some anion exchange membranes the expected pH change occurs, whereas for others it does not.[5] This is strong evidence that water dissociation can only explain high flux maintenance in certain anion-exchange membranes.

In other type anion-exchange membranes and in cation-exchange membranes it cannot. The anion-exchange membranes where the expected pH change occurs have current-voltage curves where the voltage levels out to a constant value with increasing current.[5] The other type membranes have current-voltage curves much like the one shown here with the MC-3142 membrane and Na_2HPO_4 solution .05M in Na^+ ion (see Fig 53). Since the voltage rises to much higher values with membranes of this type, it suggests that these membranes have more efficient current carrying systems.

PH changes, therefore dissociation, not being adequate to explain high flux transport, alternative current carrying mechanism were postulated to take place simultaneously with water dissociation and H^+ ion conduction (cation-exchanger membrane). Peers[48] believed that some of the excess current was carried by co-ions. The transport of co-ions is normally, at most, a few percent in commercial ion-exchange membranes. However, he suggested that under high flux the value might increase. Experimental verification of high co-ion transport has not been found and many investigators have found conductance by co-ions to be a negligible factor under all experimental conditions.[5,7,8] It has been postulated that electroosmotic solvent flow could carry ions across the membrane. This transference usually goes in the same direction as the counter-ions[14] and might supply some of the excess current. However, at all concentrations electroosmotic flow

Figure 53

Current vs Voltage Curve for Na_2HPO_4 (.05M in Na^+ ion) at 298°K

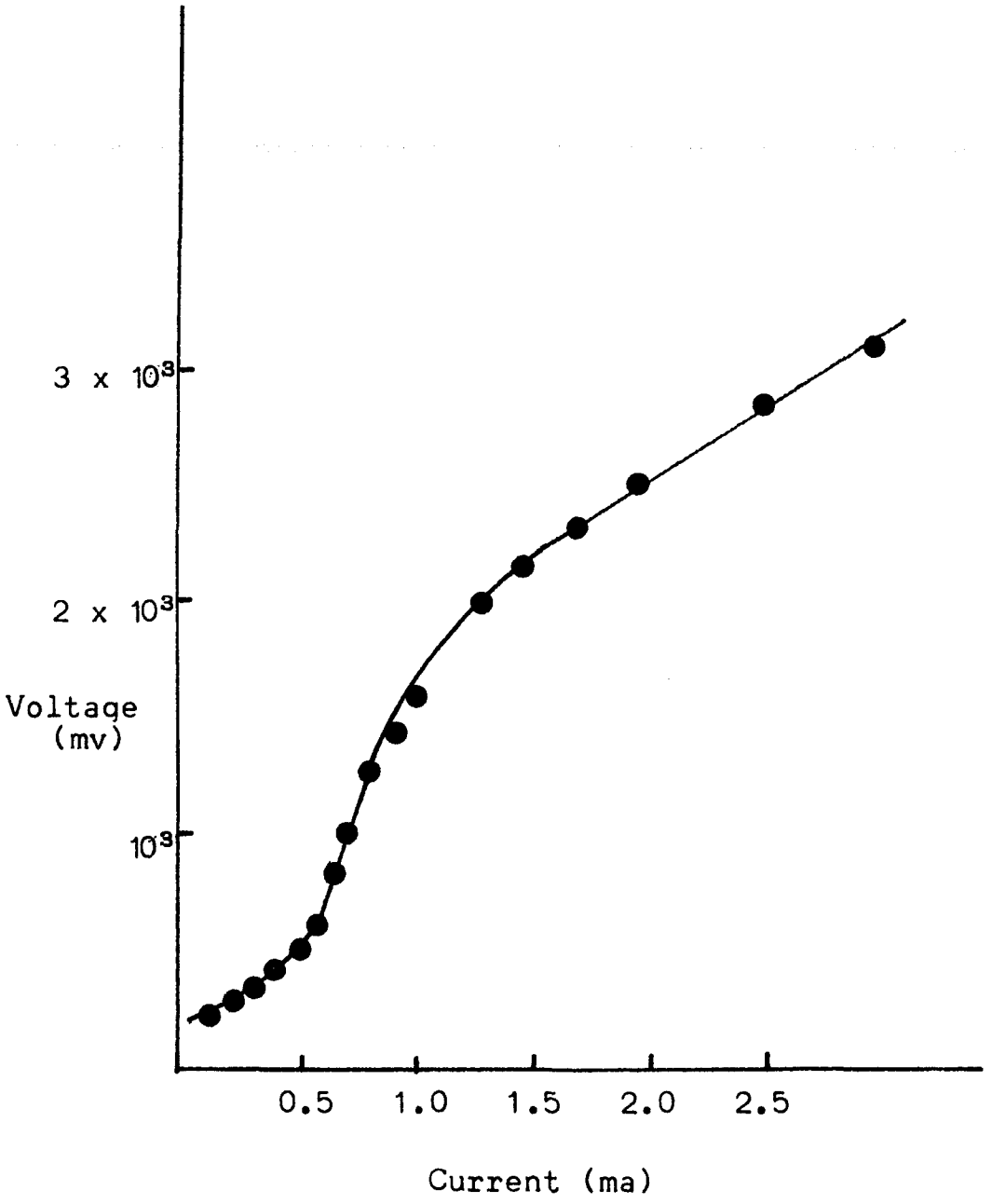

has been found to play no more than a minor role in transport of current.[5,9]

A wide variety of cation-exchange membranes electrodialysized in .01 NaCl at high flux well above the C.C.D. (660 A/M^2) showed at most 6% of current obtained in the form of H^+ ion transport.[5] This has led some investigators to talk of a breakdown in the efficient H^+ ion conduction mechanism, others of a suppression of water dissociation.[7,8,28] Cooke postulates that this suppression is due to an ion-solvent interaction. The interaction between a cation and the immediately neighboring water molecules is seen as the cause of a breakdown of the normal spatial relationships of the dipoles of water. He then goes on to say that as a result of this water loses its strong ionizing power. Block[5] postulated that hydrophobic groups on the surface of the membrane block the Grotthus chain structure of water and thereby deprive H^+ ions of their high mobility.

Additional Evidence of Turbulence

In large scale desalination as well as in many electrodialysis studies, the diluate solution is vigorously stirred.[50] This artificially created disturbance causes the concentration gradient to increase. From Fick's first law considerations, stirring would by increasing $\partial c/\partial x$ (concentration gradient) increase the supply of ions reaching the membrane surface. Similarly, with increasing solution disturbance due to bulk flow of solution, we would expect that $\partial c/\partial x$ would increase and more ions would be able to reach the membrane surface and transport current. At fluxes above the second C.C.D., increases in flux mean increases in total noise and since this is a measure of bulk flow, increasing disturbance of solution. An increase in flux (above the second C.C.D.) is maintained and steady state conditions are stabilized by a concurrent increase in bulk flow which results in an increase in $\partial c/\partial x$. Solution flow can be visualized as the systems own stirring mechanism. When the flux demands become greater, the solution stirs itself with greater intensity. It is reasonable to assume the percentage of co-ions, and solvent molecules at the membrane surface at high flux is greater than what it would be at the C.C.D. and that this percentage increases with increasing flux. This would mean that the transport number of H^+ ion in the cation-exchange membrane would be expected to decrease with increases of flux above the C.C.D. It was just this "abnormal" behavior that has been found.[6]

Block and Kitchener,[5] using Schlieren techniques have observed convection and turbulence in systems similar to ours. One of the membranes they used was MC-3142. They found turbulence only in the diluate layer, with the membrane horizontal and counterions passing upward (conditions favoring stagnation). Under these conditions, Block and Kitchener also observed that chronopotentiometric curves continued to show a rise in voltage after the initial sharp rise upon depletion (at the Sand's Law transition time). Under these conditions, the voltage decreased and no turbulence was observed.

All of our experiments were carried out using vertical mounting for the membrane, with the membrane surface a small part of an infinite plane in contact with solution. This contrasts with Block and Kitchener's geometry, where the membrane surface covered the complete cross section of a tube 1 cm. in diameter. Turbulence could be prevented by making the tube smaller.

In our chronopotentiometric studies with H^+ we found the voltage increased after the Sand's Law transition time, corresponding to cases in which turbulence occurred in Block and Kitchener's work. By contrast, with Na^+, we found a smaller increase and in a few cases a small decrease at currents slightly above the C.C.D. It may well be that in spite of vertical mounting, the other differences in geometry allow for turbulence, at least in the H^+ case.

Tchen's Turbulence Theory

The earths atmosphere is usually in a state of turbulent motion and many theories of atmospheric turbulence have been proposed. Wind velocity, temperature and humidity at every point in space are fluctuating irregularly. Noise measurements of each of the latter variables have been made and spectral densities of the correlation functions plotted.[51]

Dr. Tchen of The City University of New York developed a theory of turbulence in plasma. This theory gives power as a function of the wave vector (P(k)). To convert from spatial to frequency dependence (P(f)), a dispersion relation is required. The dispersion, however, is linear, so that the functional dependence P(f) is the same as P(k). Tchen's theory would predict turbulent noise spectra with three parts, f^{-3} at low frequency, f^{-1} in an intermediate region, and f^{-5} at high frequency. The f^{-1} region exists over a very small flux range. Tchen believes that his theory is applicable in our case.[52] Thus we would expect to find spectra with an f^{-3} dependence at low frequency and an f^{-5} dependence at high frequency.

Slope "b" of the H^+ ion spectrum gets steeper with increasing C (see Fig. 10) and slope "a" gets steeper with decreasing T (see Fig. 12). We find at .008H^+ at 283°K a $f^{-3.07}$ to $f^{-4.74}$ dependence and for .01H^+ at 283°K a $f^{-3.06}$ to $f^{-4.69}$ dependence (see Table 4). Thus Tchen's theory

of plasma turbulence could quite conceivably be applicable to turbulence in ionic solution. The theory depends on a transport equation which has an additional term due to a chemical reaction. In our case this could quite possibly be a dissociation process. Precise information on the application of Tchen's theory to our particular system will have to be left for a later date since the theory is not yet published and the details of it have not been made available to us.

The Na^+ ion power spectrum have slopes of $f^{-2.3}$ to $f^{-2.8}$ (Table 5 We believe that it is also conceivable (Tchen never saw this data) that Tchen's theory could be modified to explain turbulence in Na_2HPO_4 for the following reasons:

1) All of the arguments made previously for the second noise source apply equally well to both H^+ ion and Na^+ ion spectrum.
2) Na^+ ion spectra are steeper than f^{-2} and nowhere in literature has a frequency dependence greater than this ever been reported in a comparable system (including semiconductors)
3) The nearly identical spectrum obtained for the most concentrated H^+ ion spectrum (.021 H^+) and the most dilute Na^+ ion spectrum (.010 Na^+) at 283°K (see Tables 4 and 5) suggests that the transition from H^+ ion type spectra to Na^+ ion type spectra is not a sharp one.

4) The only other possibility for having spectrum with slopes $>f^{-2}$ would be to have a high capacitance exist across the diluate solution in such a way as to effect only the second noise source and leave the first noise source unchanged and unfiltered. This seems unlikely[11] and we have no evidence that such a capacitance of sufficient magnitude exists.

The evidence does not argue as strongly for turbulence in the Na^+ ion case as in the H^+ ion case. The Na^+ spectra are less steep, and do not consist of two straight lines (except 0.01M).

Possible Causes of Solution Turbulence

There are two possible ways of dealing with the causes of solution turbulence. One approach is to consider the system as stable to small disturbances but unstable to disturbances of sufficiently large magnitude. Such a system is considered to be of "hard self-excitation".[5] The second approach would be to consider the system as unstable with respect to infinitely small disturbances. This type of system would be considered to be of "soft self-excitation" or "absolutely unstable". The former approach will be considered first.

The change in pressure occurring in a dielectric fluid subject to an electric field is called "electrostriction". There is electrostrictive pressure in the inner depleted region which arises from the compressive effects of the diffuse layer.[16,54] A general criterion for the creation of turbulence in a "hard self-excitation" system was established by O. Reynolds (1883). This criterion is that bulk flow will remain laminar so long as the Reynolds number (Re) does not exceed the critical value (Re_{cr}), while for $Re > Re_{cr}$ it will be turbulent.[55]

$$Re = \frac{v l}{\eta / \rho_m} \qquad (34)$$

where

v = velocity
l = distance over which the solution is turbulent
η = viscosity
ρ_m = mass density

Re may be defined as the ratio of the values of the inertial and viscous forces. The minimum value needed to produce turbulence ($Re_{cr\ min}$) is ≈2030. With $Re < Re_{cr\ min}$, the flow will always remain laminar, i.e., any disturbance will be damped regardless of its intensity.[56] In order to see whether the pressure gradient established by the field is of sufficient magnitude to produce solution turbulence, we must see if the bulk velocity created by this pressure gradient will result in an Re value greater than 2030.

In the theoretical analysis of the transition of laminar to turbulent flow, we must start from the fact that the velocity and pressure fields in any fluid are solutions of the equations of fluid mechanics.[57] If p is the mechanical pressure in the liquid when it is in equilibrium with the electric volume force F_v, then the mechanical force $-\nabla p$ which is set up as a result of the pressure gradient is equal and opposite to F_v. The pressure gradient at any point within the liquid is given by[58]

$$\nabla p = F_v = \frac{\epsilon_0 \rho_m}{2} \nabla\left(E^2 \frac{dK}{d\rho_m}\right) \qquad (35)$$

where

ϵ_0 = permittivity of free space

E = Electric field

K = dielectric constant of the medium

On integration, with the assumption of a definite equation of state for the liquid, we obtain

$$\int_{P_1}^{P_2} \frac{dP}{\rho_m} = \frac{\epsilon_0}{2}\left\{\left[E_1^2 \frac{dK_1}{d\rho_{m_1}}\right] - \left[E_2^2 \frac{dK_2}{d\rho_{m_2}}\right]\right\} \quad (36)$$

This equation shows how the pressure within a dielectric liquid is a unique function of the electric field at a given point.

If the liquid is incompressible, equation 36 reduces to

$$P_2 - P_1 = \frac{\rho_m \epsilon_0}{2}\left[E_1^2 \frac{dK_1}{d\rho_{m_1}} - E_2^2 \frac{dK_2}{d\rho_{m_2}}\right] \quad (37)$$

For water at 20°C, $d \ln K / d \ln \rho_m$ is very nearly constant over a wide range of pressure, and equal to 1.34 ± 0.02.[59] Thus equation 37 reduces to

$$P_2 - P_1 = \frac{1.34 \epsilon_0 K}{2}\left[E_1^2 - E_2^2\right] \quad (38)$$

If we take the field adjacent to the membrane to be of the order of 10^8 volts/m and the field in the uncharged part of the diffuse layer to be ~0, then equation 38 becomes

$$\Delta p = 4.4 \times 10^9 \frac{kg.}{M \cdot sec^2} \qquad (39)$$

This pressure difference (ΔP) will take place over an area the size of our membrane surface ($3.1 \times 10^{-6} m^2$ for H^+ ion). The ordinary force (F) due to ΔP will be

$$F = \Delta p \times \text{AREA} = 1.4 \times 10^4 \text{ NEWTONS} \qquad (40)$$

The inertial forces which produce mixing of the different volumes of fluid moving inertially with different velocities contribute to the formation of sharp inhomogeneites in flow. The viscous forces, on the other hand, assist in smoothing out small-scale inhomogeneities. The force (F') holding back the flow of liquid is

$$F' = \eta \frac{dv}{dh} \qquad (41)$$

where

η = viscosity

$\frac{dv}{dh}$ = velocity gradient

The force (F) due to Δp must be equal to this retarding force (F') if we are to get bulk flow of constant velocity. Therefore

$$\eta \frac{dv}{dh} = 1.4 \times 10^{4} \text{ Newtons} \qquad (42)$$

$$dv = \frac{1.4 \times 10^{4}\, dh}{\eta}$$

The inner depleted region of the double layer is assumed to be of the order of 100 A^{o}. If turbulence is created initially in this region, the velocity of bulk water flow is

$$dv = \frac{\left(1.40 \times 10^{4} \frac{kg \cdot m}{sec^{2}}\right)\left(10^{-8} m\right)}{10^{-3} \frac{kg}{m \cdot sec}} \qquad (43)$$

$$dv = 0.14 \text{ m/sec}$$

Assuming that the solution is turbulent over a distance of 1mm (the radius of the membrane), and using our calculated velocity, we get Re $\simeq$ 140 from equation 34. If dh in equation was chosen to be 1000 A^{o} instead of 100 A^{o}, Re $\simeq$ 1400. The impreciseness of these calculations does not allow us to state with definite assurance whether ΔP does or does not cause solution turbulence in a "hard self-excitation" system. However, it is unlikely that ΔP will be of sufficient magnitude to cause the needed bulk velocity flow.

High fields produce considerable heating effects [60,61] and a thermal gradient was considered as a source of solution turbulence. The heat energy due to joule heating and the heat of transport of H^+ ion (3100 cal/g°ion) [62] are both approximately equal to 10^{-4} joules/sec. Rough calculations showed thermal effects even less likely to cause solution turbulence than pressure effects.

One of the simplest examples of a "soft self-excitation" system would occur when two layers slide over each other with equal and opposite velocities, thereby creating a surface of discontinuity of velocity. A small amplitude wave is formed on this surface. The streamlines above the wave creast will draw closer together, while in the troughs they will become further apart. As a result, the pressure will fall above the crest and rise in the troughs thereby creating transverse pressure gradients in the fluid which in turn increase the amplitude of the wave. The amplitude of the wave will become so large that it eventually disintegrates into individual vortices, forming the beginning of the turbulent zone. This is the simplest case of the so-called "Helmholtz instability" i.e., we have an absolutely unstable surface of tangential velocity.[63]

The system that we are investigating could be one which is absolutely unstable. Bulk water is pushed in opposite directions and this results in the propogation of a wave.

Water is pushed away from the membrane as the high pressure in the inner and charged depleted region tries to equalize itself (the pressure in a liquid wants to be the same at every point). The large difference in field between the inner and bulk region, which created the high pressure in the first place, pushes water back toward the membrane, partly via electroosmosis. Two layers of flow will create a surface of tangential velocity that is absolutely unstable and we need not have a Re value of $\simeq$ 2030 to have a turbulent zone.

Diffusional Activation Energies

Plots of J vs f_B were made for H^+ ion and Na^+ ion (see pages 69-71). The intercept of these plots we have called β (β has units of A/M^2). The β values obtained from these plots are listed in Table 18 and the slopes (χ) are listed in Table 19. At a given C and T, 1st C.C.D.< β < 2nd C.C.D. The power spectrum recorded at fluxes = β show an $f^{-1.5}$ frequency dependence; it was mentioned earlier (see page 28) that this is indicative of a diffusion process. Since there is no measurable (diffusion) noise below the 1st C.C.D. and the 1st C.C.D. is reached when diffusion of ions can no longer maintain the flux, it seems probable that we are not measuring ordinary (bulk) diffusion.

The Arrhenius equation for a diffusion process would be

$$D = D_o e^{-\frac{E_a}{RT}} \qquad (44)$$

where

Ea = the diffusional activation energy

Since β is directly dependent on a diffusion process we should be able to write

$$\beta = \beta_o e^{-\frac{E_a}{RT}} \qquad (45)$$

β' values were defined as the lowest flux at which measureable noise above background is obtained (Table 20), since the β values (in Table 18) are approximately equal to the 1st C.C.D. Plots of 2.303 log β vs $1/T^{0}K$ were made for .008H^{+}, .010H^{+}, .016H^{+} and .010 Na^{+} and plots of 2.303 log β' vs $1/T^{0}K$ were made for .021H^{+} and .040 Na^{+} (Figs. 54-57). The activation energies (Ea) obtained from these plots are listed in Table 21.

The Ea's in Table 21 are less than what we would expect for ordinary diffusion or for diffusion through the membrane. If this were an ordinary diffusion process, we would expect an Ea of 4.7 kcal/mole for Na_2HPO_4 and of 4.7 kcal/mole for H_3PO_4 (certainly not less than 3.23 kcal/mole the diffusion activation energy of the H^{+} ion). The Ea values for diffusion through a membrane are twice as large as those found for ordinary bulk diffusion.(64)

Between the 1st and 2nd C.C.D., only part of the membrane surface is fully depleted of ions (see page 123). This means there must be a concentration gradient established across the surface of the membrane. Diffusion across the surface of the membrane can be ruled out as the diffusion noise source, however. At fluxes above the 2nd C.C.D. the membrane surface has a homogeneous distribution of ions (see page 123) but the diffusion slopes are still identical to those found at fluxes below the 2nd C.C.D. (see page 131).

Figure 54

Plot of Log β vs $1/T(^{o}K)$ for H_3PO_4

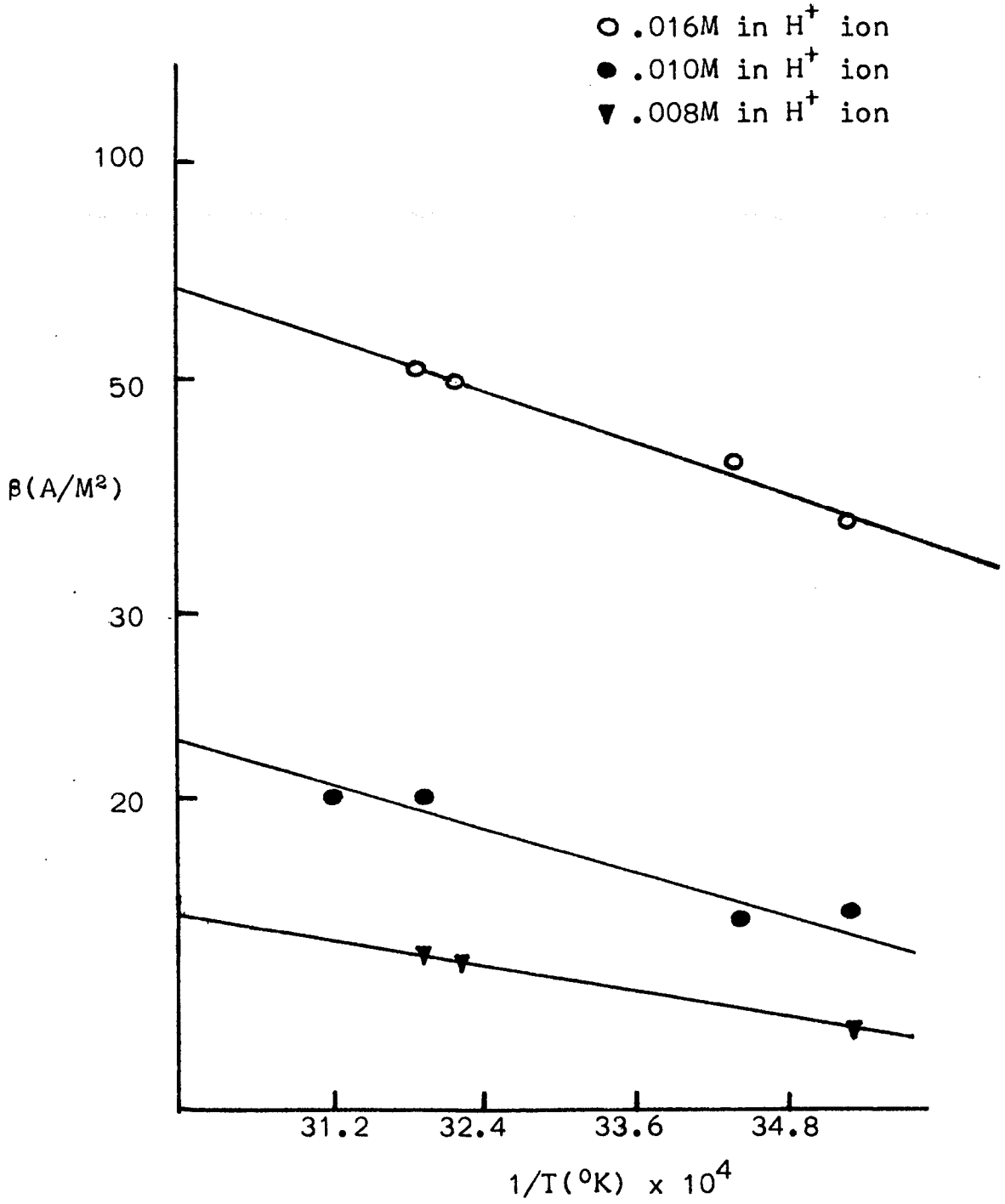

Figure 55

Plot of log β vs $1/T(^{o}K)$ for Na_2HPO_4 (.010M in Na^+ Ion)

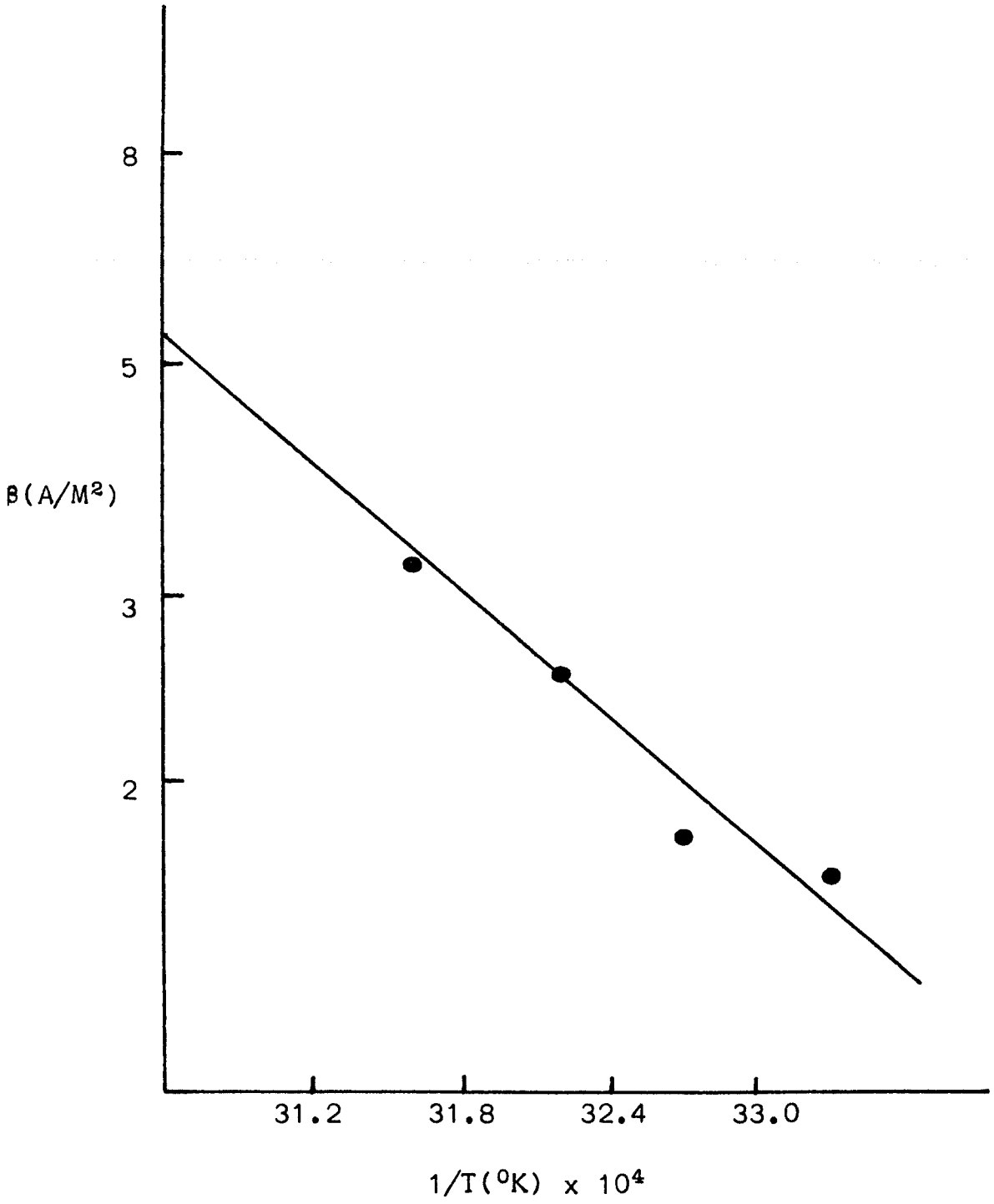

Figure 56

Plot of Log β' vs $1/T(^{0}K)$ for H_3PO_4 (.021M in H^+ Ion)

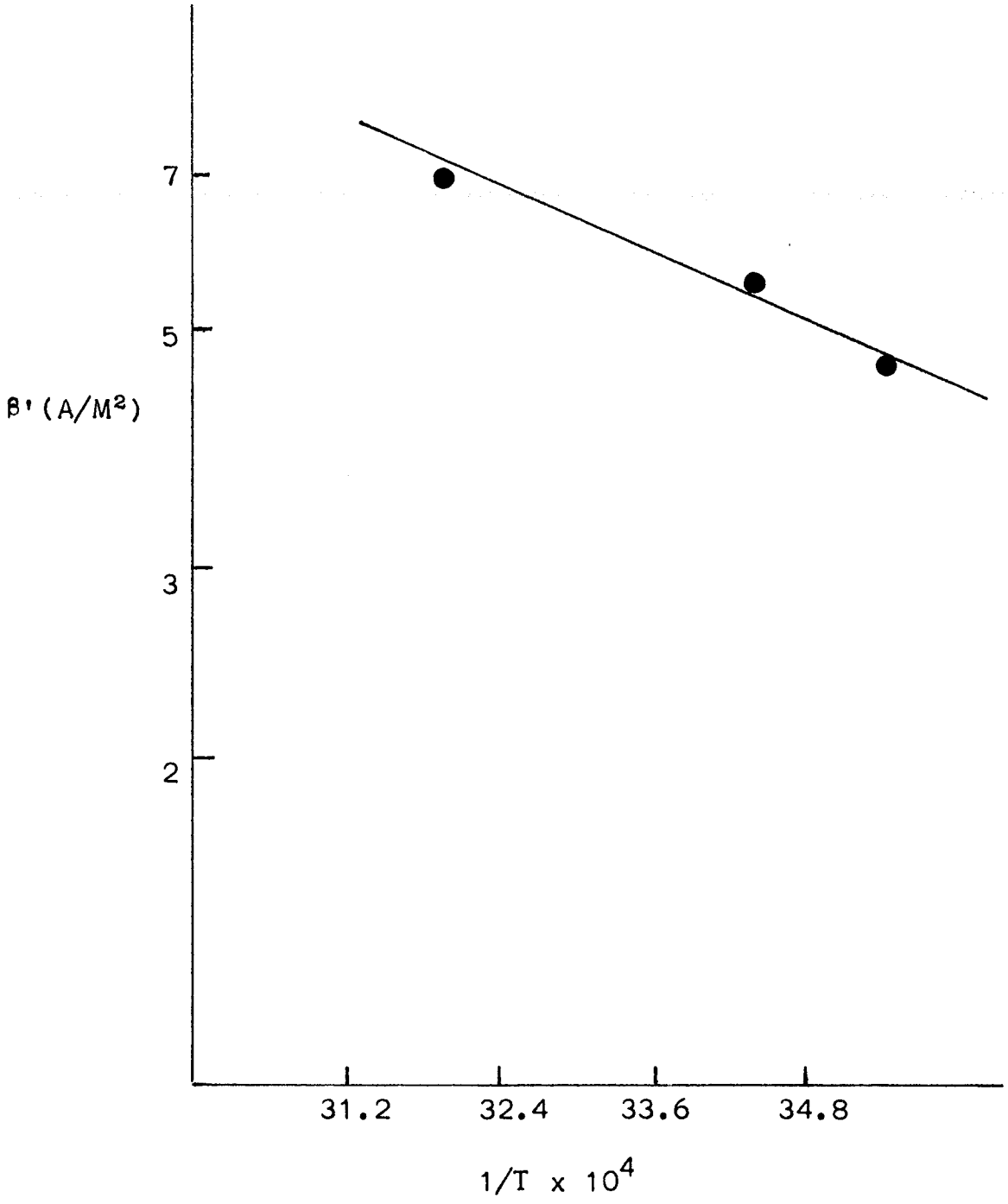

Figure 57

Plot of Log β' vs 1/T(^{o}K) for Na_2HPO_4 (.040M in Na^+ ion)

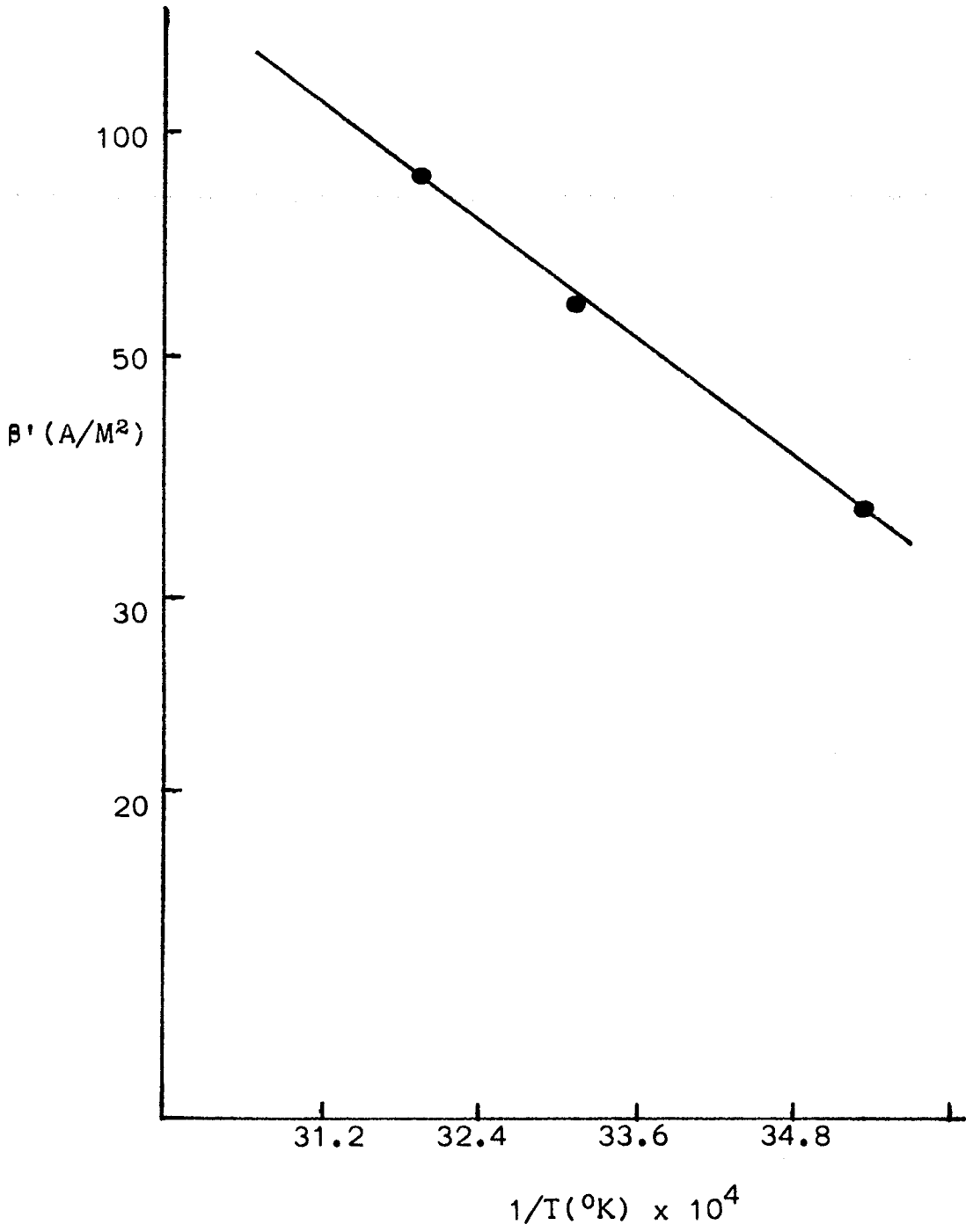

We know that obtaining measureable diffusion noise is dependent on the formation of a depleted region in solution. This depletion creates a high field and a region of dielectric saturation external to the membrane. It is well known that high fields cause the velocities of ions to become so large that the asymmetric part of the ionic atmosphere is left behind and the ions move almost independently (Wien effect).[65,66] Large increases in conductance has been found with solutions of weak acids in high fields.[67]

At the membrane-solution interface, a newly dissociated ion (of a weak electrolyte) would find itself in a region where the dielectric constant of water is very low, due to saturation. In such a region it would not be able to attract a water shell. Ions without atmosphere would cause little friction between themselves and the solvent medium and their diffusional activation energies might be expected to be very low. The only apparent stumbling block to this argument is that in the case of phosphoric acid, at a field of 3×10^7 volts/m, Schiele[68] found the increase in conductivity to be at most 3%.

The discrepancy between the very small increase in phosphoric acid conductivity and the substantial drop in Ea obtained in the work can be resolved, however. The resolution lies in the fact that the high field, weak acid conductivity data obtained by other investigators does not apply to our system. Their conductivity measurements were made with an elec-

trically neutral solution in the high field region. In this work, the high field is across the inner portion of the double layer (a region of non-electroneutrality). In the high field external to the membrane the current is carried almost entirely by counterions; co-ions being excluded from this region. Thus it seems quite likely that we would find a large increase in H_3PO_4 conductivity, since H^+ ion transport would not be retarded by $H_2PO_4^-$ ion transport moving in the opposite direction. Because the current is carried only by H^+ ions (in H_3PO_4), the Ea value should not be > 3.23 kcal/mole.

Green and Yafuso[11] obtained activation energies of 3.0 kcal/mole (0.025 M HCl) and 4.6 kcal/mole (0.050 M HCl). Lacking a reason to suspect concentration dependence, they reported an activation energy of 3.8 ± 0.5 kcal/mole. However, by combining their results with those obtained in this work, they offer further affirmation of the decrease of the diffusional activation energy of H^+ ion with decreasing concentration.

Figure 58 is a plot of Ea vs. C for H_3PO_4. It shows quite clearly how Ea increases with increasing C. That this is expected can be seen from the following:

1) Increasing C means less effective co-ion exclusion. With increasing $H_2PO_4^-$ participation in transport in the depleted region, the transport of H^+ will be increasingly opposed.

2) Increasing C means less dielectric saturation in the high field region. Thus more highly solvated ions will be transporting the current. Electrophoretic effects will be increasingly more important.

The decrease in activation energy of diffusion required at the lowest concentration is about 3 kcal/mole. It is known that in some circumstances a high field can affect the activation energy of diffusion of ions in solids.[69] Our situation is slightly different, and we have not been able to estimate the reduction quantitatively. The evidence does suggest that the decrease in activation energy with decreasing concentration is mediated by an increase in field.

Figure 58

The Diffusional Activation Energy of Phosphoric Acid as a Function of the Concentration of H^+ Ions

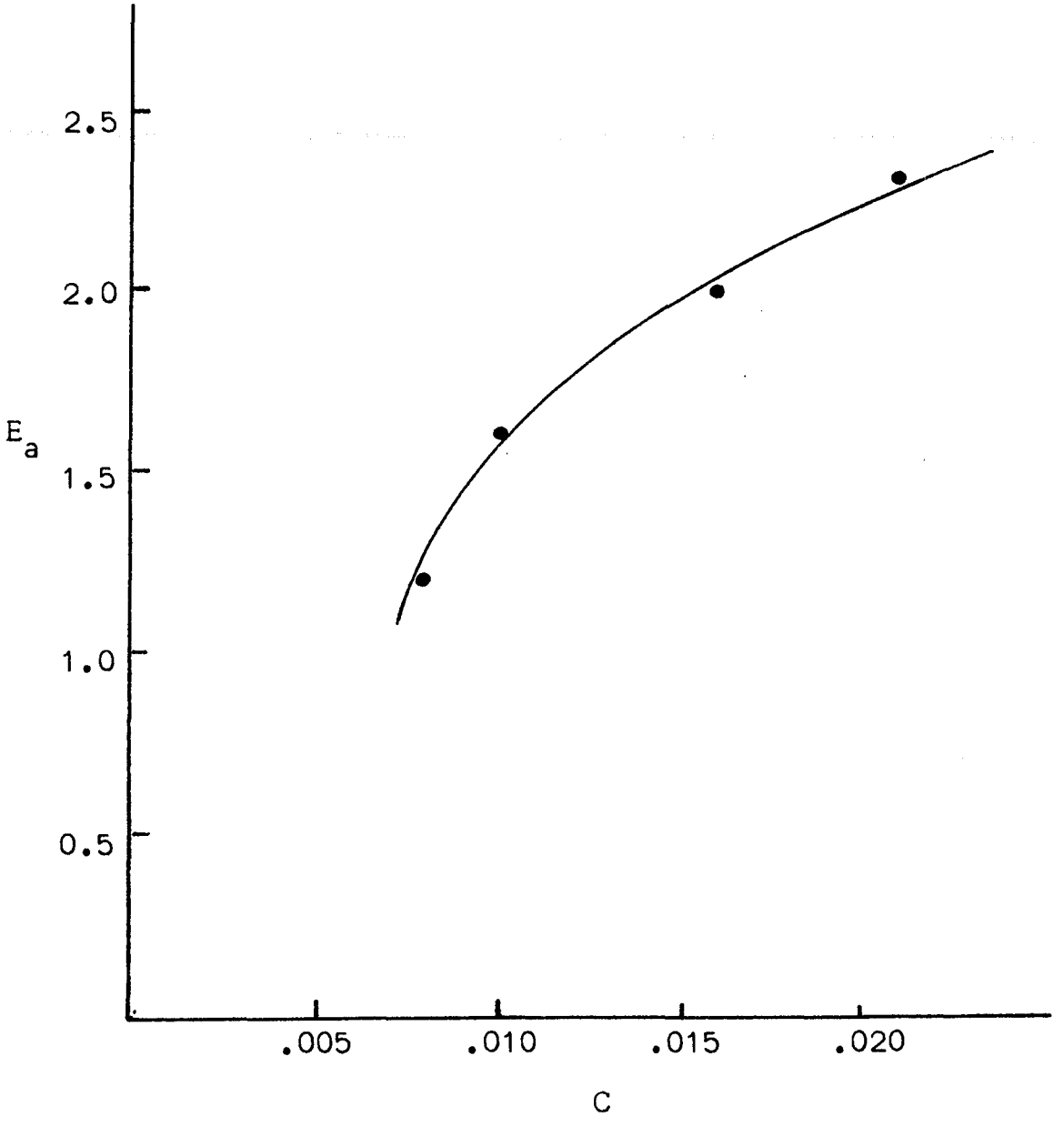

Sand's Equation

For a uni-univalent electrolyte, the diffusion coefficient can be shown to be[70]

$$D = \frac{RT}{F}\left(\frac{2\mu^{+}\mu^{-}}{\mu^{+}+\mu^{-}}\right) \qquad (46)$$

where

D = Diffusion coefficient

R = Gas Constant

μ^{+} = mobility of cation

μ^{-} = mobility of anion

In the depletion layer, we cannot be certain that $HPO_4^{=}$ is present in non-negligible amounts, since this region is depleted of ions and a weak electrolyte will dissociate with increasing dilution. For an electrolytic solution containing a univalent electrolyte and a univalent and divalent-anion

$$D = \frac{4RT}{F}\left(\frac{\mu^{+}\mu_1^{-}\mu_2^{-}}{3\mu_1^{-}\mu_2^{-}+\mu^{+}(\mu_2^{-}+2\mu_1^{-})}\right) \qquad (47)$$

where

μ_1^{-} = mobility of univalent anion

μ_2^{-} = mobility of divalent ion

Both of the above diffusion coefficients were derived with the assumption that diffusion is taking place across a region of electroneutrality, and as such equations 46 and 47 are applicable to the bulk solution and non-charged part of the depletion layer only. The charged region of the depletion layer is not electrically neutral and equations 46 and 47 can not be used here. In the bulk solution, at all concentrations of phosphoric acid used here, there is essentially no $HPO_4^=$ ion present (see page 56). The total diffusion coefficient calculated from equation 46 is 1.59×10^{-9} m^2/sec. In the electrically neutral part of the depletion layer, the total diffusion coefficient calculated from equation 47 is 0.95×10^{-9} m^2/sec.

The transport numbers of the ions carrying current in solution must add up to one.

$$t_A^+ + t_B^- = 1 \qquad (48)$$

The ratio of the transport numbers must equal the ratio of the respective diffusion coefficients.

$$\frac{t_A^+}{t_B^-} = \frac{D_A^+}{D_B^-} \qquad (49)$$

Since

$$D_A^+ = D_A'^+ e^{-\frac{E_A^+}{RT}}$$
$$D_B^- = D_B'^- e^{-\frac{E_B^-}{RT}} \qquad (50)$$

where

E_A^+ = diffusional activation energy of the cation

E_B^- = diffusional activation energy of the anion

We can write

$$\frac{t_A^+}{t_B^-} = \left(\frac{D_A'^+}{D_B'^-}\right) e^{-(E_A^+ - E_B^-)/RT} \qquad (51)$$

Therefore

$$t_B^- = \frac{1}{1 + \left(\frac{D_A'^+}{D_B'^-}\right) e^{-(\Delta E)/RT}} \qquad (52)$$

where

$$\Delta E = E_A^+ - E_B^-$$

We shall show that $t_{H_2PO_4^-}$ will increase with increasing T (t_{H^+} decrease), whereas $t_{HPO_4^=}$ and t_{Na^+} remain constant over all T.

A comparison of plots of log $RT\Lambda_{H_3PO_4}/F^{2(71)}$ vs $1/T^oK$ to plots of log $RT\Lambda_{H^+}/F^{2(72)}$ vs $1/T^oK$ show them to have nearly identical slopes. Thus the increase of the molar conductance of H_3PO_4 with increasing T is due almost entirely to the increase in conduction of H^+ ion. This follows from the fact that the transport number of H^+ ion (t_{H^+}) is appreciably greater

than $t_{H_2PO_4^-}$.

The following evidence shows why t_{H^+} cannot be constant with increasing T.

1) If we assume that t_{H^+} does remain constant and use η_{H^+} [12], we can calculate $\eta_{H_2PO_4^-}$ values as a function of T. Plots of log $RT\eta_{H_2PO_4^-}/F^2$ vs $1/T^oK$ give a diffusion activation energy of 2.8 kcal/mole for $H_2PO_4^-$. Such an $Ea_{H_2PO_4^-}$ is impossible, as at the very least $Ea_{H_2PO_4^-}$ must be greater than 3.2 3.2 kcal/mole (Ea_{H^+} = 3.2 kcal/mole).[13]

2) Molar conductances of phosphoric acid are determined from η_{H^+} and $\eta_{H_2PO_4^-}$ values in No. 1 above ($\Lambda'_{H_3PO_4}$). When plots of $RT\Lambda_{H_3PO_4}/F^2$ vs $1/T^oK$ are compared with plots of $RT\Lambda'_{H_3PO_4}/F^2$ vs $1/T^oK$, the slopes of the latter are nearly four times greater than those of the former (1.9×10^3 compared to 0.5×10^3).

The transport number of Na^+ ion (t_{Na^+}) in Na_2HPO_4 is independent of T. Molal conductivities of Na_2HPO_4 were computed ($\Lambda'_{Na_2HPO_4}$) on the basis of t_{Na^+} being constant with T (η_{Na^+} found in literature [11] were used). A comparison of log $RT\Lambda'_{Na_2HPO_4}/F^2$ vs $1/T^oK$ and log $RT\Lambda_{Na_2HPO_4}/F^2$ vs $1/T_oK$ shows the slopes to be identical (0.9×10^3). A plot of log $RT\eta_{HPO_4^=}/F^2$ vs $1/T^oK$ shows the diffusion activation energy of $HPO_4^=$ ($Ea_{HPO_4^=}$) equal to ~4.6 kcal/mole. This is almost identical to that of Na^+ ion (Ea_{Na^+} = 4.7 kcal/mole).[13]

From equation 52 we can see that $e^{-\Delta E/RT}$ will decrease with increasing T. Thus $t_{H_2PO_4^-}$ must increase and t_{H^+} decrease. Both t_{Na^+} and $t_{HPO_4^=}$ remain constant with T since $\Delta E=0$.

Sands equation can be written in the form

$$J^2 = \frac{c^2}{k}\left(\frac{1}{\tau}\right) \qquad (25)$$

$$\text{WHERE } k = \frac{4(1-t_+)^2}{\pi z^2 F^2 D} \qquad (25')$$

If our system obeys Sands law predictions, plots of J^2 vs $1/\tau$ should be linear at a given C and T. The charge (δ) formed at the membrane-solution interface at times before τ has no effect on Sand's equation since it is only a small fraction of the total charge. Figures 31 to 43 show that for both Na^+ ion and H^+ ion Sands law holds. Experimental error is somewhat larger for H^+ ion than for Na^+ ion.

For the Na^+ ion case, the numerator of k (equation 25'), will remain constant over all T. Since k is proportional to the total diffusion coefficient (D) and

$$D = D_0 e^{-E_a/RT} \qquad (50)$$

k should decrease exponentially with increasing T. This is born out experimentally. At a given C, plots of log $dJ^2/d(1/\tau)$ vs $1/T^0K$ have linear slopes (see Fig. 59). In the H^+ ion case, $(1-t_{H^+})^2$ is not constant over T. Therefore, k would not be expected to show a clear trend with T, at a given C, and none is found.

Figure 59

A Plot of Reciprocal Temperature vs the Slope of

The Sands Equation Plots (J^2 vs $1/\tau$)

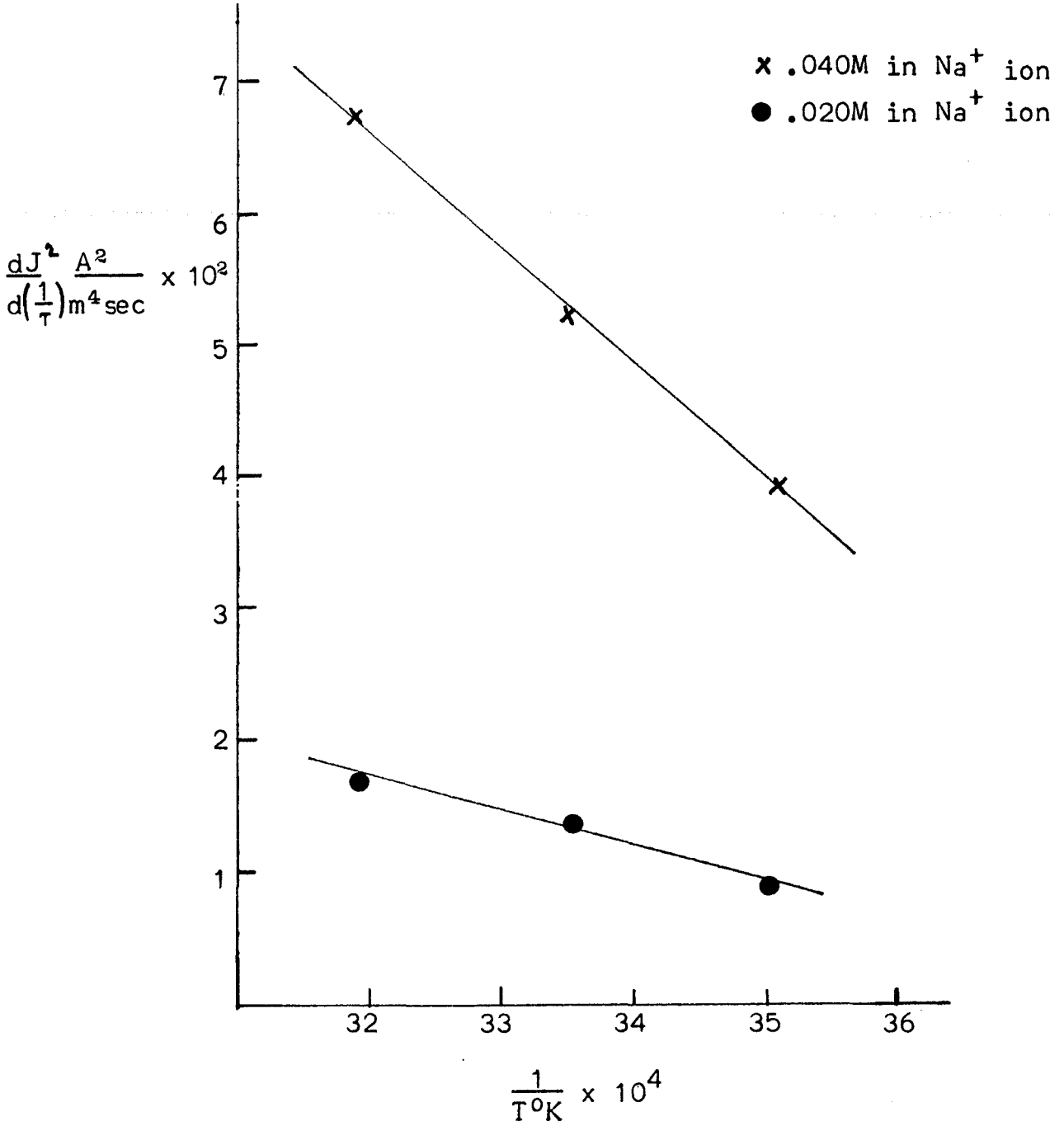

Equation 25 predicts that $\left[\frac{dJ'^2}{d(\frac{1}{t'})}\right] \div \left[\frac{dJ^2}{d(\frac{1}{t})}\right]$ should vary vs C'^2/C^2, at a given T. For Na^+ ion experimental results conform closely to theoretical expection. For H^+ ion, this is not the case (see % Difference columns in Table 15). It appears that $k \neq f(c)$ for Na^+ ion but $k = f(c)$ for H^+ ion. The only term in k that could depend on C is the cation transport number (t_+). Equal changes in t_+ in both cases will produce greater changes in k for H^+ ion than for Na^+ ion. This can be seen from the following:

1) $D^0_{H^+} = 9.30 \times 10^{-9} m^2/sec$ [75] and $D^0_{Na^+} = 1.33 \times 10^{-9} m^2/sec$. [75] This means that the numerator of k is approximately seven times larger in the H^+ ion case.
2) $t^0_{H^+} = 0.913$ [75][76] and $t^0_{Na^+} = .675$. [75][77] This makes the $(1-t_+)^2$ term (the denominator of $1/k$) more sensitive to change in t_+.

As the concentration of Na_2HPO_4 solutions changes from .060M in Na^+ ion to .010M in Na^+ion, t_{Na^+} decreases by 0.06 (this was calculated from literature values of Λ_{NaCl} [78], $\Lambda_{Na_2HPO_4}$ [74] and λ_{Na^+} [78][79] as a function of concentration. If both t_{Na^+} and t_{H^+} are changed by 0.06 the change in k for H^+ ion (ΔK_{H^+}) and the change in k for Na^+ ion (Δk_{Na^+}) will be:

$$q(\Delta k_{H^+}) = \frac{9.30}{(1-.913)^2} - \frac{9.30}{(1-.853)^2} \qquad (53)$$

$$q(\Delta k_{Na^+}) = \frac{1.30}{(1-.675)^2} - \frac{1.30}{(1-.615)^2}$$

where $q = \pi z^2 F^2 \times 10^{-8}$

$$g(\Delta k_{H^+}) = 790$$

$$g(\Delta k_{Na^+}) = 3.58$$

$$\frac{\Delta k_{H^+}}{\Delta k_{Na^+}} \simeq 220 \qquad (54)$$

Since Δk_{H^+} is 220 times greater than Δk_{Na^+} over a comparable change in t_{H^+} and t_{Na^+}; k is approximately independent of C for Na^+ ion only. Since $\left[\frac{dJ'^2}{d(\frac{1}{t'})}\right] \div \left[\frac{dJ^2}{d(\frac{1}{t})}\right]$ would equal C'^2/C^2 only if k is nearly independent of C we should expect to find the predicted values for Na^+ ion only.

Interfacial Concentrations

The Nernst idealization supposes a sharply bounded film of thickness δ to exist at the membrane solution interface and that diffusion along a uniform concentration gradient across the film is the only ion-transfer mechanism besides electrolytic migration. This leads to the relation

$$\pm (c - c') = \frac{i\delta(\bar{t} - t)}{FD} \qquad (55)$$

where

c = bulk concentration of counterion

c' = interfacial concentration of counterion

i = current density

δ = film thickness

$\bar{t}$ = counterion transport number in the membrane

t = counterion transport number in the bulk solution

F = Faraday's Constant

D = mean diffusion coefficient of electrolyte in the range c to c'.

For the limiting current c' = 0 and

$$i_{Lim} = \frac{FDc}{\delta(\bar{t} - t)} \qquad (56)$$

Cooke[7,8] showed that the Nernst idealization could account quite successfully for what he called the "total overpotential" below the limiting current density. Cooke's "total overpotential" is equivalent to our V_B(11KΩin). In an effort to extend his theoretical work to events above the limiting current Cooke assumed the Nernst idealization to be applicable at steady state conditions at fluxes above the C.C.D. He then showed that it was possible to estimate the interfacial concentration (c') at such fluxes if no ionic species other than those provided by the electrolyte in solution are near the interface. The expression he derived is

$$\eta_t' = \left[\frac{2RT}{F}\left(\bar{t}-t\right) + \frac{FD}{(\bar{t}-t)\Lambda}\right] \ln \frac{C_o}{C'} - \frac{FD}{(\bar{t}-t)\Lambda} \qquad (57)$$

where

η_t' = total overpotential

Λ = molar conductance

C_o = bulk concentration

Using the values in the previous section and rearranging the above equation we obtain for phosphoric acid

$$\ln c' = \frac{-\eta_t'}{.273} + \ln C_o - .981 \qquad (58)$$

This assumes $(\bar{t} - t) = .087$. All values used are those found at infinite dilution. Table 22 shows how c' of H^+ ion will change with $V_B(11K\Omega in)$ in the phosphoric acid case. In Cooke's experimental work he stirred the concentrate solution (the solution on the anode side of the membrane). Ideally, the concentration buildup at the membrane-solution interface in the concentrate solution should be equal in magnitude to the concentration loss or depletion in the diluate solution. However, such is never the case in the electrodialysis of ion-exchange membranes. The depletion is always far greater than the buildup. Nevertheless, stirring the concentrate solution will help to nullify its effect on the measurement of the overpotential. We did not stir the concentrate solution when $V_B(11K\Omega in)$ was measured, and thus our measured Back Emf's should be somewhat smaller than those shown in Table 9 . The effect that this would have on the reported c' of H^+ ion concentrations is small, however, because the H^+ ion c' does not change much with relatively large changes in $V_B(11K\Omega)$ (see Table 22). This is not the case for Na^+ ion (see Table 23). The c' of Na^+ ion changes quite drastically with relatively small changes in $V_B(11K\Omega in)$. Thus any correction that should have been made in the Back Emf might be significant in this case. The equation applicable to Na_2HPO_4 is:

$$\ln c' = \frac{\eta_t'}{A} + \ln C_o - .585 \qquad (59)$$

In the above equation A is approximately 50 times smaller than 2.75 (see equation 58). Because A is so small a number, large changes in c' will result from small errors in V_B(11KΩin) values. The calculation of c' in the Na^+ case is made more difficult by the presence of H^+ ion in solution. We cannot assume that all counter-ion transport through the membrane is due to Na^+ ion, since non-negligible amount of H^+ ion might exist near the membrane surface once the depletion process has begun. The H^+ ion could come from the bulk solution or from any dissociation process taking place in the depleted region.

Since all counter-ion transport can no longer be assumed to be due to Na^+ ion, $\bar{t}_{Na^+} \neq 1$. This makes the choice of $\bar{t}_{Na^+} - t_{Na^+}$ very speculative. The calculation of c' for Na^+ is therefore made more unreliable since small differences in $\bar{t}_{Na^+} - t_{Na^+}$ would be a critical factor in c' determinations. c' values for Na^+ ion were determined with $\bar{t}_{Na^+} - t_{Na^+} = 0.14$ (Table 23) and with $\bar{t}_{Na^+} - t_{Na^+} = 0.34$ (Table 23). The range of possible values for $\bar{t}_{Na^+} - t_{Na^+}$ was felt to be between 0.14 and 0.34.

Although the absolute values of c' in Table 23 are not very reliable, they do show that a large V_B(11KΩin) values the Na^+ ion interfacial concentration gets so small that the ions at the surface are more likely to be H^+ ion than Na^+ion. It was mentioned earlier that for .020, .040 and .060M Na^+ ion bulk concentration, one must obtain a V_B(11KΩin) value of sufficient magnitude before one will find a break in the

Na^+ ion power spectrum (see Table 10). Table 23 reveals that when V_B(11KΩin) values are comparable to those found in Table 10 H^+ ions could well come to dominate transport at the surface of the membrane in Na_2HPO_4 solutions .02, .04 and .06M in Na^+ ion. Cooke estimated that if .05M NaCl is used at 25°C, a' c' of 10^{-7}M in Na^+ ion would cause an "overpotential" of ~690mv. This offers some verification of our findings since the V_B(11KΩin) values in Table 10 are roughly of this magnitude.

The interfacial concentrations of H^+ ion in the phosphoric acid case tell us that the surface is never quite as depleted of ions as might have been expected. The phosphoric acid interfacial calculations are more reliable, and if Cooke's assumptions are correct, they must be considered seriously. The relatively large interfacial concentration would be possible if bulk flow was responsible for providing enough ionic agitation to have a constant supply of ions ready to carry the current.

Steady State Voltages and Back Emf's

Steady state resistances (R_{ss}) were calculated from Ohm's law using

$$R_{ss} = \frac{V_T(11K\Omega_{out})_{ss}}{i_{ss}} \qquad (24)$$

where

$V_T(11K\Omega out)_{ss}$ = total voltage at steady state (11KΩout)

i_{ss} = current at steady state

The calculated R_{ss} values Fig. 26-30 show that the system does not always behave ohmically with changes in J. Whether or not the system behaves ohmically depends on the type of counter-ion, the value of C and the magnitude of J above the C.C.D. R_{ss} tends to be independent of J when the counterion is Na^+, when C is large and when J is much greater than the C.C.D. (see Figs. 26 - 28). R_{ss} tends to behave non-ohmically when the counterion is H^+, when C is low and when J is at or slightly above the C.C.D. (see Figs. 29 to 30).

The behavior of $V_B(11K\Omega in)$ at steady state tends to parallel that of R_{ss} with changes in steady state J values (see Figs. 31 - 34). This results from the fact that the ohmic or non-ohmic behavior of the system is not a function of having an 11KΩ resister between the measuring electrodes. What the

measured R_{ss} and V_B(11KΩin) values at steady state tell us is that in solutions of .020, .040 and .060M in Na^+ ion the power spectra were recorded under solution conditions quite different than those found in the spectrum of .008, .010 and .016M H^+ ion. For instance, power spectra of .010 H^+ ion were measured when the entire system was in a non-ohmic region; whereas when the power spectrum were measured in .060Na^+, the system was behaving in an ohmic way with changes in J.

The arrows on Figs. 31 and 34 indicate the lowest flux at which we find the first break in the power spectrum (see Table 10). At fluxes at and above those indicated by the arrows there is little difference between power spectrum of .020, .040 and .060 Na^+ ion. All of these spectra were obtained with the system in an ohmic region. On the other hand, .01 Na^+ spectrum are quite different from those obtained for the other Na^+ ion concentrations. It has been mentioned earlier that .01 Na^+ ion spectra resemble the H^+ ion spectrum more closely than they do those of other Na^+ ion concentrations. Since .01 Na^+ ion spectrum were obtained with the system in a non-ohmic region and since the H^+ ion spectra were also, for the most part, obtained with the system in a non-ohmic region, the data seem to suggest that there is a relationship between the type of spectra obtained and whether the system is in a non-ohmic or ohmic region. The above relation-

ship is not quite as clear-cut as we might have hoped, however. For instance, .01 Na^+ and .021 H^+ have similarly shaped spectra at 283°K but in this particular case the H^+ ion is in an ohmic region. It should be pointed out that the steady state resistance and Back Emf values obtained in .01 Na^+ are somewhat erratic, certainly much more so than for all other H^+ ion and Na^+ ion concentrations. This seems to indicate, once again, that .01 Na^+ solutions are in a unique transition region between Na^+ ion dominated and H^+ ion dominated noise spectra.

Steady-State Voltages (11KΩin ⇄ 11KΩout)

If we are at steady state with no 11KΩresistor in the circuit and then we place an 11KΩresistor into the circuit, the system immediately begins to adjust itself to the new conditions. Since the total voltage is now higher than it should be at 11KΩin steady state conditions, a voltage decay (two-step) begins.

Non-equilibrium situations have been created and studied in double layers adjacent to electrodes.[80,81] Although they were created in a somewhat different manner, they also showed a two-step voltage decay back to equilibrium. What was found was an initial sharp drop in voltage, followed by a slow fall in voltage back to equilibrium. These investigators[80,81] suggested that the initial short time (1msec) decay was the result of the decay of extended charge. For the voltage drop at long times (80msec), the back diffusion of salt into the relatively pure solvent in the disturbance region was believed responsible. The decay in our system involves time constants of 1sec and 10sec for the rapid and slow voltage drop, respectively. The long time constant seems to suggest that the decay takes place through a large capacitance somewhere in the system. An additional complication in our system is that the voltage decay takes place while charge builds up at the membrane-solution interface.

The difference in time constants must be understood in the light of the following differences in the systems involved:

1) No current was running when the electrode measurements were made. Our measurements were made with a large steady state flux being maintained.
2) The non-equilibrium situation in the electrode case was created with a large rapid burst of charge onto the electrode. This is quite different from what we have done.

It would seem plausible that the voltage buildup when the 11KΩ resistor is removed at steady state would also take place in two steps, (i.e., a sharp voltage increase, followed by a slower increase in potential as salt diffuses into the bulk solvent). Such two-step increases are found at all C and T values with J slightly above the C.C.D. At somewhat higher J values, we find "S-shaped" curves (see Fig. 45 and 46). The curves, after time t_B (the break time), also follow the expected two-step decay. The voltage buildup after time τ looks to be just what we might expect for a rapid buildup of extended charge followed by diffusion of salt into the electrolyte.

It was mentioned that the 11KΩ out → 11KΩ in situation is complicated by the necessity of building up a charged layer at the membrane-solution interface. Similarly, in going in

the reverse direction, charge must be dissipated before 11KΩ out steady-state conditions can be reached. Figures 35 to 36 and Table 12, show that the charge (δ) formed on the membrane in the 11KΩin case increases linearly with increase in J. (Charge (δ) formed on the membrane at time t", where $0<t"<\tau$ is not the final charge ($t>\tau$) on the membrane at steady state.) Since plots of J vs t_B (Fig. 47 to 49) also increase linearly with increasing J, this suggests that t_B might be dependent on δ. This would mean that if there is to be a time delay (break time) there must be a sufficient amount of charge created on the membrane surface. The lowest t_B value which is clearly discernable in our measurements is 0.5 sec. From the J vs. t_B curves (Fig. 47 to 49), J values corresponding to t_B = 0.5 sec (J_t) were determined at various C and T values. At $J < J_t$, we do not have an S-shaped curve (there is no time delay). From the J vs. ΔV curves (Fig. 35 to 36), ΔV values corresponding to J_t values (ΔV_t) were determined (see Table 24). The ΔV_t values are seen to be of large magnitude and independent of C. Averaged over C, the ΔV_t values at 298°K are ~450 mv. This corresponds to a charge of 2-3 x 10^{-8} coul/m^2 (see page 126) on the membrane surface (at $t<\tau$). Table 12 shows that a ΔV (or δ) of this magnitude is only attained when J lies somewhat above the C.C.D., i.e., when $J \simeq J_t$. This suggests that a significant amount of charge must be formed on the membrane surface, regardless of C and T, if we are to see a time delay in going from the 11KΩin steady

state to the 11KΩ out steady state. This appears to be true even though this charge is later modified by depletion at the membrane surface.

Summary:

1. Noise and chronopotentiometric measurements were used to study Na^+ and H^+ ion transport across cation exchange membranes.
2. Two types of noise source appear to be present, diffusion and bulk flow.
3. The bulk flow, in the case of H^+ at least, appears to be turbulent.
4. The two noise sources coexist and must be spatially separated.
5. Diffusion activation energies, obtained from the noise investigations, fall to relatively low values at low concentrations. This is postulated to be due to an increase in electric field.
6. The chronopotentiometric results were found to verify both Sand's law predictions and conductivity data found in the literature for both Na^+ and H^+ ions.
7. Steady state d.c. resistances, obtained from the chronopotentiometric data, show that the system can behave either ohmically or non-ohmically with changes in J. Conditions under which each type of behavior could be found were determined.
8. The surface charge on the membrane was obtained (to a rough order of magnitude). This charge was found to increase linearly with J at a given C and T. When J is slightly greater than J_{VT}, the magnitude of the charge on the membrane surface is $2\text{-}3 \times 10^{-8}$ coul/m^2.

9. Interfacial ionic concentrations of both H^+ ion and Na^+ ion at $J > J_{VT}$ were obtained (the values are more reliable for H^+ than for Na^+). H^+ interfacial concentrations were $\sim 10^{-3}$ moles/liter. These relatively large values offer additional evidence for bulk flow in the H^+ ion case.

Table 2

Total Noise as a Function of Concentration, Temperature and Flux.

Conc. (m/l)	T°K	J_{H^+} (A/M^2)	Total Noise RMS (10^{-3}MV.)
.008 H^+	283	106	14.5
	"	121	450.
	"	255	5000.
.016 H^+	"	325	20.
	"	395	875.
	"	462	2250.
.021 H^+	"	462	8.2
	"	557	220.
	"	656	1650.
.010 H^+	"	156	60.
	"	191	1200.
.008 H^+	313	121	13.5
	"	156	170.
	"	255	2700.
.021 H^+	"	691	12.5
	"	758	25.
	"	837	750.
.016 H^+	"	608	835.
.010 H^+	"	255	800.
	"	395	5250.
.010 H^+	292	156	12.
	"	172	90.
	"	191	650.
.016 H^+	"	462	550.
.021 H^+	"	557	11.
	"	573	25.
	"	601	230.
	"	697	1230.

Continued

Table 2 (Cont)

Conc. (m/l)	T°K	J_{Na^+} (A/M²)	Total Noise RMS (10^{-3}MV.)
.060 Na^+	301	147.	330.
.060 Na^+	292	84.0	9.5
	"	147.	365.
.060 Na^+	313	116.	4.6
	"	196.	500.
.060 Na^+	283	147.	575.
.010 Na^+	301	30.6	370.
.010 Na^+	313	63.2	1050.
	"	94.7	2600.
	"	116.	4100.
.010 Na^+	292	63.2	2000.
.010 Na^+	283	3.9	145.
	"	19.3	240.
	"	25.5	500.
.020 Na^+	301	40.7	165.
	"	84.0	625.
	"	116.	1050.
.020 Na^+	292	63.2	475.
	"	84.0	775.
	"	116.	1650.
.020 Na^+	313	30.6	5.2
	"	35.7	28.
	"	40.7	95.
.020 Na^+	283	19.3	8.
	"	25.5	20.
	"	30.6	230.
	"	116.	2900.
.040 Na^+	283	35.7	12.
	"	63.2	230.
	"	116.	600.

Table 2 (Cont)

Conc. (m/l)	T°K	J_{Na^+} (A/M^2)	Total Noise RMS (10^{-3}MV.)
.040 Na^+	301	51.0	4.1
	"	56.0	13.5
	"	84.0	210.
	"	94.7	625.
	"	147.	650.
.040 Na^+	313	71.3	15.
	"	84.0	50.
	"	116.	380.
	"	147.	580.
	"	196.	800.

Table 3a

Slopes of H_3PO_4 Power Spectra

Conc.(m/l)	T°K	$J_H+(A/M^2)$	"a"	"b"	"c"
.008	318	191	2.42	4.60	--
		223	2.58	4.60	--
		323	2.70	4.44	--
	313	121	--	--	1.71
		255	2.65	4.76	1.64
		525	2.76	4.82	
	310	121	--	--	1.52
	283	106	--	--	1.49
		121	3.28	5.06	1.58
		255	2.88	4.53	--
		322	3.05	4.65	--
		395	3.08	4.71	--
.010	318	233	--	--	1.47
		322	2.42	4.94	
		350	2.56	4.71	
	313	255	2.45	4.60	1.33
		395	2.70	4.40	
		592	2.76	4.44	
	291	156	--	--	1.44
		172	--	3.70	1.46
		191	3.20	4.41	1.33
		287	2.99	4.71	1.37
	283	156	--	--	1.58
		191	3.23	5.26	
		395	2.88	4.21	
		726	3.08	4.60	1.35

Table 3a (Cont)

Conc.(m/l)	T°K	J_{H^+}	"a"	"b"	"c"
.016	313	607	2.74	4.35	1.19
		656	2.70	4.21	1.83
		758	2.90	4.12	1.35
	291	462	2.99	4.30	1.48
		525	2.92	4.35	--
	283	395	2.68	4.17	1.41
		462	3.05	4.40	1.47
		557	2.90	4.12	--
		758	2.94	4.12	1.54
.021	313	691	--	--	1.39
		758	--	--	1.38
	309	691	--	--	1.59
		758	--	--	1.47
	291	557	--	--	1.32
		573	--	--	1.38
	283	462	--	--	1.58
		557	3.05	4.12	1.38
		658	2.88	3.85	
		758	2.86	3.92	1.73

where

-- not found

"a" low and high frequency slopes, respectively

"b" of high noise spectra

"c" low noise diffusion slope

Table 3b

Slopes of Na_2HPO_4 Power Spectra

Conc.	T°K	J_{Na^+}	"x"	"x-y"	"y"	"C"
.010 Na^+	313	63.2		2.94		
		94.7	2.88		3.28	
		116.	2.84		3.45	
	310	--		2.70		
	301	30.6	2.56		3.23	
		63.2	2.58		3.20	
		94.7	2.67		3.18	
		147.	2.55		3.18	
	291	63.2	2.82		3.01	
		197	2.56		3.18	
	283	3.9		3.51		
		19.3	2.92		3.81	
		25.6	2.82		3.88	
		40.7	3.13		3.92	
		63.2	2.78		3.64	
.020 Na^+	313	30.6				1.65
		35.7			3.02	1.78
		40.7			2.92	1.85
.020 Na^+	301	40.7		2.76		
		84.0	2.47		2.84	
		116.	2.45		2.92	
		147.	2.40		2.61	
	291	63.2		2.31		
		84.0	2.20		2.84	
		116.	2.25		2.69	
		147.	2.16		2.94	
		197.	2.04		3.33	
	283	19.3				1.39
		25.6			3.05	1.52

Table 3b (Cont)

Conc.	T°K	J_{Na^+}	"x"	"x-y"	"y"	"C"
.020 Na^+	283	30.6		2.84		
		84.0	2.35		2.69	
		116.	2.13		2.80	
		196.	2.31		2.82	
.040 Na^+	313	71.3			2.63	1.70
		84.0			2.78	1.31
		116.		2.38		
		147.	--		2.65	
		196	2.37		2.70	
		249	2.55		2.74	
	301	51.0	2.31			1.31
		56.0			2.67	1.78
		84.0		2.50		
		94.7		2.50		
		147.	2.31		2.78	
		249.	2.22		2.70	
	283	35.7			2.96	1.56
		63.2		2.48		
		116.	2.22		2.84	
		147.	2.26		2.67	
		196.	2.15		2.76	
		249.	2.15		2.96	
.060 Na^+	313	116.				1.56
		196	2.53		3.08	
		249.	2.48		3.17	
	301	147.	2.29		2.66	
		196.	2.20		2.65	
		249.	2.13		2.61	

Table 3b (Cont)

Conc.	T°K	J_{Na^+}	"x"	"x-y"	"y"	"C"
.060 Na^+	291	84				1.30
		147	1.99		2.44	
		196	2.03		2.55	
		249	1.92		2.66	
	283	147	2.20		2.56	
		196	2.09		2.76	
		249	2.15		2.72	

where

"x" low and high frequency slopes, respectively, of
"y" high noise Na^+ ion spectrum.

"x-y" slope of straight line Na^+ ion spectra.

"C" low noise diffusion slope

Table 4

Slopes Averaged Over Flux for H_3PO_4 Power Spectra

Conc. (m/l)	T°K	"a"	"b"	"c"	
.008	283	3.07	4.74	(1.58)	σ_a = .225
.008	313	2.70	4.44	1.45	σ_b = .136
.008	318	2.56	4.55		σ_c = .092
	Avg.	2.78	Avg. 4.58	Avg. 1.52	
.010	283	3.06	4.69	(.935)	σ_a = .250
.010	291		4.26	1.39	σ_b = .239
.010	313	2.73	4.49	(1.33)	σ_c =
.010	318	2.48	4.82		
	Avg.	2.76	Avg. 4.57	Avg. 1.22	
.016	283	2.96	4.21	1.47	σ_a = .101
.016	291	2.95	4.33	(1.48)	σ_b = .069
.016	313	2.78	4.21	1.41	σ_c = .032
	Avg.	2.90	Avg. 4.25	Avg. 1.45	
.021	283	2.93	3.96	1.56	σ_a = .251
.021	291	(2.53)	4.0	1.29	σ_b = .140
.021	313	((2.38))	3.74	(1.19)	σ_c = .191
	Avg.	2.61	Avg. 3.90	Avg. 1.43	

Table 5

Slopes Averaged Over Flux for Na_2HPO_4 Power Spectra

Conc. (m/l)	T°K	"X"	"Y"	
.010	283	2.90	3.81	σ_x = .140
.010	291	2.68	3.09	σ_y = .316
.010	301	2.58	3.20	
.010	313	2.80	3.36	
	Avg.	2.74	Avg. 3.37	
.020	283	2.26	2.76	σ_x = .142
.020	291	2.16	2.92	σ_y = .087
.020	301	2.44	2.78	
	Avg.	2.29	Avg. 2.82	
.040	283	2.20	2.80	σ_x = .102
.040	291	2.26	2.74	σ_y = .051
.040	313	2.40	2.70	
	Avg.	2.29	Avg. 2.75	
.060	283	2.15	2.74	$\sigma_{x_{2.11}}$ = .154
.060	291	1.98	2.55	
.060	301	2.20	2.65	$\sigma_{x_{2.50}}$ = .294
.060	313	(2.50)	((3.13))	σ_y = .095
	Avg.	2.11/2.21	Avg. 2.65	

Table 6

Effect of Temperature on Slope "a"(H_3PO_4) at Constant Total Noise

C	T°K	Approximate Total Noise RMS(10^{-3}MV.)	"a"
.008	283	8000	3.05
	318		2.70
.010	283		2.88
	313	5700	2.70
	318		2.56
.010	291		2.99
	318	3700	2.42
.016	283	4000	2.90
	313		2.90
.016	283		2.68
	291	750	2.99
	313		2.74
.016	283		3.05
	291	1950	2.92
	313		2.70
.016	291		(2.92)
	313	1750	2.70
.021	283	25	(3.05)
	291		2.63
.021	283	~1400	2.88
	291		2.42

Table 7

Break Frequency as a Function of Experimental Variables

Conc. (m/l)	T°K	J(A/M²)	Total Noise RMS(10^{-3}MV.)	Break freq. (Hz)
.008 H^+	318	191	2450	334
		223	5500	630
		323	8250	890
.008 H^+	313	172	1500	334
		191	850	224
		255	2700	530
		287	7000	890
		322	6150	794
		395	7900	1060
		525	17000	3160
.008 H^+	310	172	725	123
		191	2400	246
		239	4250	473
		287	6250	666
		322	7750	794
.008 H^+	283	121	425	94
		156	1650	168
		191	2500	334
		255	5000	615
		322	7000	1060
		395	9000	1290
		525	15000	3420
.010	318	239	375	158
		255	2230	354
		322	3750	500
		350	6000	630
.010	313	255	800	158
		395	5250	794
		592	9000	1410
		726	14000	5620

Table 7 (Cont)

Conc. (m/l)	T°K	J(A/M²)	Total Noise RMS(10^{-3}MV.)	Break freq. (Hz)
.010 H^+	291	191	650	174
		223	1550	294
		255	2400	455
		287	3650	595
.010 H^+	283	191	1200	162
		255	2700	446
		323	4500	683
		395	6500	1080
		525	9750	2060
		726	15575	3980
.016 H^+	313	607	825	251
		656	1700	334
		758	4100	595
		837	6000	794
.016 H^+	309	557	600	224
		607	1100	316
		691	2650	666
.016 H^+	291	462	550	224
		525	1800	396
		592	2950	630
.016 H^+	283	395	875	94
		462	2250	376
		557	4000	446
		691	5750	794
		758	6500	1260
.021 H^+	291	607	230	158
		691	1230	543
.021 H^+	283	557	220	84
		658	1650	155
		758	2650	298
		837	4000	530

Table 7 (Cont)

Conc. (m/l)	T°K	J(A/M²)	Total Noise RMS(10^{-3}MV)	Break freq. (Hz)
.010 Na^+	283	19.3	240	411
		25.6	500	749
		40.7	1400	2820
		63.2	3400	5120
	291	19.3	105	158
		22.1	185	251
		25.0	295	411
		27.5	380	595
	301	40.7	625	1120
		63.2	1500	5600
		116.	4850	8800
		147.	6500	10600
	313	63.2	1050	1060
		94.7	2600	5600
		116.	4100	7060
		147.	5850	10000
.02 Na^+	283	84.0	1400	3980
		116.	2900	5950, 7310
		147.	4250	9750
		169.	--	10200
		196	6000	10350
.02 Na^+	291	84.0	775	5300
		116.	1650	5950
		147.	2500	10000
.04 Na^+	301	116.	430	4210
		147.	650	5610
		196.	950	8880
		249.	1350	10000
.04 Na^+	313	147.	580	4200
		196.	800	7940
		249.	1350	10000

Table 7 (Cont)

Conc. (m/l)	T°K	J(A/M²)	Total Noise RMS(10^{-3}MV.)	Break freq. (Hz)
.06 Na^+	283	147.	575	2810
		196.	850	5600
		249.	1300	10000
.06 Na^+	291	116.	190	4200
		147.	365	5610
		196.	600	7940
		249.	800	11200

Table 8

Break Frequency as a Function of Concentration

Conc.	T°K	Total Noise RMS(10^{-3}mv.)	f_B
.008	285	1650	168
.010	"	1200	162
.021	"	1650	155
.008	"	2500	334
.010	"	2700	446
.016	"	2250	376
.021	"	2650	300
.008	"	5000	615
.010	"	4500	683
.016	"	4000	446
.016	"	5750	794
.021	"	4000	530
.008	"	7000	1060
.010	"	6500	1080
.016	"	6500	1260
.008	313	850	224
.010	"	800	158
.016	"	830	251
.008	"	1500	334
.016	"	1700	334
.008	"	6150	794
.010	"	5250	794
.016	"	6000	794

Table 9

The Effect of Flux on Steady State Resistance and Back Emf

Conc. (m/l)	T°K	J(A/M²)	Resistance (K)	Back Emf (-volts)
.010 Na^+	285	10.2	3.62	.224
		15.3	3.08	.460
		25.5	2.15	--
		30.6	4.16	.790
.020 Na^+	285	25.5	1.32	.350
		30.6	1.31	.450
		35.7	1.15	.510
.040 Na^+	285	56.0	.700	.530
		71.3	.696	.540
		86.6	.609	.700
		102.	.575	--
		127.	.510	.760
.060 Na^+	285	102.	.438	.615
		127.	.420	.600
		153.	.358	.850
		204.	.312	1.100
.010 Na^+	298	15.3	2.15	.250
		20.4	2.08	.360
		25.5	3.20	.864
		30.6	1.66	.510
.020 Na^+	298	30.6	.875	.285
		35.7	.919	.350
		45.8	.917	.515
.040 Na^+	298	56.0	.364	.225
		71.3	.447	.410
		86.6	.465	.525
		127.	.390	.700

Table 9 (Cont)

Conc. (m/l)	T°K	J(A/M²)	Resistance (K)	Back Emf (-volts)
.060 Na^+	298	127.	.310	.560
		153.	.317	.625
		204.	.300	.760
.010 Na^+	313	15.3	1.66	.300
		35.7	1.73	--
		45.8	1.44	.625
.020 Na^+	313	35.7	.688	.350
		45.8	.794	--
		71.3	.660	.585
.040 Na^+	313	86.6	.344	.430
		102.	.400	.450
		127.	.370	.775
		153.	.325	.755
.060 Na^+	313	127.	.190	.250
		153.	.222	.440
		204.	.219	.835
.008 H^+	285	138.	2.32	.504
		172.	1.85	.586
		191.	1.79	.475
		223.	1.67	--
		287.	1.53	--
	285	191.	1.14	.440
		287.	1.37	.600
		350.	1.22	.425
		366.	1.30	-1.10
.016 H^+	285	411.	.585	--
		462.	.732	.585
		656.	.631	.500
.021 H^+	285	608.	.474	.335
		691.	.486	.425
		837.	.455	.425

Table 9 (Cont)

Conc. (m/l)	T°K	J(A/M²)	Resistance (K)	Back Emf (-volts)
.008 H^+	298	138.	1.27	.260
		172.	1.82	.570
		191.	1.750	.625
		223.	1.60	.600
		287.	1.38	.640
.010 H^+	298	191.	.958	.320
		280.	1.36	.725
		350.	1.20	.690
		411.	.377	.426
.016 H^+	298	525.	.538	.600
		608.	.553	.690
		656.	.552	.730
		691.	.238	.600
.021 H^+	298	726.	.313	.550
		837.	.352	.510
		888.	.348	.665
		1054.	.397	.630

Table 10

Minimum Back Emf Values for the First Break in Spectrum

Conc. Na^+ ion in moles/liter	T°K	V_B (volts)
.020	285	-.920
.040	285	-.670
.060	285	-.680
.010	298	~-.500
.020	298	-.590
.040	298	-.610
.060	298	-.590
.040	313	-.650
.060	313	-.630

Table 11

Average Steady State Resistance as a Function of Concentration and Temperature

Conc. Na^+	T^oK	R_{ss}avg (Kilohms)
.010	285	--
.020	"	1.26
.040	"	.610
.060	"	.380
.010	298	--
.020	"	.904*
.040	"	.417
.060	"	.309
.010	313	1.62
.020	"	(.674)
.040	"	.360
.060	"	.210

Conc. H^+	T^oK	Avg. Res (Kilohms)
.010	285	1.25
.016	"	.649
.021	"	.473
.016	298	.548
.021	"	.353

*The R_{ss}avg for .02 Na^+ ion at a flux of 25 A/M^2 was ignored.

Table 12

The Effect of Flux on the Initial Drop in V_T(11KΩin)

Conc. (m/l)	T°K	J A/M^2	ΔV(volts)	$\delta^* \times 10^8$ coulombs/m^2
.010 Na^+	313	20.4	.176	.920
		35.7	.382	2.0
		45.8	.527	2.8
	298	15.3	.203	1.1
		20.4	.294	1.5
		25.5	.412	2.2
		30.6	.441	2.3
		35.7	.616	3.2
	285	10.2	.265	1.4
		25.5	.470	2.5
		30.6	.646	3.4
.020 Na^+	313	35.7	.147	.77
		45.8	.176	.92
		71.3	.500	2.6
		102.	.587	3.0
	298	30.6	.235	1.2
		35.7	.294	1.5
		45.8	.412	2.2
		71.3	.587	3.0
.040 Na^+	313	86.6	.294	1.5
		102.	.352	1.9
		127.	.412	2.2
		153.	.528	2.8
	298	56.	.264	1.4
		71.3	.323	1.7
		86.6	.440	2.3
		102.	.616	3.2
		127.	.616	3.2

Table 12 (Cont.)

Conc. (m/l)	T°K	J A/M^2	ΔV(volts)	δ^* x 10^8 coulombs/m^2
.060 Na^+	313	127.	.352	1.9
		153.	.470	2.5
		204.	.735	3.8
	298	127.	.470	2.5
		153.	.528	2.8
		204.	.910	4.8
	285	102.	.352	1.9
		127.	.500	2.6
		153.	.941	4.9
		204.	1.12	5.9

*calculation of δ will be discussed in the next section.

Table 13

The Effect of Concentration, Temperature and Flux on the Transition Time

Conc. (m/l)	T°K	J(A/M²)	τ(sec)
.010 Na^+	285	10.2	25.5
		15.3	12.6
		25.5	4.5
		30.6	3.0
	298	15.3	17.1
		20.4	8.4
		25.5	5.4
		30.6	3.8
		35.7	3.0
	313	15.3	23.3
		20.4	12.5
		30.6	5.3
		35.7	3.9
		45.8	2.25
.020 Na^+	285	20.4	31.5
		25.5	21.0
		30.6	12.6
		35.7	6.3
		45.8	5.9
		71.3	1.9
	298	25.5	30.8
		30.6	17.4
		35.7	12.3
		45.8	6.6
		56.0	5.0
		71.3	2.9
.020 Na^+	313	30.6	24.0
		35.7	18.6
		45.8	9.6
		71.3	3.6
		102.	2.0

Table 13 (Cont)

Conc. (m/l)	T°K	J(A/M²)	τ(sec)
.040 Na^+	285	56.0	13.8
		71.3	7.5
		86.6	5.3
		102.	3.8
		127.	2.3
	298	56.0	20.4
		71.3	10.2
		86.6	7.1
		102.	5.6
		127.	3.0
	313	71.3	19.5
		86.6	9.9
		102.	6.9
		127.	4.2
		153.	3.2
.060 Na^+	285	102.	9.6
		127.	5.4
		153.	4.2
		204.	2.0
	298	86.6	20.4
		127.	7.8
		153.	5.0
		204.	3.0
.060 Na^+	313	127.	12.0
		153.	7.5
		204.	4.1

Table 13 (Cont)

Conc. (m/l)	T°K	J(A/M²)	τ(sec)
.008 H^+	285	121.	33.8
		138.	24.0
		172.	16.5
		191.	12.9
		223.	9.6
	298	138.	32.3
		172.	18.9
		223.	9.9
		287.	6.0
	313	172.	20.6
		191.	15.9
		223.	11.9
		287	6.8
.010 H^+	285	172.	28.5
		191.	25.2
		223.	16.2
		287.	9.8
		350.	6.3
	313	255.	17.1
		350.	8.0
		395.	5.7
.016 H^+	285	366.	25.2
		411.	20.4
		462.	15.8
		525.	11.6
		608.	8.1
		656	7.13
	298	462.	16.1
		525.	12.0
		608.	9.1
		656	7.8

Table 13 (Cont)

Conc. (m/l)	T°K	J(A/M²)	τ(sec)
.016 H^+	313	525.	13.0
		608.	18.7
		656.	7.4
		726.	5.7
.021 H^+	285	608.	21.0
		691.	14.4
		837.	10.4
		1054.	5.6
	298	691.	25.2
		726.	15.3
		837.	12.3
		888.	11.7
		1054.	7.8

Table 14

Effect of Concentration and Temperature on $dJ^2/d(1/\tau)$

Na^+ ion

Conc. (m/l)	T^oK	Slope (A^2/m^4 sec x 10^{-2})	Conc. $(m/l)^2 x\ 10^4$
.010	285	.28	1.0
.020	"	.91	4.0x
.040	"	3.9	16.
.060	"	8.4	36.
.010	298	.33	
.020	"	1.4	
.040	"	5.2	
.060	"	13.	
.010	313	.47	
.020	"	1.7	
.040	"	6.7	
.060	"	17.	

H^+ ion

.008	285	.55	.64
.010	"	.77	1.0
.016	"	3.1	2.6
.021	"	5.8	4.4
.008	298	.55	
.016	"	3.6	
.021	"	8.1	

Table 15

Comparison of Experimental Values of $\frac{dJ'^2}{d\frac{1}{\tau'}}$ $\frac{dJ^2}{d\frac{1}{\tau}}$ With Values Calculated From Equation 25

Na^+ Ion

Values From Eq	$\frac{C'^2}{C^2}$	Experimental Values $\frac{k'}{k}$ 285°K	298°K	313°K	% Difference 285°K	298°K	313°K
$(.02/.01)^2=4.0$		3.3	4.1	3.6	-18	+ 2.5	-10
$(.04/.01)^2=16$		14.	16.	14.	-13	0.0	-13
$(.06/.01)^2=36$		30.	39.	36.	-17	+ 0.8	0.0
$(.04/.02)^2=4.0$		4.3	3.8	3.9	+ 7.5	- 5.0	- 2.5
$(.06/.02)^2=9.0$		9.2	9.4	10.	+ 2.2	+ 4.4	+11.
$(.06/.04)^2=2.3$		2.2	2.5	2.5	+ 4.3	+13.	+13.

H^+ Ion

$(.010/.008)^2 = 1.6$	--	1.4	--	-13.	
$(.016/.008)^2 = 4.0$	6.5	5.7	+ 63.	+43.	
$(.021/.008)^2 = 6.3$	16.	11.	>100.	+75.	

where

$C'^2/C^2 = \frac{dJ'^2}{d\frac{1}{\tau'}} \quad \frac{dJ^2}{d\frac{1}{\tau}}$ from equation

$\frac{k'}{k}$ " obtained experimentally

$$\% \text{ Difference} = \frac{\frac{k'}{k} - \frac{C'^2}{C^2}}{\frac{C^{2\prime}}{C^2}} \times 100$$

Table 16

Effect of Concentration, Temperature and Flux on Break Time

Conc. (m/l)	T°K	J A/M^2	t_B(sec)
.010 Na^+	286	20.4	1.5
		25.5	3.8
		30.6	6.8
		35.7	10.2
		45.8	17.1
	299	15.3	N
		25.5	N
		35.7	1.4
		45.8	2.8
		56.0	7.8
	313	35.7	N
		45.8	0.6
		56.0	1.7
		71.3	3.9
.020 Na^+	286	35.7	0.8
		45.8	4.7
		56.0	8.6
		71.3	N
	299	25.5	N
		35.7	N
		45.8	N
		56.0	N
		71.3	4.1
		81.5	5.9
	313	71.3	N
		102.	1.1
		127.	3.5
		153.	5.5

Table 16 (Cont)

Conc. (m/l)	T°K	J A/M^2	t_B(sec)
.040 Na^+	286	56.0	N
		71.3	1.4
		86.6	6.1
		102.	10.2
	299	56.0	N
		86.6	N
		102.	1.5
		127.	7.1
	313	153.	1.5
		178.	3.6
		204.	6.0
.060 Na^+	286	102.	2.0
		127.	10.2
		153.	N
		204.	N
	299	127.	N
		153.	4.5
		178.	7.2
		204.	9.0
.008 H^+	285	137.8	0.3
		171.9	6.3
		191.0	8.7
		222.8	15.3
		286.5	N
	298	156.0	N
		171.9	0.9
		191.0	1.8-2.1
		222.8	10.2
		286.5	N

Table 16 (Cont)

Conc. (m/l)	T°K	J $^{A}/M^{2}$	t_B(sec)
.008 H^+	313	191.0	N
		222.8	2.1
		254.7	3.9
		286.5	N
.010 H^+	298	254.7	1.1
		286.5	5.9
		321.5	7.1
		350.1	14.0
	313	222.8	N
		254.7	1.2
		286.5	1.4
		350.1	4.7
.016 H^+	285	366.1	1.0
		410.6	6.9
		461.6	13.8
		525.2	24.4
		592.1	28.5
.021 H^+	285	525.2	2.9
		607.8	10.8
		690.7	20.4
		837.2	N
		1053.6	N

where

N indicates that an "S-shaped curve" was not found.

Table 17

The Lowest Fluxes at Which Measureable Noise and Non-linear Voltage-Time Curves were Found, as a Function of Concentration and Temperature

Conc. (m/l)	T°K	Total Noise RMS(mv.x10^3)	J_N(A/M²)	J_{VT}(A/M²)
.008 H^+	283	14.5	106	121
.008 H^+	313	13.5	121	172
.016 H^+	283	20.0	325	366
.021 H^+	283	8.2	462	608
.021 H^+	313	12.5	690	758
.020 Na^+	283	8.0	19.3	20.4
.020 Na^+	313	5.2	30.6	35.7
.040 Na^+	301	4.1	51.0	56.0
.060 Na^+	313	4.6	116	127

where

J_N = lowest J values at which noise appears

J_{VT}= lowest J values where chronopotentiometry shows membrane depletion.

Table 18

β as a Function of Concentration and Temperature

Conc. (m/l)	T°K	$1^{\circ}/T\ K \times 10^{-4}$	β (A/M^2)
.008 H^+	283	35.3	118
	310	32.2	138
	313	31.9	142
.010 H^+	283	35.3	154
	291	34.4	151
	313	31.9	200
	318	31.2	200
.016 H^+	283	35.3	360
	291	34.4	409
	310	32.2	495
	313	31.9	505
.010 Na^+	282	35.4	16
	292	34.2	17.5
	301	33.2	25.
	313	31.9	32.

Table 19

χ as a function of Concentration and Temperature

Conc. (m/l)	T°K	ma/cm²-sec x 10^{-3}
.005 H^+	10	21.0
	37	21.8
	40	22.5
	45	22.2
.010 H^+	10	23.0
	18	22.5
	36	22.5
	40 + 45	25.0
	45	24.5
.016 H^+	10	35.6
	18	27.7
	37	26.2
	40	26.8
	40	42.2
.021 H^+	10	56.2
.010 Na^+	10	.96
	19	1.75
	28	1.16
	40	1.20
.040 Na^+	28	2.1
	40	2.0

where

$$\chi = dJ/df_B$$

Table 20

β' as a Function of Concentration and Temperature

Conc. (m/l)	T°K	$\frac{1}{T}$°K x 10^{-4}	β'(A/M²)	RMS(10^3mv)
.008 H^+	283	35.3	106	14.5
.008 H^+	313	31.9	121	13.5
.021 H^+	283	35.3	162	8.2
	291	34.4	557	11.0
	313	31.9	691	12.5
.040 Na^+	283	35.3	35.7	12.
	301	33.2	56.0	13.5
	313	31.9	73.0	15.

Table 21

The Diffusional Activation Energy (Ea) as a Function of Concentration and Temperature

H^+ ion		Na^+ ion	
Conc. (m/l)	Ea(kcal/mole)	Conc. (m/l)	Ea(kcal/mole)
.008	1.2	.01	4.1
.01	1.6	.04	4.0
.016	2.0		
.021	2.3		

Table 22

H^+ Ion Concentration at the Membrane Surface as a Function of Back Emf

η'_t(mv)	Co=.008H^+ c'x10^3	Co=.010H^+ c'x10^3	Co=.016H^+ c'x10^3	Co=.021H^+ c'x10^3
50	2.50	3.12	5.00	6.56
100	2.08	2.6	4.16	5.46
150	1.73	2.16	3.46	4.54
200	1.45	1.81	2.90	3.80
250	1.21	1.51	2.42	3.18
300	1.01	1.26	2.02	2.65
350	.84	1.05	1.68	2.20
400	.70	.88	1.40	1.84
450	.58	.73	1.16	1.52
500	.49	.61	.98	1.29
550	.41	.51	.82	1.08
600	.34	.43	.68	.89
650	.28	.35	.56	.79
700	.24	.30	.48	.63
800	.16	.20	.32	.42
900	.11	.14	.22	.29
1000	.08	.10	.16	.21

$$\bar{t}_{H^+} - t_{H^+} = .087$$

$$\eta'_t = V_B(11K \text{ in})$$

Table 23

Na^+ Ion Concentration at the Membrane Surface as a Function of Back Emf

	$Co=.01Na^+$	$Co=.02Na^+$	$Co=.04Na^+$	$Co=.06Na^+$
η'_t(mv)	C'	C'	C'	C'
100	1.05×10^{-3}	2.10×10^{-3}	4.20×10^{-3}	6.37×10^{-3}
200	1.99×10^{-4}	3.98×10^{-4}	7.96×10^{-4}	1.20×10^{-3}
300	3.75×10^{-5}	7.50×10^{-5}	1.50×10^{-4}	2.27×10^{-4}
400	7.10×10^{-6}	1.42×10^{-5}	3.84×10^{-5}	4.29×10^{-5}
500	1.34×10^{-6}	2.68×10^{-6}	5.35×10^{-6}	8.1×10^{-6}
600	2.53×10^{-7}	5.06×10^{-7}	1.01×10^{-6}	1.53×10^{-6}
700	4.77×10^{-8}	9.55×10^{-8}	1.91×10^{-7}	2.89×10^{-7}
800	--	--	3.64×10^{-8}	5.45×10^{-8}

a) where $\bar{t}_{Na^+} - t_{Na^+} = 0.14$

	$Co=.01Na^+$	$Co=.02Na^+$	$Co=.04Na^+$	$Co=.06Na^+$
η'_t(mv)	C'	C'	C'	C'
100	5.20×10^{-4}	1.04×10^{-3}	2.1×10^{-3}	3.15×10^{-3}
200	4.87×10^{-5}	9.74×10^{-5}	1.96×10^{-4}	2.95×10^{-4}
300	4.56×10^{-6}	9.12×10^{-6}	1.82×10^{-5}	2.76×10^{-5}
400	4.26×10^{-7}	8.52×10^{-7}	1.71×10^{-6}	2.58×10^{-6}
500	3.98×10^{-8}	7.96×10^{-8}	1.60×10^{-7}	2.41×10^{-7}
600	3.70×10^{-9}	7.40×10^{-9}	1.49×10^{-8}	2.25×10^{-8}
700	--	--	1.3×10^{-9}	2.10×10^{-9}

b) where $\bar{t}_{Na^+} - t_{Na^+} = 0.34$

$\eta'_t = V_B$(11K in)

Table 24

ΔV_t as a Function of Concentration and Temperature

Conc. of Na^+ ion	T^oK	ΔV_t(mv)
.01	298	455
.01	313	530
.02	298	420
.02	313	--
.04	298	470
.04	313	490

where

ΔV_t - voltage drop at which sufficient charge is built at mem-solution interface to cause a break time delay of 0.5 sec.

REFERENCES

1. S.J. Sethu, J. Appl. Polymer Sci. 8, 2249 (1964).

2. J.D. Blainey and H.J. Yardley, Nature 83, (1956).

3. T. Yamabe, M. Seno and N. Fakai, Bull. Chem. Soc. Japan 32, 1383 (1959).

4. C. Forgacs, Desalination 4, 111 (1969/70).

5. M. Block and J.A. Kitchener, J. Electrochem. Soc. 113, 947 (1966).

6. T. Sata, R. Yamane, and Y. Mizutani, Bull. Chem. Soc. Japan 42, 279 (1969).

7. B.A. Cooke, Electrochimica Acta 3, 307 (1961).

8. B.A. Cooke, Electrochimica Acta 4, 179 (1961).

9. V.J. Frilette, J. Phys. Chem. 61, 168 (1957).

10. M.E. Green and M. Yafuso, J. Phys. Chem. 72, 4072 (1968).

11. M. Yafuso and M.E. Green, J. Phys. Chem. 75, 654 (1971).

12. P. Resibois and N. Hasselle-Schuermans, "Advances in Chemical Physics" (I. Prigonine, ed.), p.159 (1967).

13. D.G. Miller, Chem. Rev. 60, 15 (1960).

14. N. Lakshminarayanariah, Chem. Rev. 65, 491 (1965).

15. F. Helfferich, "Ion Exchange" p. 134. McGraw Hill, New York, 1962.

16. J.R. MacDonald and C.A. Barlow, Jr., J. of Chem. Phys. 36, 3062 (1962).

17. G. Gouy, J. Physique 9, 457 (1910).

18. D.L. Chapman, Philm Mag. 25, 473 (1913).

19. O. Stern, Z. Elektrochem. 30, 508 (1924).

20. M. Olmstead and R. Nicholson, J. of Phys. Chem. 72, 1650 (1968).

21. R.S. Rodgers and L. Meites, J. of Electroanal. Chem. 16, 1 (1968).

22. J. R. MacDonald, J. of Chem. Phys. 54, 2026 (1971).

23. A.L. McWhorter, "Semiconductor Surface Physics" (R.H. Kingston, ed.), p.207. Univ. of Pennsylvania Press, Philadelphia, 1957.

24. T.E. Firle and H. Winston, J. of Appl. Phys. 26, 716 (1955).

25. D.K.C. MacDonald, "Noise and Fluctuations," Wiley, New York, 1962.

26. I. Prigogine, "Non-Equilibrium Statistical Mechanics", p. 63. Interscience Publishers, New York, 1962.

27. A. Van der Ziel, "Noise," p. 316. Prentice Hall, New York, 1954.

28. M. Eigen and L. de Maeyer, "Physical Methods in Organic Chemistry" (A. Weissberger, ed.), Interscience Publishers, New York, 1963.

29. K.M. Van Vliet and J. Fassett, "Fluctuation Phenomena in Solids" (R. Burgess, ed.), p. 334. Academic Press, New York, 1965.

30. F.N. Hooge, Physics Letters 29A, 139 (1969).

31. F.N. Hooge and A.M.H. Hoppenbrouwers, Physica 45, 386 (1969).

32. F.N. Hooge, H.J.A. Van Dujk and A.M.H. Hoppenbrouwers, Philips Res. Repts. 25, 81 (1970).

33. F.N. Hooge and J.L.M. Gaal, Philips Res. Repts. 26, 77 (1971).

34. F.N. Hooge and J.L.M. Gaal, Philips Res. Repts. 26, 345 (1971).

35. J.H.J. Lorteige and A.M.H. Hoppenbrouwers, Philips Res. Repts. 26, 29 (1971).

36. M.H. Fishman, Biophysical Abstracts 119a, SaAM-E4, (1971).

37. M. Lax and P. Menqart, J. Phys. Chem. Solids 14, 248 (1960).

38. T. Yamabe and M. Seno, Desalination 2, 148 (1967).

39. A.P. Christodoulou and H.L. Rosano, Advances in Chemistry 84, (1968).

40. Mason and Blum, J. Am. Chem. Soc. 69, 1246 (1947).

41. K.L. Elmore, J.D. Hatfield, R.L. Dunn and A.D. Jones, J. Phys. Chem. 69, 3520 (1965).

42. J. Clay, N.S. Goel and F.P. Buff, J. Chem. Phys. 56, 4245 (1972).

43. F.W. Sears and M.W. Zemansky, "University Physics", p.438 Addison-Wesley Pub., Readinq, Mass., 1955.

44. S. Rice and M. Nagasawa, "Polyelectrolyte Solutions", p. 318. Academic Press, New York, 1961.

45. "Handbook of Chemistry and Physics - 46th edition" (R.E. Weast -ed.) p.D79. The Chemical Rubber Co., 1965/66.

46. L. Onsager, J. Chem. Phys. 2, 599 (1934).

47. C. Forgacs, Nature 190, 339 (1961).

48. A.M. Peers, Disc. Faraday Soc. 21, 124 (1956).

49. N.W. Rosenberg and C.E. Tirrell, Industr. Engng. Chem. 49, 780 (1957).

50. W. Kooistra, Desalination 2, 139 (1967).

51. V.I. Tatarski, "Wave Propagation in a Turbulent Medium" (Translated by R.A. Silverman), p. 8. Dover Pub. Inc., New York, 1967.

52. Dr. Tchen, Private communications.

53. A.S. Monin and A.M. Yaglon, "Statistical Fluid Mechanics: Mechanics of Turbulence - Vol 1" (J.L. Lumley -ed.), p.88. The MIT Press, Cambridge, Mass., 1971.

54. B.E. Conway, "Theory and Principles of Electrode Processes" p. 38. The Ronald Press Co., New York, 1965.

55. A.S. Monin, op. cit., p. 73.

56. Ibid., p. 76.

57. Ibid., p. 85.

58. W.K.H. Panofsky and M. Phillips, "Classical Electricity and Magnetism", p. 111. Addison Wesley, Reading, Mass., 1962.

59. I.W. Jacobs and A.W. Lawson, J. Chem. Phys. 20, 1161 (1952).

60. D.A. MacInnes, "The Principles of Electrochemistry", p. 349. Reinhold Pub. Co., New York, 1939.

61. H. Harned and B. Owen, "The Physical Chemistry of Electrolytic Solutions", p. 214. Reinhold Pub. Co., New York, 1943.

62. J.N. Agar, "The Structure of Electrolytic Solution", (J. Hammer -ed.), p. 207. Wiley, New York, 1959.

63. A.S. Monin, op. cit., p. 89.

64. J.H.B. George and R.A. Courant, J. Phys. Chem. 71, 246 (1967).

65. S.W. Provenchu, Ph.D. Thesis, Yale University, New Haven, Conn., 1967.

66. A. Patterson, Jr., Proc. Nat'l. Acad. Sci. 39, 146 1953.

67. D.A. MacInnes, op. cit., p. 352.

68. J. Von Schiele, Annelen Der Physik - V Folge, Band 13, 811 (1932).

69. K.J. Vetter, "Electrochemical Kinetics", p. 160. Acad. Press, NY 1967.

70. E.A. Moelwyn-Hughes, "Physical Chemistry", p. 863. The Macmillan Co., New York, 1961.

71. A.A. Noyes, "The Electrical Conductivity of Aqueous Solutions", p. 257. The Carnegie Inst. of Washington, Wash. D.C., 1907.